

A STUDY OF
BROADBAND VARACTOR HARMONIC GENERATORS

THESIS

SUBMITTED IN PARTIAL FULFILMENT OF THE REQUIREMENTS

FOR THE DEGREE OF

MASTER OF ENGINEERING

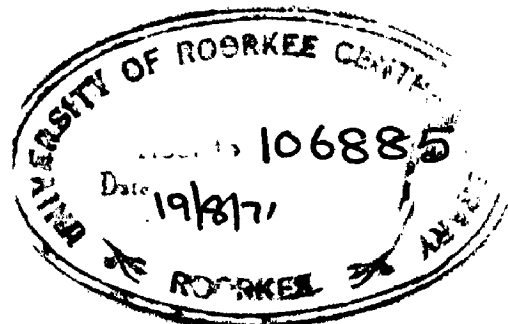
IN

ELECTRONICS & COMMUNICATION ENGINEERING
(MICROWAVES)

BY

NEELAM RANI GUPTA

November, 1970



DEPARTMENT OF ELECTRONICS & COMMUNICATION
UNIVERSITY OF ROORKEE
ROORKEE
(U.P.)

ELECTRONICS AND COMMUNICATION ENGINEERING DEPARTMENT

UNIVERSITY OF ROORKEE

ROORKEE (U.P.)

C E R T I F I C A T E

I hereby certify that the thesis entitled " A Study of Broadband Varactor Harmonic Generator" which is being submitted by Miss NEELAM RANI GUPTA in partial fulfilment of the requirement for the award of Degree of Master of Engineering in Electronics and Communication (Microwaves) is a record of her own work. She worked for about 4½ months in the Department of Electronics & Communication Engineering and for about 3 months at Tata Institute of Fundamental Research, Bombay.

INCHARGE OF THESIS

A.K.Kamal.

(A.K.KAMAL)

**Head of the Department
Electronics & Communication
Engineering, University of
Roorkee, Roorkee.**

SUMMARY

This dissertation presents a study of the varactor harmonic generator type frequency multipliers and describes the design and development of a broadband harmonic generator operating in L-Band.

The primary objective of this exercise has been to obtain broadband frequency multiplication consistent with a good overall performance.

The frequency multiplier was actually designed, fabricated and tested.

The schematic of this unit consists of a mechanically tunable UHF transistor oscillator followed by a single stage frequency quadrupler.

The output filter was of the interdigital type with a passband bandwidth of 200 MHz centred at a frequency of 1840 MHz. The complete design, fabrication and testing of the output bandpass filter and input low pass filter are described in detail in this thesis.

A frequency multiplier consisting of these units and a diode mount together with the matching networks, was assembled and its characteristics of operation were studied. The final measurements on the frequency multiplier indicate a 3 db bandwidth of 135 MHz, with all other spurious and harmonic frequencies down to a minimum of 40 db.

ACKNOWLEDGEMENTS

The work described in this thesis was carried out in the Solid State Microwave circuits Laboratory of the Tata Institute of Fundamental Research, Bombay. The author wishes to acknowledge the kind permission and facilities provided by the authorities of that institute for carrying out the experimental work. A special debt of gratitude is owed to Dr. V.F. Kodali, head of the Microwave solid state circuits and components group, T.I.F.R., for his valuable guidance, helpful discussions and for his keen interest at all stages of my work. Thanks are also due to Professor D.Y. Phadke, Head of Microwave Engineering Group, T.I.F.R., for his interest and encouragement during my work.

The author is deeply indebted to Dr. A.K. KAMAL, Professor and head of Electronics and Communication Engineering Department, University of Roorkee, for his thoughtful guidance of theoretical work and suggestion of the topic.

Thankful appreciations are also due to all the members of Microwave Engineering Group and workshop who helped unstintingly but for which the work could not have been completed successfully. Among the members of Microwave Engineering Group, special thanks^{go}/to Mr. D. K. Irivedi, scientist, for his encouragement in the completion of the work.

TABLE OF CONTENTS

Certificate	(i)
Summary	(ii)
Acknowledgements	(iii)
<u>CHAPTER I : VARACTOR DIODES</u>	1

1.1	Introduction.
1.2	A varactor diode.
1.2.1	Varactor characteristics.
1.3	Conventional depletion layer varactors.
1.3.1	The abrupt-junction diode.
1.3.2	The graded-junction diode.
1.4	The step-recovery diode.
1.5	Harmonic generation using conventional and step-recovery diodes.
1.5.1	Harmonic generation using conventional varactors.
1.5.2	Harmonic generation using step-recovery diodes.
1.5.2.1	Impulse generator circuit.
1.5.2.2	Conduction interval.
1.5.2.3	Depletion interval.
1.5.2.4	Spectrum of impulse generator.

<u>CHAPTER II : VARACTOR MULTIPLIERS</u>	30
---	-----	-----	----

2.1	Introduction
2.2	Large signal analysis of narrowband varactor harmonic generators with and without idlers.

- 2.2.1 Varactor capacitance-voltage relationship.
- 2.2.2 Resonant varactor multipliers without diodes.
- 2.2.3 Calculation of efficiency.
- 2.2.4 Abrupt-junction case.
- 2.2.5 Resonant varactor multipliers with diodes.
- 2.3 Broadband frequency multipliers.
- 2.3.1 Bandwidth limitations in multipliers.

CHAPTER XXV: DESIGN OF FILTERS FOR DETERMINED FREQUENCY MULTIPLIERS

- 2.1 Introduction
- 2.2 General principles of multiplier circuit design.
- 2.3 Theory of low-pass filter design.
 - 2.3.1 Design of a low-pass filter.
- 2.4 Theory of interdigital band-pass filter design.
 - 2.4.1 Low-pass to band-pass transformation.
 - 2.4.2 Band-pass filters and their relation to low-pass prototype.
 - 2.4.3 Design principles.
 - 2.4.4 Band-pass filter characteristics.
 - 2.4.5 Comparison between theoretical design and experimental performance.
- 2.5 Design of transistor power oscillator mechanically tunable from 420 to 650 MHz.
 - 2.5.1 Oscillator design.

<u>CHAPTER IV : MEASUREMENTS ON THE BROADBAND HARMONIC GENERATOR</u>	105
4.1 Introduction			
4.2 Experimental set-up.			
4.2.1 Multiplier testing.			
4.3 Design of output matching network.			
4.4 Results.			
<u>CHAPTER V : SUMMARY, CONCLUSION AND SCOPE FOR FURTHER STUDY</u>	119
5.1 Summary and conclusion.			
5.2 Scope for further study.			
REFERENCES	124

SECRET

SECRET

The generation of microwave frequencies at the milliwatt power level has in the past been the exclusive domain of vacuum and similar electron beam devices. But in recent years the need for a solid state source of microwave power has been increasingly felt due to the advent of situations where space and weight have become of prime importance in the selection of components and systems for mobile military and civil installations. Important additional benefits gained from the use of solid state sources are an increased reliability and lifetime. The most obvious choices for solid state microwave sources are the tunnel diodes, varactor diodes and the silicon transistors. The tunnel diode suffers from the disadvantage of low power output. The very recent devices which show promise of both high power and high frequency operation are the 'Cruz effect' oscillator and avalanche oscillator. But of all the solid state microwave sources, the varactor multipliers have relatively low noise, high frequency stability and proven reliability of operation. Because of a large power availability from UHF transistors, it has now become possible to obtain useful power at microwave frequencies from varactor harmonic generators. At present these are among the more powerful semiconductor devices, but the circuit complexity of a high-efficiency frequency multiplier chain is an insuperable problem in this case.

A new type of varactor diode, called step recovery diode or step back diode overcomes some of these complex conditions. A single stage of step recovery

diode can multiply to the hundredth order without idlers. These multipliers are more efficient and have a high power handling capability. In addition to this, the multiplier circuits are somewhat simpler than those using conventional varactors and the circuit tuning is also very simple.

1.2 A VARACTOR DIODE⁽¹⁾

A varactor diode is a semiconductor device that is used as a variable reactance circuit element. This variable reactance is provided by the junction capacitance, which varies as a function of the applied voltage. The variation of capacitance with voltage is nonlinear in the case of a varactor diode and this nonlinearity can produce three substantially different effects. One of these is the switching or modulation of a microwave signal through variation of reactance by means of an externally applied bias. In a second usage, the nonlinearity causes the generation of harmonic frequencies of an applied signal. In the third case, two microwave signals of different frequencies may be applied, resulting in parametric amplification and/or up conversion of one of these signals.

The active element in a varactor diode consists of a semiconductor wafer containing a junction, usually formed by diffusion. The equivalent circuit of the wafer is shown in fig. 1.1. Here

C_j is the junction capacitance, which is a function of the applied voltage.

R_j is the junction resistance, which is in shunt with C_j and which is also a function of bias.

R_s is the series resistance, which is a function of bias, includes the resistance of the semiconductor on either side of the junction

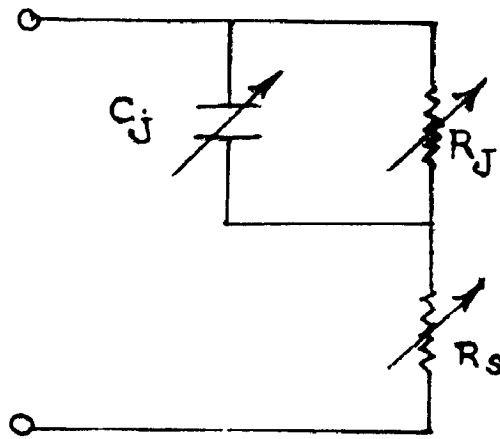


FIG. 1.1.

WAFER EQUIVALENT CIRCUIT

through which the conduction current passes and the resistance of the ohmic electrical contacts to the wafer. But the variation in R_s with bias is generally negligible in normal varactors.

Varactor diodes are normally operated under reverse bias, where the junction resistance, which is ordinarily $10 \text{ M}\Omega$ or more is negligible in comparison with the microwave capacitive reactance of the junction. Therefore, the equivalent circuit of a reverse biased wafer at microwave frequencies is simply a capacitance and resistance in series. The equivalent circuit of a forward-biased varactor at microwave frequencies is generally more complicated, since it must include the diffusion capacitance of the injected carriers as well as the effect of these carriers on the conductance of the semiconductor material.

1.24. VARACTOR CHARACTERISTICS ⁽²⁾

When operating as a frequency multiplier, the important varactor characteristics are: efficiency as a multiplier, power handling capability and, in some applications, the linearity of power output with changes in input power. The efficiency of a varactor is a function of the cut-off frequency of the device which in turn is dependent on the diode quality factor. The quality factor Q_V at a specified bias V and frequency is given as

$$Q_V = \frac{1}{2\pi f R_s C_{jV}}$$

For high Q device, R_s should be extremely low. But there is a low limit ^{or} on its value which cannot be further reduced for a particular reverse breakdown voltage.

The cut-off frequency is defined as that frequency at which quality factor is unity. Accordingly, the cut-off frequency at a specified bias V is given as

$$f_{cV} = \frac{1}{2\pi R_0 C_{jV}}$$

The power handling capability of the varactor is given by

$$P_T = \frac{\omega C_j V_B^2}{2}$$

where V_B is the breakdown voltage of the junction.

For a large power handling capability, it is desirable to make V_B as large as possible; which in turn requires the resistivity of the material near the junction to be high. Yet a high resistivity leads to a relatively high R_0 , which in turn lowers the Q factor and efficiency of the diode. Therefore, the varactor diode design, normally, is a compromise between high power handling capability and high efficiency.

1.2 CONVENTIONAL DEPLETION LAYER VARACTORS⁽³⁾

In conventional varactors, the dielectric capacitance variation is due to varying width of depletion region. A schematic of a high frequency depletion layer varactor is shown in fig. 1.2.

For forward voltages, the electrons of the moderately doped n-type region extend over a distance ΔL and occupy almost all of the epitaxial layer in ordinary operation. The capacity of the diode in this state is given by

$$C_{max} = \frac{A}{L - \Delta L} \dots (1.1)$$

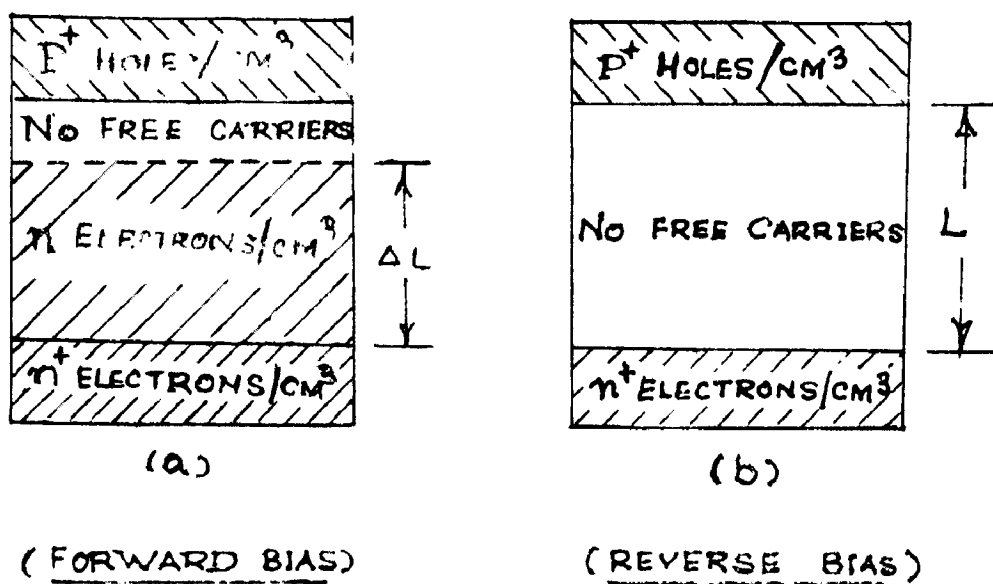


FIG 1.2

IDEALIZED MODEL OF A
"DIELECTRIC" VARACTOR.

and can be quite large before appreciable amounts of charge penetrate the remaining 'barrier' and introduce loss.

For peak reverse voltage, the carriers are swept out of the entire n-type region, which for optimum design usually occurs at reverse voltage just below avalanche breakdown. Here the capacity of the junction can be written as

$$C_{\min} = \frac{\epsilon A}{L} \quad \dots \quad (1.2)$$

Thus the depletion layer varactor exhibits a capacitance that varies with the applied voltage and can thus be employed as a harmonic generator, the mathematical proof for which is given in the next article 1.51. The main disadvantage of such types of harmonic generators is that, the output is not proportional to the input.

The conventional varactors commonly used are of two types:

1. Abrupt - junction diode
2. Graded-junction diode.

1.51 THE ABRUPT - JUNCTION DIODE

The abrupt or step junction has a constant resistivity near the depletion region which means that, the doping changes abruptly from an excess of acceptors to an excess of donors at the junction. This resistivity or impurity profile leads to an inverse half-power dependence of the junction capacitance on the voltage given by

$$C_j = \frac{C_0}{\left(1 - \frac{V}{V_0}\right)^{1/2}} \quad \dots \quad (1.3)$$

where C_0 is the capacitance at zero bias determined by the impurity and doping levels and the geometrical configuration and the structure of the diode.

ϕ is the contact potential, which appears across the junction in the absence of any applied bias.

v is the voltage across the diode (reverse bias)

Both the doping and the resistivity profiles are shown in fig. 1.3. It is found that with the abrupt-junction diode except for the doubler, it is impossible to generate harmonics without idlers, the mathematical proof of which is given in Chapter II.

1.32 THE GRADED - JUNCTION DIODE

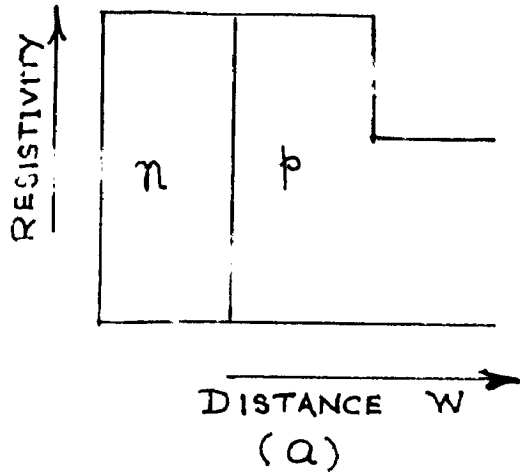
The graded-junction has an impurity concentration that decreases linearly as the depletion region is approached. This resistivity or impurity profile leads to an inverse third-power dependence of the junction capacitance and the voltage given by

$$C_j = \frac{C_0}{\left(1 - \frac{V}{\phi}\right)^{1/3}} \dots \quad (1.4)$$

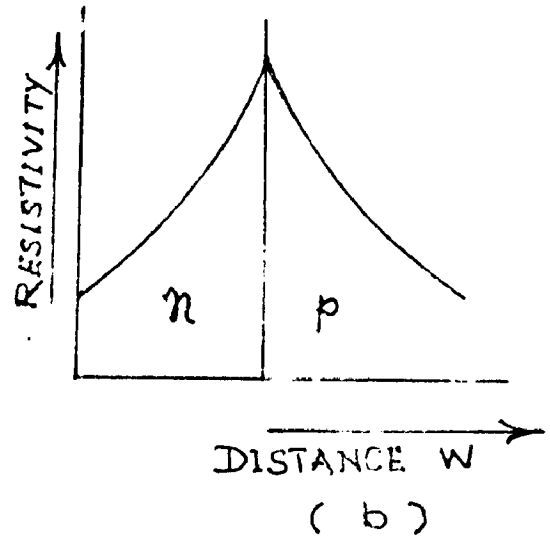
The graded-junction diodes have high power handling capability since resistivity peaks near the depletion region which gives high breakdown voltage. This high breakdown voltage contributes to a high power handling capability.

1.4 THE STEP RECOVERY DIODE^{(1), (4)}

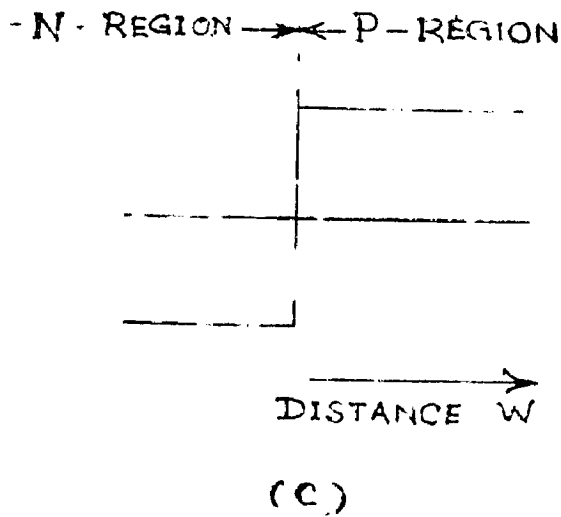
Krakauer⁽⁵⁾ and Schaffner⁽⁶⁾ have found that the diode frequency multipliers employing minority carrier charge storage effect have a performance, which



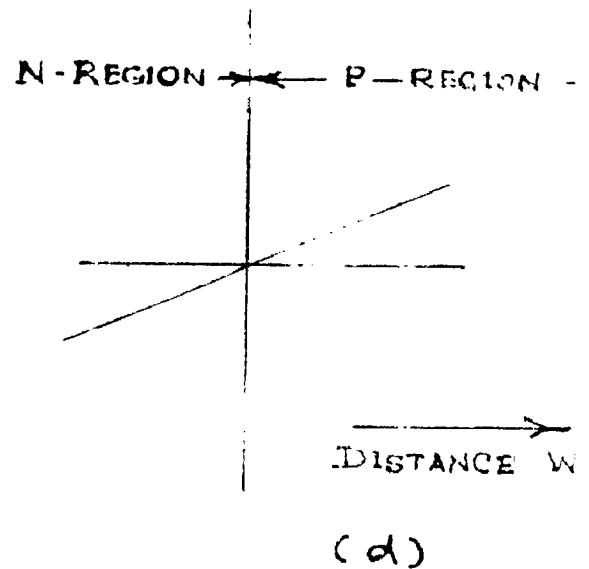
TYPICAL RESISTIVITY PROFILE
FOR THE ABRUPT OR STEP JUNCTION



TYPICAL RESISTIVITY
PROFILE FOR THE
LINEAR GRADED JUNCTION



TYPICAL IMPURITY PROFILE
FOR THE ABRUPT OR STEP
JUNCTION



TYPICAL IMPURITY PROFIL
FOR THE LINEAR GRADED
JUNCTION

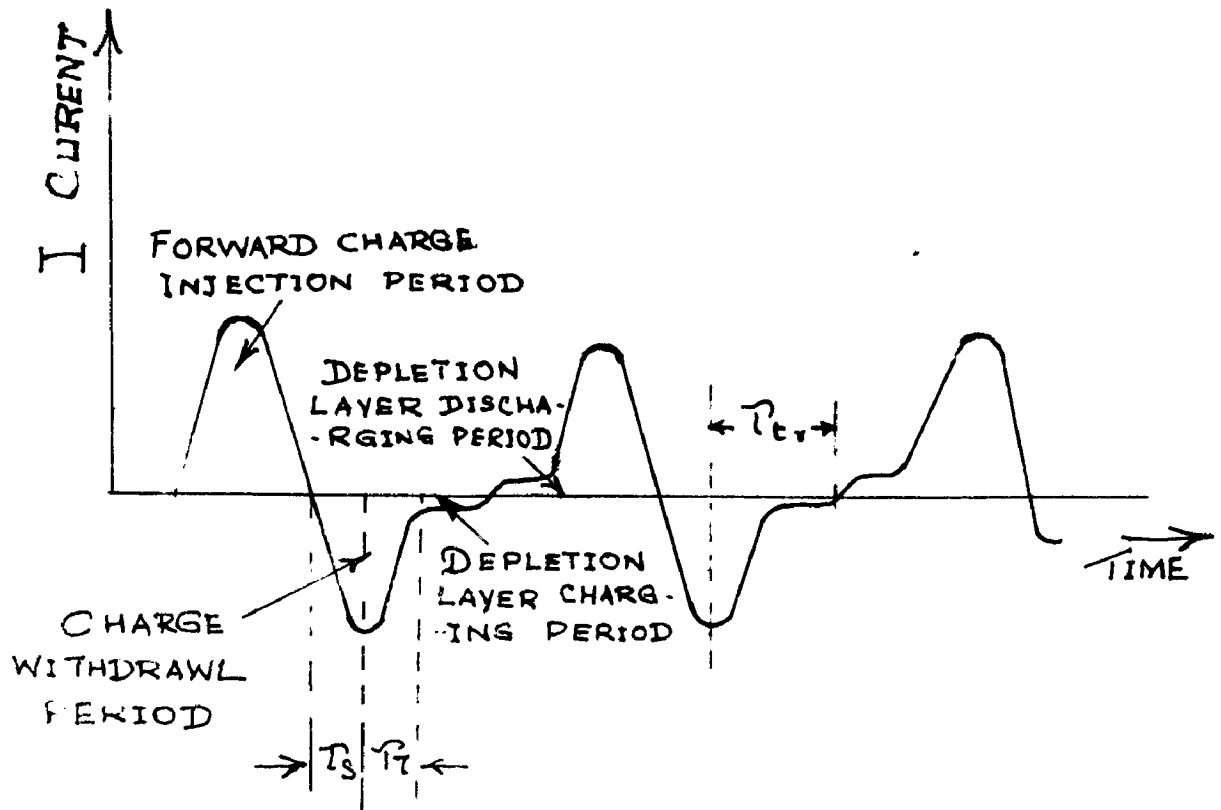
FIG. 1-3

is superior to that of the normal varactor diodes. Charge storage results from driving the varactor into forward voltage region. When the diode is forward biased, the charged carriers from one region are injected into the other to form minority carriers. These minority carriers are effectively stored charges contributing to junction capacitance. This stored charge is removed by reverse current during the reverse bias. Thereafter, the reverse current falls abruptly and this sudden cessation of reverse current produces charge discontinuity responsible for harmonic generation.

Step recovery diodes are optimized for maximum charge storage under forward current consistent with: (1) controlled release of the stored charge (as reverse current) and (2) fast transition from reverse-current conduction to the normal reverse-bias condition.

Although the capacitance of a step recovery diode varies with reverse-bias, the effect is small and relatively unimportant compared to the difference in charge storage between forward and reverse polarities (forward charge storage in the step recovery diode is typically 10^4 - 10^5 times greater than in the reverse direction).

When the forward stored charge has been exhausted by reverse current and carrier recombination, the reverse current falls abruptly and the diode assumes its reverse-bias equivalent circuit of a resistance in series with a variable capacitance. The reverse current then begins to charge the reverse-bias capacitance of the diode. Thereafter, the diode performs as a passive circuit element until the next reversal of the voltage across the diode. When a large sinusoidal voltage signal is applied to such a diode, biased near zero, the current in the diode follows a waveform shown in fig. 1.4.



T_s = STORAGE TIME

T_t = TRANSITION TIME

T_{tr} = REVERSE RECOVERY TIME

FIG. 1.4

CURRENT WAVE FORM OF A
SINUSOIDALLY SWITCHED STEP RECOVERY DIODE

With an optimum design of the impurity profile, the transition time may be made very small (down to a few picoseconds) the transition period, which may be viewed as a harmonic-rich switching transient, permits an approach to frequency multiplication that is substantially different in concept from the usual varactor operation.

The charge storage varactors have specially graded junctions. The resistivity profile of these special graded junctions adds the step recovery property because the electric fields set up by the steep resistivity gradient are a short distance, about 0.2 mil, away from the center of the depletion region. This keeps the minority carriers close to the depletion layer rather than permitting them to wander to random depths in the opposite regions. Thus, when the voltage is reversed, they return to their point of origin.

A more important figure of merit for step recovery diodes is the ratio of minority carrier life time to the transition time. This figure of merit should be very high for efficient operation. Since if minority carrier life time is long compared to an r.f. period; then injected carriers which are stored under forward bias are fully recovered by reverse current without any carrier recombination.

The step recovery property also results in a device with more linear power characteristics because the percentage of harmonic-current generation is not a function of the signal level. It is a function only of the waveform and the abruptness of the decline of the reverse current. And if self-biasing is employed, as it should be for linearity, the shape of the current wave remains constant over a considerable power input range. Further, the circuit-detuning effects which occur with changes in the bias level are minimized because of the relative insensitivity of the capacitance to voltage changes.

Both charge storage and step recovery add to the power handling capability of the varactors. Since charge is stored during forward voltage and not recombined, here the voltage swing is not limited to be between zero volts and breakdown voltage. Considerable forward voltage and therefore, considerable extra power because of the large currents involved, can be tolerated without dissipating excess power in the varactor. In addition, to obtain step recovery action, the resistivity must peak near the depletion region. Thus, the breakdown voltage is high because of its dependence on the resistivity and this high breakdown voltage contributes to a high power, handling capability.

1.5 HARMONIC GENERATION USING CONVENTIONAL AND STEP RECOVERY DIODES

Harmonics are generated when a sinusoidal source drives a nonlinear impedance, i.e. an impedance whose resistance, capacitance or inductance varies with the current or voltage as a nonlinear function. The nonlinear resistance of a semiconductor diode has been used extensively to generate millimeter wave frequencies. However, Page⁽⁷⁾ has shown that the efficiency of a nonlinear-resistance harmonic generator can not be greater than $\frac{1}{n^2}$, where n is the order of the harmonic, due to losses inherent in the resistance. On the other hand simple energy considerations, supported by the relations of Manley & Rowe⁽⁸⁾, show that all of the power introduced at a single fundamental frequency into a lossless nonlinear reactance must be converted into power at harmonic frequencies of the driving frequency. Ideally such a diode can not convert any of the incident power into dc power, nor does it dissipate any power. Such generators have become practicable because of the availability of high quality varactors and step recovery diodes.

1.51 HARMONIC GENERATION USING CONVENTIONAL VARACTORS⁽¹⁾

The varactor junction capacitance (C_j) varies in accordance with the relation

$$C_j = \frac{C_0}{\left(1 - \frac{V}{\phi}\right)^\gamma}$$

where γ is a constant (nonlinearity parameter) determined by the impurity gradient.

= 1/2 for abrupt junction diodes

= 1/3 for graded junction diodes.

= 0 for step recovery diodes

and V is the applied voltage.

A typical plot of the junction capacitance versus bias voltage is shown in Fig. 1.5 (a). The a.c. elastance (incremental elastance) $S(V) =$

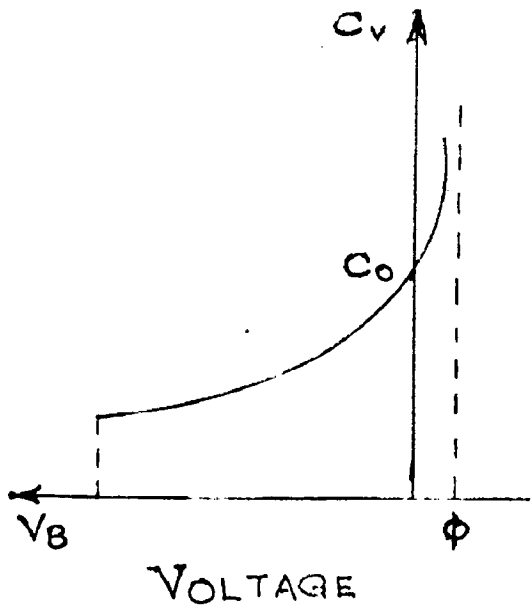
$$\frac{1}{C(V)} = \frac{\partial V}{\partial Q}$$

$$\frac{S}{S_{\max}} = \left(\frac{\phi - V}{\phi - V_B}\right)^\gamma \quad \text{for } V \leq \phi \quad \dots\dots (1.5)$$

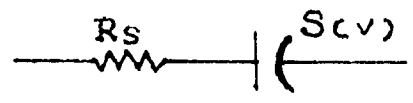
$$\frac{S}{S_{\max}} = 0 \quad \text{for } V \geq \phi \quad \dots\dots (1.6)$$

where V_B is the reverse breakdown voltage

and Q is the stored charge.



(a)



(b)

CAPACITANCE VOLTAGE CURVE

AC EQUIVALENT
CIRCUIT OF A VARACTOR

FIG. 1.5

Equation (1.5) is a good approximation for back biased diodes only.

The agreement is poorer for positive values of bias where the diffusion capacitance is significant.

Equation (1.6) is a good approximation for frequencies where minority carrier lifetime is long compared to r.f. period.

By integrating $S = \frac{\partial V}{\partial q}$ and using equation (1.5), we get

$$\frac{d - v}{d - V_B} = \left(\frac{q_d - q}{q_d - Q_B} \right)^{1/(1-\gamma)} \quad \text{for } v \leq \beta \text{ \& } q \leq q_d \quad \dots (1.7)$$

and

$$v = \beta \quad \text{for } q \geq q_d \quad \dots \dots \quad (1.8)$$

where q_d (positive) is the charge stored at $v = \beta$

and Q_B (negative) is the charge stored at reverse breakdown ($v = V_B$).

Since the conventional varactors are normally operated under reverse bias, by restricting to voltage operation $v \leq \beta$,

Equation (1.7) can be written as

$$\frac{d - v}{d - V_B} = \left(\frac{q_d - q}{q_d - Q_B} \right)^m \quad \dots \dots \quad (1.9)$$

$$\text{where } m = \frac{1}{1-\gamma} \quad \dots \dots \quad (1.10)$$

If the charge is constrained to be a single sinusoid, then

$$q = Q_0 + Q_1 \sin \omega t \quad \dots \dots \quad (1.11)$$

where Q_0 is the average value of the stored charge or bias charge.

Simplifying equation.(1.9) for v , we have

$$v = \beta - \frac{v - V_B}{(Q_1 - Q_0)^n} (Q_1 - q)^n \quad \dots \quad (1.12)$$

$$S_0 \frac{\partial v}{\partial q} = \frac{n(\beta - V_B)(Q_1 - q)^{n-1}}{(Q_1 - Q_0)^n} \quad \dots \quad (1.13)$$

$$S_0 = \left. \frac{\partial v}{\partial q} \right|_{Q_0} = \frac{n(\beta - V_B)(Q_1 - Q_0)^{n-1}}{(Q_1 - Q_0)^n} \quad \dots \quad (1.14)$$

where S_0 is the average value of a.c. elastance.

Combining equations.(1.11), (1.12) and (1.14), we have

$$v = \beta - \frac{S_0(Q_1 - Q_0)}{n} \left[1 - \left(\frac{Q_1}{Q_1 - Q_0} \right) \sin \omega t \right]^n \quad \dots \quad (1.15)$$

Expanding above equation in a binomial series, we have

$$v = \beta - \frac{S_0}{n}(Q_1 - Q_0) \left[1 - n \left(\frac{Q_1}{Q_1 - Q_0} \right) \sin \omega t + \frac{n(n-1)}{2!} \left(\frac{Q_1}{Q_1 - Q_0} \right)^2 \sin^2 \omega t - \frac{n(n-1)(n-2)}{3!} \left(\frac{Q_1}{Q_1 - Q_0} \right)^3 \sin^3 \omega t \dots \right] \quad (1.16)$$

Thus, it is seen from the above analysis that voltages at all harmonic frequencies appear at the output even though the charge is constrained to be a single sinusoid.

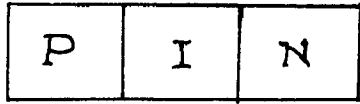
1.52 HARMONIC GENERATION USING STEP RECOVERY DIODES⁽⁹⁾

The step recovery diode is a highly non-linear element in that the forward stored charge results in a low device impedance, while the reverse stored charge gives high impedance. Thus, during a normal drive cycle, the impedance varies as a function of time, depending on the charge. The conductivity variation for this diode during reverse recovery approximates a step function. The transition from reverse storage conduction to cut off can occur in about a nanosecond, and it produces associated discontinuities up to about an ampere and/or a hundredvolts. This step recovery action converts the energy of each input cycle into a narrow, large amplitude, voltage pulse that occurs once per input cycle. An ideal impulse (i.e., a pulse having infinite height, infinitesimal width and unity area) has a frequency spectrum containing all frequencies.

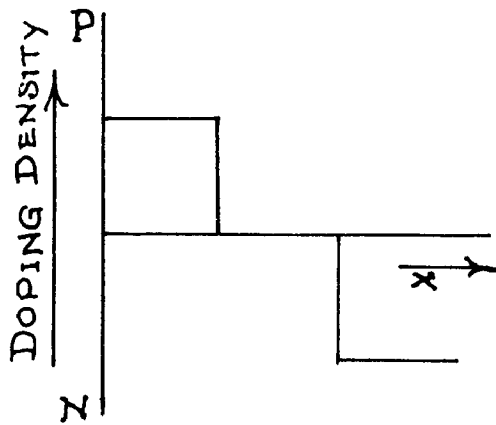
The ideal step recovery diode characteristic is shown in fig. 1.6. Here, because of the intrinsic center region, the capacitance as a function of reverse voltage would be a constant, and the diffusion capacitance in the forward direction is very large. Fig. 1.7(a) and 1.7(b) show the equivalent circuits of a step recovery diode during conduction and depletion ("impulse") intervals.

1.521 IMPULSE GENERATOR CIRCUIT

The impulse generator circuit (Fig.1.8) consists of a voltage generator, a drive inductance, the SRD (the time varying element), a bias battery, and the load. There are two equivalent circuits of the impulse generator; one for the time during which the diode is in its low impedance state, and

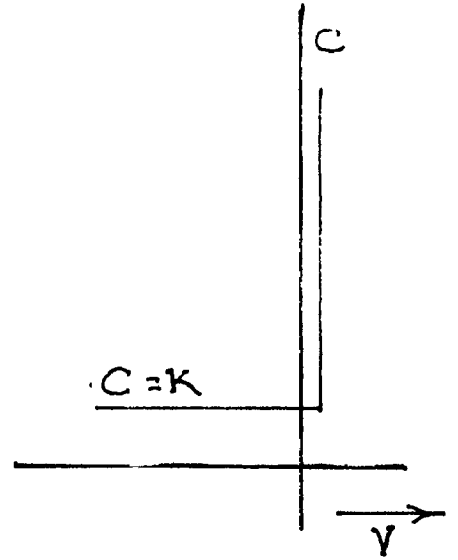


$x \rightarrow$



(a)

DOPING PROFILE



(b)

SRD IDEAL CAPACITANCE

IDEAL STEP RECOVERY DIODES

VOLTAGE CURVE

FIG. 1.6

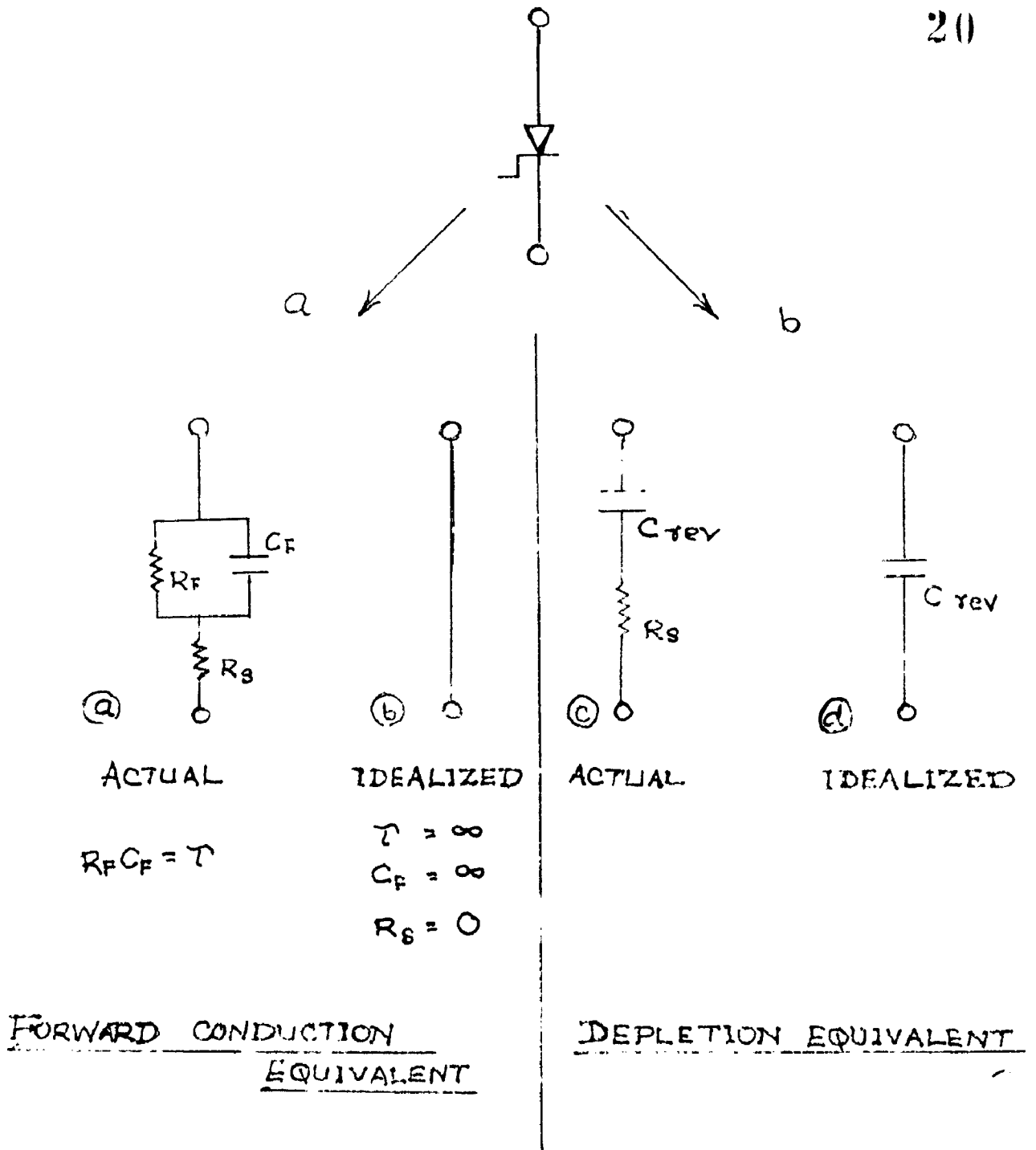


FIG. 1-7.

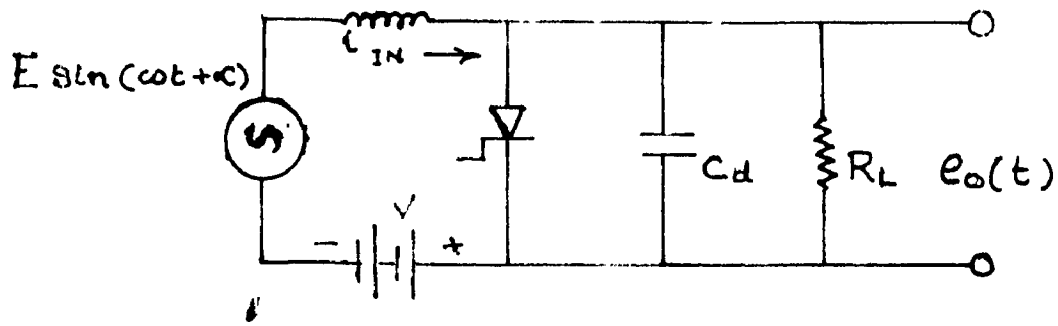
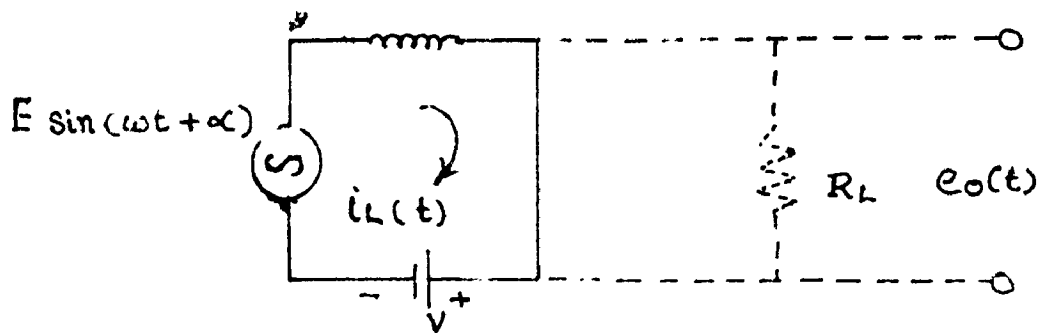
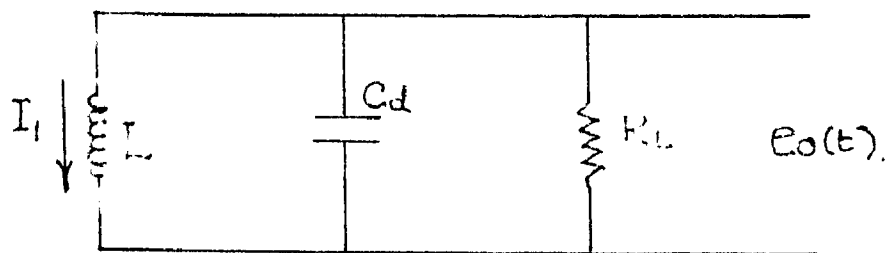
(a) IMPULSE GENERATOR CIRCUIT(b) EQUIVALENT CIRCUIT DURING CONDUCTION INTERVAL(c) EQUIVALENT CIRCUIT DURING IMPULSE INTERVAL

FIG. 1.8

the other for the time when the diode is in its high impedance state. Current and voltage waveforms of the impulse generator are shown in fig. 1.9. The first frame shows the conduction interval; the second, the depletion interval; and the third frame shows the second complete cycle.

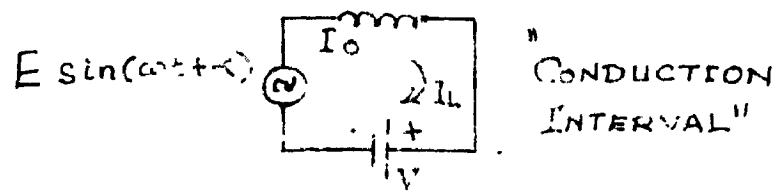
1.5.2 CONDUCTION INTERVAL

During the conduction interval (Fig. 1.9-1st frame), the equivalent circuit (Fig. 1.8 a) is an inductance, a battery, and the generator whose voltage is $E \sin(\omega t + \alpha)$. The input current through the inductance L is

$$i_{IN}(t) = I_0 + \frac{E}{\omega L} \left[\cos \alpha - \cos(\omega t + \alpha) \right] - \frac{(V + \phi) \omega t}{\omega L} \quad \dots (1.17)$$

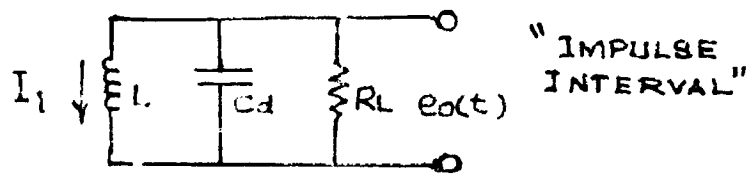
where ϕ is the contact potential of the diode. This current consists of three terms. The first is an initial value, I_0 , the second is a sinusoidal component of current, and the third is a linear ramp term due to the bias battery. This current waveform is shown in fig. 1.9. When the two areas, above and below the $i = 0$ axis, are equal, it can be stated that all the charge stored in the diode during forward current is recovered fully. At the instant this is true, the equivalent circuit will change to the depleted I -layer equivalent, as shown in Fig. 1.8 (b).

The voltage across the diode during the conducting phase will simply be the contact potential of the diode (about 0.7 volts for silicon diodes).



$$i_L = I_0 + \frac{E}{\omega L} \left[\cos(\omega t + \alpha) - \cos(\omega t + \alpha - \phi) \right] - \frac{(V + \phi) \omega t}{\omega L}$$

$\phi = \phi$



$$i_L = I_1 \exp\left(-\frac{\varphi \omega N t}{\sqrt{1-\varphi^2}}\right) \left[\cos \omega N t + \frac{\varphi \sin \omega N t}{\sqrt{1-\varphi^2}} \right]$$

$$e_0(t) = \frac{I_1 \sqrt{\frac{L}{C_d}}}{\sqrt{1-\varphi^2}} \exp\left(-\frac{\varphi \omega N t}{\sqrt{1-\varphi^2}}\right) \sin \omega N t$$

1) $\omega N = \frac{\sqrt{1-\varphi^2}}{\sqrt{L C_d}} \quad \omega = N \omega$

2) $\left. \begin{matrix} I_1' = I_0 \\ I_0' = I_1 \end{matrix} \right\} \begin{matrix} \text{FOR STABLE STEADY} \\ \text{STATE OPERATION} \end{matrix}$

3) $I_1 = I_0 \exp\left(\frac{-\pi \varphi}{\sqrt{1-\varphi^2}}\right)$

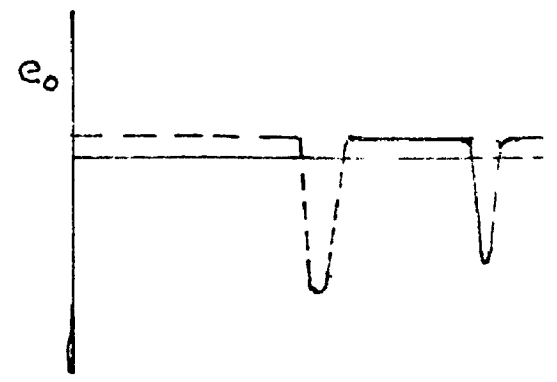
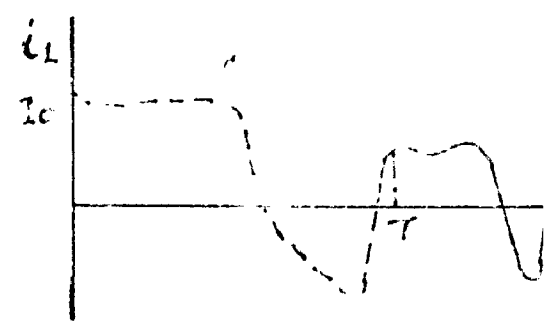
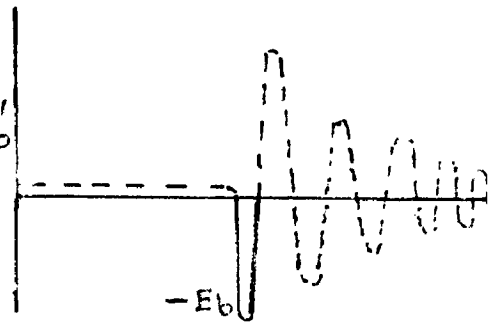
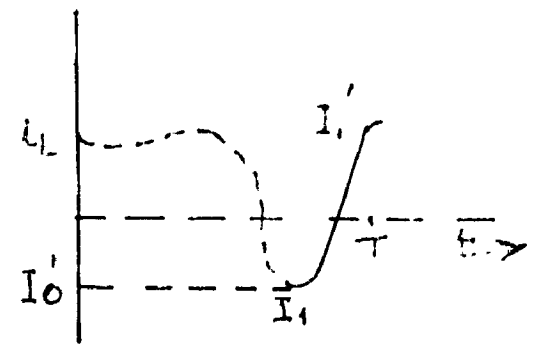
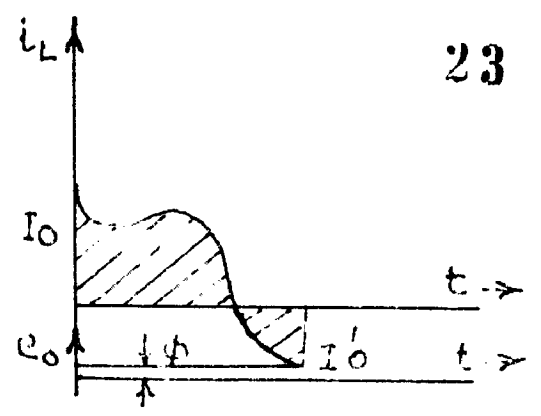


FIG 1.9

IMPULSE GENERATOR CIRCUIT & VOLTAGE WAVEFORMS.

1.5.23 DEPLETION INTERVAL

It is found that by adjusting the bias voltage, V , the stored charge can be returned to zero at the time when the current has its maximum negative value, i.e., $\frac{di}{dt} = 0$. The voltages across the diode and inductor are then both zero. This in turn means that at the beginning of the depletion interval, the instantaneous value of the generator voltage is equal and opposite in sign to the battery voltage, V . Therefore, the generator is neglected during the "impulse" or depletion interval, as shown in Fig. 1.8 (e).

The output voltage, e_o across R_L and the current i_L in the inductor are found from linear circuit analysis with constant parameters R_L , L and C_d .

$$e_o(t) = \frac{I_1 \sqrt{\frac{L}{C_d}}}{\sqrt{1 - \varphi^2}} \exp\left(-\frac{\varphi}{\sqrt{1 - \varphi^2}} \beta t\right) \sin(\beta t) \dots \quad (1.18)$$

where

$$\beta = \sqrt{\frac{1 - \varphi^2}{L C_d}} = \omega_H$$

$$\varphi = \frac{1}{2 R_L} \sqrt{\frac{L}{C_d}} \quad (\text{damping factor})$$

The voltage, e_o appearing across R_L is a half sine pulse, the height of which is limited to the breakdown voltage of the diode, and the width is controlled by R_L , L and C_d . The pulse width t_p , is

$$t_p = \pi \sqrt{\frac{L C_d}{1 - \varphi^2}} = \frac{\pi}{\beta} \dots \dots \quad (1.19)$$

The current i_L in the inductor, L , during the depletion interval is determined by integrating the voltage that appears across it. The integration results in the following expression for the inductor current

$$i_L(t) = I_1 \exp\left(-\frac{\beta t}{\sqrt{1-\phi^2}}\right) \left[\cos \beta t + \phi \frac{\sin \beta t}{\sqrt{1-\phi^2}} \right] \dots \quad (1.20)$$

This current is shown in the second frame of fig. 1.9.

1.524 SPECTRUM OF IMPULSE GENERATOR

The spectral content of the impulse can be found by Fourier analysis.

Assuming that the impulse formed is a perfect half sine pulse of loaded height equal to E_b , the amplitude, C_n , of the voltage in frequency line, n fin is found as follows:

Referring to Fig. 1.10

$$v_o = -E_b \sin \beta t \quad \text{for } t = 0 \text{ to } t = t_p \dots \quad (1.21)$$

$$v_o = 0 \quad \text{for } t = t_p \text{ to } t = 1/f_1 \dots \quad (1.22)$$

The alternate form of Fourier series may be written as

$$V_o = \sum_{n=-\infty}^{\infty} \frac{C_n}{j} \cdot jn \omega t \dots \quad (1.23)$$

The Fourier coefficient C_n is a complex number defined as

$$C_n = a_n - j b_n = \sqrt{a_n^2 + b_n^2} \cdot e^{j\theta_n} \dots \quad (1.24)$$

$$|C_n| = \sqrt{a_n^2 + b_n^2} \quad \text{is the desired amplitude spectrum} \dots \quad (1.25)$$

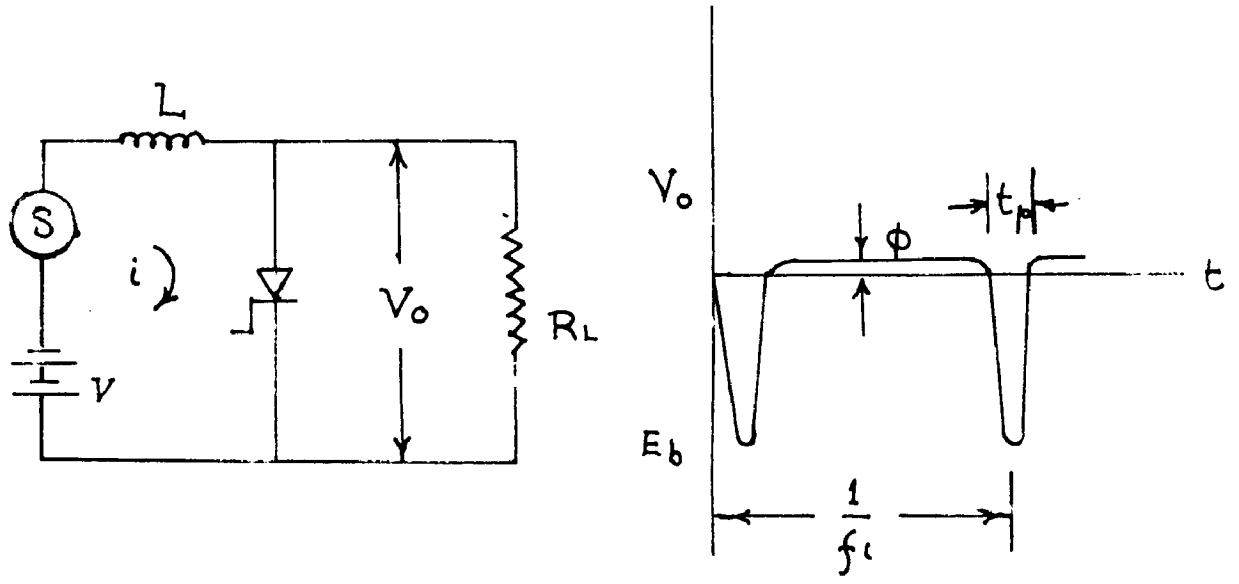


FIG. 1.10

IMPULSE GENERATING OUTPUT VOLTAGE

and $\theta_n = \tan^{-1} \left(\frac{-b_n}{a_n} \right)$ represents phase characteristic .. (1.26)

Now

$$C_n = \frac{2}{T} \int_{t=0}^{t_p} E_b \sin n \omega t \cdot e^{-j \omega n t} dt \dots (1.27)$$

where $T =$ input period $= 1/f_{in}$

$n =$ harmonic of f_{in}

$N = T/t_p$

$t_p =$ pulse width

Integrating (1.27), we have

$$\begin{aligned} C_n \left[1 - \frac{n^2}{N^2} \right] &= \frac{2 E_b}{T N} \left[1 - e^{-j \frac{\pi N}{N}} \cos \pi \right] \\ &= \frac{E_b}{\pi N} \left[1 + e^{-j \frac{\pi N}{N}} \right] = \frac{E_b}{\pi N} \left[1 + \cos \left(\frac{\pi N}{N} \right) - j \sin \left(\frac{\pi N}{N} \right) \right] \end{aligned}$$

Therefore,

$$\begin{aligned} |C_n| &= \frac{E_b}{\pi N \left(1 - \frac{n^2}{N^2} \right)} \cdot \sqrt{\left(1 + \cos \frac{\pi N}{N} \right)^2 + \sin^2 \frac{\pi N}{N}} \\ &= \frac{2 E_b}{\pi N \left(1 - \frac{n^2}{N^2} \right)} \cdot \cos \frac{\pi}{2} \left(\frac{n}{N} \right) \end{aligned}$$

or

$$|C_n| = \frac{C_0 \cos \frac{\pi}{N} \left(\frac{n}{N} \right)}{1 - \left(\frac{n}{N} \right)^2} \quad \begin{array}{l} \text{is the desired amplitude} \\ \text{spectrum} \quad \dots \quad (1.29) \end{array}$$

where

$$C_0 = \frac{2 E_p}{\pi N}$$

A plot of $\frac{|C_n|}{C_0}$ (the Fourier amplitude coefficients) is shown in fig. 1.11.

The Fourier integral, which is the envelope of the lines shown, has its first zero at 3π rad. The "flatness" of the line spectrum between any two arbitrary lines is determined by the pulse width. Narrower the pulse, the higher is the first "zero crossing". In the limit, if it were physically possible, zero pulse width would correspond to a flat amplitude line spectrum to $f = \infty$.

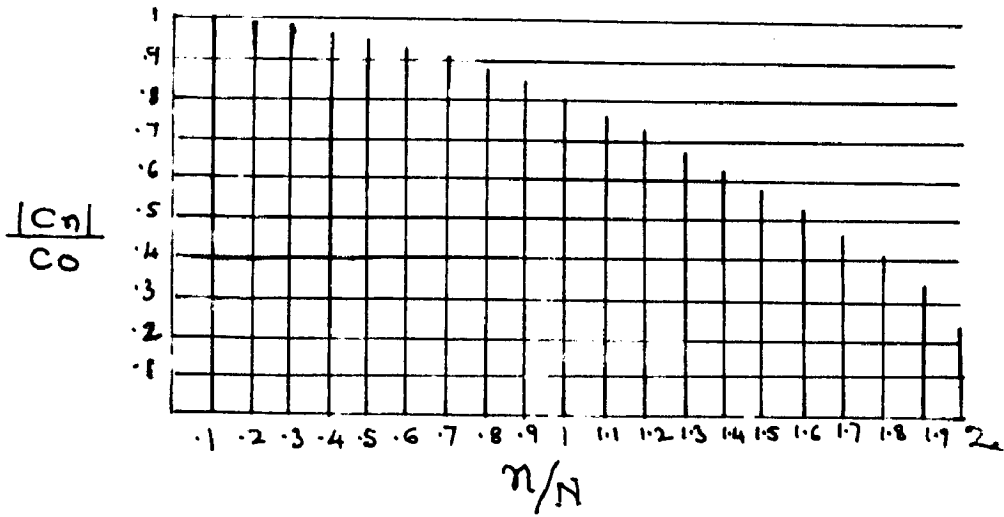


FIG. 1.11

FOURIER AMPLITUDE COEFFICIENTS
FOR IMPULSE WAVE FORMS

CHAPTER IIVARACTOR MULTIPLIERS2.1 INTRODUCTION

Microwave solid state sources assure high reliability, even under the severe conditions encountered in space and missile programs. Because of their rugged construction, low-power consumption, light weight and small size, varactor multipliers are ideally suited for this type of requirements. Typical power outputs of the order of several watts in L band and several hundreds of milliwatts at X-band are feasible by using present varactor and step recovery diode multiplier technology. For efficient higher order frequency multiplication with varactor chains, several idler circuits are essential. These idler circuits, however present some difficult problems when considering broadband applications. If the idlers have a high Q, the efficiency would be good but the bandwidth is limited to one or two percent. When the Q is lowered to facilitate a broader bandwidth, the efficiency drops because of the idler losses. However, step recovery diodes being rich in high order harmonics, multiply to the hundredth order with efficiencies better than 1/n without idlers. The resulting circuit simplicity from omitting these idlers leads to an ease of and freedom from parametric oscillations and spurious frequencies.

2.2 LARGE-SIGNAL ANALYSIS OF NARROW BAND VARACTOR HARMONIC GENERATORS
WITH AND WITHOUT IDLERS ^{(10), (11)}

In varactor harmonic generators, two distinct modes of operation are possible. In one case only the fundamental and the desired harmonic frequency currents

are allowed to flow in the varactor, while in the second case other selected harmonic current also flow. The latter are known as idling currents or simply 'idlers'. The efficiencies obtainable using idlers are higher than the corresponding efficiencies without idlers, this increase in efficiency being obtained at the expense of increased circuit complexity.

2.21 VARACTOR CAPACITANCE-VOLTAGE RELATIONSHIP

The nonlinear capacitance-voltage law of the varactor is described by an equation of the type

$$C(v) = \frac{C_0}{\left(1 - \frac{v}{\beta}\right)^\gamma} \quad \dots \quad (2.1)$$

where v is the applied voltage

and β is the contact potential of the junction.

At reverse breakdown voltage V_B

$$C(v) = C_{VB}$$

Letting $V_0 = \beta - V_B$, we find

$$C(v) = C_{VB} \left(\frac{V_0}{\beta - v}\right)^\gamma \quad \dots \quad (2.2)$$

now

$$\begin{aligned} Q &= \int C(v) dv \\ &= \frac{C_{VB} V_0^\gamma}{1 - \gamma} (\beta - v)^{1-\gamma} + K \end{aligned}$$

When $v = V$, the voltage across the junction is zero and therefore the charge is also zero, which gives $k = 0$, so that

$$Q = -\frac{CV_B V_0^\gamma}{(1-\gamma)} (\beta - v)^{1-\gamma} \dots (2.3)$$

The charge at the reverse breakdown voltage, Q_B is given by

$$Q_B = -\frac{CV_B V_0}{(1-\gamma)} \dots (2.4)$$

Rearranging and letting

$$m = \frac{1}{1-\gamma}$$

gives

$$V - V_B = V_0 \left[1 - \left(\lambda + \frac{Q - Q_B}{Q_B} \right)^m \right] \dots (2.5)$$

m takes values from 1.5 to 3.0 depending on the doping.

2.18 NARROW BAND VARACTOR MULTIPLIERS WITHOUT IDEAS

The circuit to be analysed is shown in fig. 2.1. Filters F_1 and F_2 are such that the current at the fundamental frequency ω can only flow in the input circuit, and only that current at frequency 2ω can flow in the output circuit. L_1 and L_2 are tuning inductances for fundamental and output frequencies, respectively.

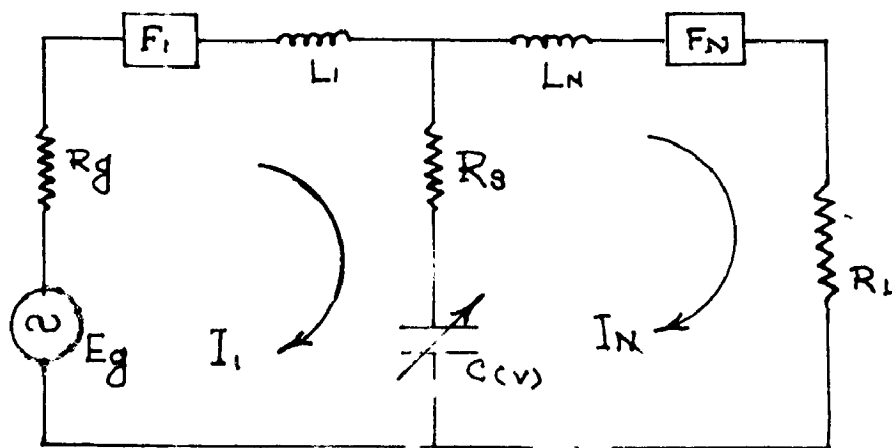


FIG. 2.1.

CIRCUIT OF VARACTOR HARMONIC
GENERATORS WITHOUT IDLERS

Let the charge on the varactor at the fundamental frequency, Q_1 , be given by

$$Q_1 = q_1 \cos \omega t$$

So that

$$I_1 = \omega q_1 \sin \omega t$$

Similarly, for output circuit,

$$Q_N = q_N \cos (N \omega t + \theta)$$

$$\text{and } I_N = i_N \sin (N \omega t + \theta)$$

where θ is the initial phase angle between I_1 and I_N .

For maximum charge swing, the alternating charge components must swing about $Q_0/2$, thus

$$Q = \frac{Q_0}{2} + Q_1 - Q_N$$

hence, from equation (2.5),

$$v - V_D = V_0 \left[1 - \left(\frac{Q_1 - Q_N + \frac{Q_0}{2}}{Q_0} \right) \right]^n$$

$$= V_0 \left[1 - \frac{1}{2^n} \left\{ 1 + \frac{q_1 \cos \omega t}{Q_0/2} - \frac{q_N \cos (N \omega t + \theta)}{Q_0/2} \right\} \right]^n \dots (2.6)$$

Expanding this expression as a Fourier series, we have

$$v - V_2 = \frac{V_0}{2^n} a_0 + \sum_{n=1}^{\infty} (a_n \cos n \omega t + b_n \sin n \omega t) \dots (2.7)$$

where a and b are given by

$$a_n = -\frac{1}{\pi} \int_{-\pi}^{\pi} \left[1 + \frac{q_1}{Q_0/2} \cos \omega t - \frac{q_2}{Q_0/2} \cos (N \omega t + \theta) \right]^n \cos n \omega t d(\omega t) \dots (2.8)$$

$$b_n = -\frac{1}{\pi} \int_{-\pi}^{\pi} \left[1 + \frac{q_1}{Q_0/2} \cos \omega t - \frac{q_2}{Q_0/2} \cos (N \omega t + \theta) \right]^n \sin n \omega t d(\omega t) \dots (2.9)$$

Writing the circuit equations, we find

$$\begin{aligned} E_g \sin (\omega t + \alpha) &= i_1 (R_g + R_2) \sin \omega t + i_1 L_1 \omega \cos \omega t \\ &+ \frac{V_0}{2^n} a_1 \cos \omega t + \frac{V_0}{2^n} b_1 \sin \omega t \dots (2.10) \end{aligned}$$

and

$$\begin{aligned} \frac{V_0}{2^n} a_N \cos N \omega t + \frac{V_0}{2^n} b_N \sin N \omega t \\ = i_N (R_L + R_2) \sin (N \omega t + \theta) + i_N L_N N \omega \cos (N \omega t + \theta) \end{aligned} \dots (2.11)$$

2.22 CALCULATION OF EFFICIENCY

It will be assumed that maximum efficiency occurs when both input and output circuits are resonant at the fundamental and harmonic frequencies, respectively. Resonance in the input circuit is defined (at a particular drive level) as the condition in which the (nonlinear) input impedance is purely real. Equation (2.10) then gives

$$\alpha = 0 \quad L_1 = -\frac{V_0 a_1}{z^n \omega i_1} \quad \dots \quad (2.12)$$

$$E_g = i_1 (R_g + R_p) + \frac{V_0 b_1}{z^n} \quad \dots \quad (2.13)$$

For resonance in the output circuit, the desirable condition is that the maximum possible power should be developed in the load resistance, for a given value of the peak voltage appearing across the varactor. The peak voltage for a given value of E_g is a function of the phase angle of the output charge. Since the problem is essentially nonlinear, no direct method exists for determining the optimum phase condition in the output circuit. However, if a "linearized" resonance condition, as described below is used, results which differ by only a small amount from the true optima can be found.

The "linearized" resonance condition consists in assuming that the inductance in the output circuit is chosen to resonate with some "effective" capacitance, which is a function of the drive level, at the output frequency.

The voltage given by $(a_n \cos N\omega t + b_n \sin N\omega t)$ is composed of two parts, one a function of q_n and one independent of q_n . The portion independent

of e_N may be regarded as a constant voltage generator as far as the N^{th} harmonic is concerned, and the remainder represents the voltage across a nonlinear impedance. If the portion independent of e_N is $(K_N \cos N\omega t + I_N \sin N\omega t)$, then "linearized" resonance occurs when the N^{th} harmonic current is in phase with this voltage. This arrangement is shown for the output circuit in fig. 2.2.

Now

$$K_N = \frac{1}{\pi} \int_{-\pi}^{\pi} \left(1 + \frac{Q_1}{Q_0/2} \cos \omega t \right)^n \cos N\omega t \, d(\omega t) \quad \dots \quad (2.14)$$

$$I_N = \frac{1}{\pi} \int_{-\pi}^{\pi} \left(1 + \frac{Q_1}{Q_0/2} \cos \omega t \right)^n \sin N\omega t \, d(\omega t) \quad \dots \quad (2.15)$$

since $\left(1 + \frac{Q_1}{Q_0/2} \right)^n$ is an even function of ωt , I_N is zero.

Equation (2.10) for the output circuit can now be written as

$$\begin{aligned} \frac{V_0}{2^n} K_N \cos N\omega t &= -\frac{V_0}{2^n} (a_N - K_N) \cos N\omega t \\ &- \frac{V_0}{2^n} b_N \sin N\omega t + i_N L_N N\omega \cos (N\omega t + \theta) \\ &+ i_N (R_L + R_p) \sin (N\omega t + \theta) \end{aligned}$$

Now, since K_N is independent of I_N , we require for resonance, that I_N have the same phase as $\frac{V_0}{2^n} K_N \cos N\omega t$, which gives $\theta = \pm \frac{\pi}{2}$ and

$$\pm I_N N\omega L_N = \frac{V_0 b_N}{2^n}$$

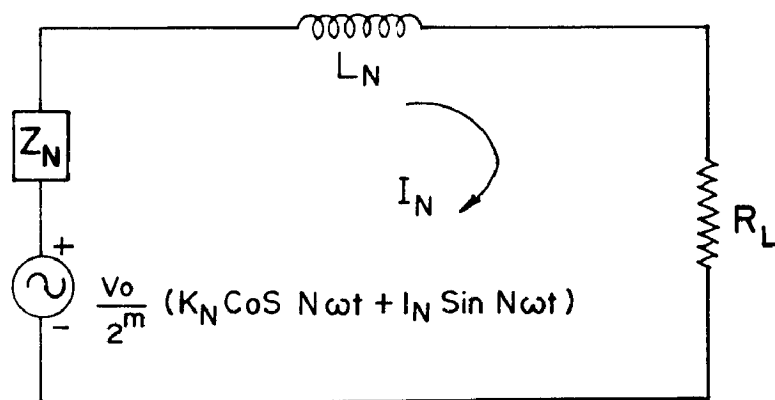


FIG. 2·2 EQUIVALENT OUTPUT CIRCUIT

From equation (2.14), it is clear that K_N is negative, if N is even and k_N is positive when N is odd.

At resonance,

$$\frac{V_0}{2^n} k_N \cos^2 N \omega t = - \frac{V_0}{2^n} (a_N - k_N) \cos N \omega t$$

$$\ddagger \quad i_N (R_L + R_g) \cos N \omega t$$

If k_N is negative, the negative sign applies in the last term, so that

$$\theta = -\pi/2$$

and

$$L_N = \frac{V_0 b_N}{2^n N \omega i_N}$$

now

$$i_N = \frac{V_0 a_N}{2^n (R_L + R_g)} \dots \dots (2.16)$$

Defining efficiency as

$$\eta = \frac{\text{Output power}}{\text{Available power from source}}$$

We have

$$\text{Output power} = \frac{i_N^2 R_L}{2} = \frac{V_0^2 a_N^2}{2^{2n} (R_L + R_g)^2} \cdot \frac{R_L}{2}$$

$$\text{Available power from the source} = E_g^2 / 8 R_g$$

So

$$\eta = \frac{4 R_g R_L V_o^2 a_N^2}{2^{2m} (R_L + R_g)^2 \left\{ i_1 (R_g + R_g) + \frac{V_o b_1}{2^m} \right\}^2}$$

Optimising efficiency with respect to R_g , gives

$$R_g = R_g + \frac{V_o b_1}{2^m i_1} \dots \dots \dots (2.17)$$

so that

$$\eta = \frac{V_o^2 a_N^2}{2^{2m} i_1^2} \cdot \frac{R_L}{R_L + R_g} \cdot \frac{1}{R_g + \frac{V_o b_1}{2^m i_1}} \dots \dots (2.18)$$

Introducing the following normalizations

$$\frac{2 q_1}{Q_B} = P_1$$

$$\frac{2 q_N}{Q_B} = P_N$$

$$\frac{R_L}{R_g} = \bar{R}_L$$

$$\frac{R_g}{R_g} = \bar{R}_g$$

and $Q_F = \frac{1}{R_g C_{VBL} \omega}$ (fundamental frequency Q factor of the diode at the reverse breakdown voltage)

Substituting these in eqn. (2.18) and using eqn. (2.4)

$$\eta = \frac{a_N^2 Q_F^2 \bar{R}_L}{2^{m-1} P_1^m (1 + \bar{R}_L)^2 (2^{m-1} P_1^m + Q_F b_1)} \dots (2.19)$$

2.24 ABRUPT - JUNCTION CASE

Substituting $m = 2$ in the expression for $v - V_B$, we have

$$v - V_B = V_0 \left[1 - \frac{1}{2^2} \left(1 + \frac{q_1 \cos \omega t}{Q_B/2} - \frac{q_N \cos (N \omega t + \theta)}{Q_B/2} \right)^2 \right]$$

or

$$\frac{v - V_B}{V_0} = 1 - \frac{1}{2^2} \left[\left(1 + \frac{q_1 \cos \omega t}{Q_B/2} \right)^2 + \left(\frac{q_N \cos (N \omega t + \theta)}{Q_B/2} \right)^2 - 2 \left(1 + \frac{q_1 \cos \omega t}{Q_B/2} \right) \left(\frac{q_N \cos (N \omega t + \theta)}{Q_B/2} \right) \right] \dots (2.20)$$

From Eqn. (2.20) it is obvious that in the case of an abrupt junction diode there will be no output at frequencies other than the second harmonic.

2.25 NARROW BAND VARACTOR MULTIPLIERS WITH IDLERS^{(11), (15)}

Fig. 2.3 shows the equivalent circuit of a harmonic generator with idlers. The filters are such that the i^{th} filter allows current only at the i^{th} harmonic to flow.

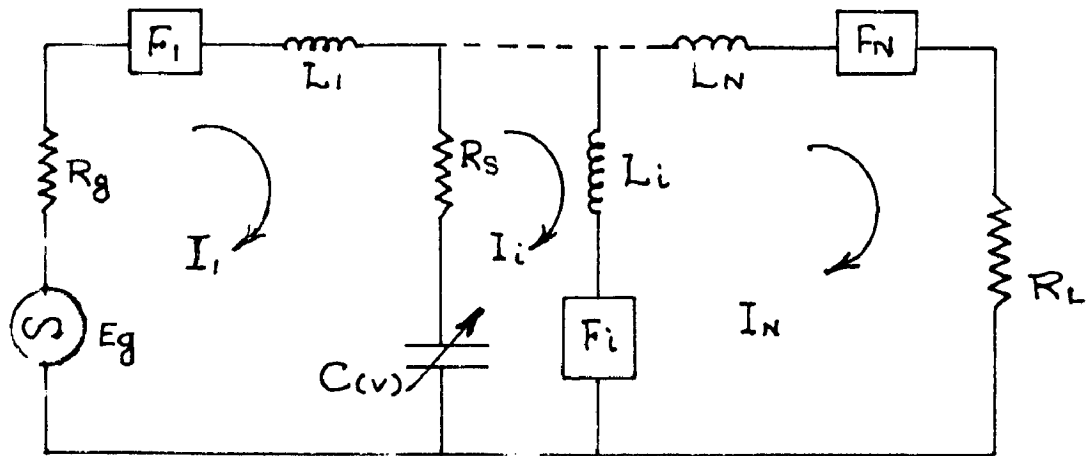


FIG. 2.3.

CIRCUIT OF A VARACTOR HARMONIC
GENERATORS WITH IDLERS.

Let the mean charge on the diode be Q_D and the i^{th} harmonic charge

$$q_i = q_i \cos (i \omega t + \theta_i)$$

So that

$$I_i = -i \omega q_i \sin (i \omega t + \theta_i) = I_i \sin (i \omega t + \theta_i)$$

Equation (2.5) then gives

$$v - V_D = V_0 \left[1 - \frac{1}{2^n} \left(\frac{Q_D}{Q_D/2} + \frac{q_1 \cos \omega t}{Q_D/2} - \sum \frac{q_i \cos (i \omega t + \theta_i)}{Q_D/2} \right)^n \right] \dots \dots (2.21)$$

where the summation is taken over all harmonic currents which are allowed to flow, including the output frequency. Expanding this expression as a Fourier series, we have

$$v - V_D = \frac{V_0}{2^n} \left[a_0 + \sum_{n=1}^{\infty} (a_n \cos n \omega t + b_n \sin n \omega t) \right] \dots (2.22)$$

a_n and b_n are given by

$$a_n = -\frac{1}{\pi} \int_{-\pi}^{\pi} \left[\frac{Q_D}{Q_D/2} + \frac{q_1 \cos \omega t}{Q_D/2} - \sum \frac{q_i \cos (i \omega t + \theta_i)}{Q_D/2} \right]^n \cos n \omega t d(\omega t) \dots \dots (2.23)$$

and

$$b_n = -\frac{1}{\pi} \int_{-\pi}^{\pi} \left[\frac{Q_D}{Q_D/2} + \frac{q_1 \cos \omega t}{Q_D/2} - \sum \frac{q_i \cos (i \omega t + \theta_i)}{Q_D/2} \right]^n \sin n \omega t d(\omega t) \dots \dots (2.24)$$

Writing the circuit equations, we find

$$E_g \sin(\omega t + \alpha) = i_1 (R_g + R_p) \sin \omega t + L_1 \omega i_1 \cos \omega t \\ + \frac{V_0}{2^n} a_1 \cos \omega t + \frac{V_0}{2^n} b_1 \sin \omega t \quad \dots \quad (2.25)$$

$$\frac{V_0}{2^n} (a_n \cos N \omega t + b_n \sin N \omega t) = i_n (R_L + R_p) \sin(N \omega t + \theta_n) \\ + i_n L_n N \omega \cos(N \omega t + \theta_n)$$

and at idler frequency

$$\frac{V_0}{2^n} (a_1 \cos i \omega t + b_1 \sin i \omega t) = i_1 R_p \sin(i \omega t + \theta_1) \\ + i_1 L_1 i \omega \cos(i \omega t + \theta_1) \quad \dots \quad (2.26)$$

Resonating the input circuit for maximum efficiency requires

$$L_1 = - \frac{V_0 a_1}{2^n \omega i_1}$$

So that

$$E_g = i_1 (R_g + R_p) + \frac{V_0 b_1}{2^n} \quad \dots \quad (2.27)$$

Introducing the following normalizations

$$\bar{E}_g = \frac{2^n E_g}{V_0}$$

$$\bar{R}_g = \frac{R_g}{R_p}$$

$$\bar{R}_L = \frac{R_L}{R_g}$$

$$Q_T = \frac{1}{R_g C_{VB} \omega}$$

$$P_1 = \frac{Q_1}{Q_B/2}$$

$$P_H = \frac{Q_H}{Q_B/2}$$

$$P_1 = \frac{Q_1}{Q_B/2}$$

Eqn. (2.27) becomes

$$\bar{E}_g = P_1 \left(1 + \bar{R}_g \right) \frac{n 2^{n-1}}{Q_T} + b_1 \quad \dots \quad (2.28)$$

Now, for optimum power transfer, at a given power level, from the generator to the varactor, the generator resistance should be made equal to the (non-linear) input impedance at the particular drive level. Therefore, from equation (2.28)

$$\bar{R}_g = 1 + \frac{Q_T b_1}{n 2^{n-1} P_1} \quad \dots \quad (2.29)$$

and equation (2.28) becomes

$$\bar{E}_g = \frac{n 2^n}{Q_T} P_1 \left(1 + \frac{Q_T b_1}{n 2^{n-1} P_1} \right) \quad \dots \quad (2.30)$$

using the normalization given above, equations (2.25) and (2.26) become

$$\frac{1}{n 2^{n-1}} (a_n \cos n \omega t + b_n \sin n \omega t) = \frac{n P_n}{Q_f} (R_L + 1) \sin (n \omega t + \theta_n) \\ + \frac{L_n n^2 \omega}{Q_f R_n} P_n \cos (n \omega t + \theta_n) \dots \dots \dots (2.31)$$

and

$$\frac{1}{n 2^{n-1}} (a_1 \cos 1 \omega t + b_1 \sin 1 \omega t) = \frac{1 P_1}{Q_f} \sin (1 \omega t + \theta_1) \\ + \frac{L_1 1^2 \omega}{Q_f R_n} P_1 \cos (1 \omega t + \theta_1) \dots \dots \dots (2.32)$$

Rearranging eqn. (2.32) gives

$$P_1 = \frac{Q_f}{1 n 2^{n-1}} (a_1 \sin \theta_1 + b_1 \cos \theta_1) \dots \dots \dots (2.33)$$

$$\frac{L_1 1 \omega}{R_n} = \frac{Q_f}{1 n 2^{n-1} P_1} (a_1 \cos \theta_1 - b_1 \sin \theta_1) \dots \dots \dots (2.34)$$

The power in the load is $\frac{1_n^2 R_L}{2}$, and, defining the efficiency as the

ratio of the power in the load to the available power from the source

($\frac{E_g^2}{8 R_g}$), we have

$$\eta = \frac{1_n^2 R_L / 2}{E_g^2 / 8 R_g}$$

But since it is assumed that the input is matched

$$E_G = 2 I_1 R_G$$

and
$$\eta = \frac{I_H^2 R_L}{I_1^2 R_G}$$

$$= \frac{P_H^2 \bar{R}_L}{P_1^2 \bar{R}_G}$$

From eqn. (2.21) this becomes

$$\eta = \frac{\left(\frac{Q_T}{m^2 - 1}\right)^2 (a_H \sin \theta_H + b_H \cos \theta_H)^2 \bar{R}_L}{P_1^2 (1 + \bar{R}_L)^2 \bar{R}_G}$$

Substituting the matched value for \bar{R}_G from equation (2.29)

$$\eta = \frac{\left(\frac{Q_T}{m^2 - 1}\right)^2 (a_H \sin \theta_H + b_H \cos \theta_H)^2 \bar{R}_L}{P_1 (1 + \bar{R}_L)^2 \left(1 + \frac{Q_T b_1}{m^2 - 1} P_1\right)} \dots (2.35)$$

Expressions for efficiency given in equations (2.19) and (2.35) can be solved for special cases of abrupt and graded junctions. η vs P_1 and η vs f/f_0 plots for the cases with and without idlers are given in references (10) and (11), respectively. From the above given plots, it is found that an abrupt junction varactor with a second harmonic idler is most efficient for tripler or quadrupler. This is because the essential doubling

action is most efficient with an abrupt junction. An increase in efficiency from 15% to 44% is obtained in the case of a graded junction tripler, using 2nd harmonic idler, while an abrupt junction tripler with optimum load and second harmonic idler yields 87% efficiency.

2.3 BROAD BAND FREQUENCY MULTIPLIERS

Most varactor multiplier chains are narrow band. Resonant circuits of limited bandwidth are used as input and output circuits for individual stages. Although individual stages can be built with moderate bandwidths; however, when a number of multipliers are cascaded, the resultant chains have usually very narrowband.

Present varactor and SSB multiplier technology provides instantaneous bandwidths of the order of 10% to 30% with fully stable output power with respect to VSWR and temperature variations. Large number of low noise multipliers have been built with 5 to 10% bandwidths, 60 to 80 db harmonic spurious rejection, and complete freedom from spurious oscillation over 3:1 VSWR.

The usual approach to increase the tuning range is to replace the simple input and output tuned circuits of each harmonic generator by more complex matching networks, thus increasing their individual bandwidths and hence bandwidth of the chain.

The block schematic of a basic broadband harmonic generator is shown in fig.2.4. The networks N_1 , N_2 and N_3 are linear and passive. N_1 matches the diode to the source at the input frequency, and N_2 , the load to the diode at the output frequency. N_3 enables any desired 'idler frequency' currents to flow through the diode. For example in simplest tripler circuit;

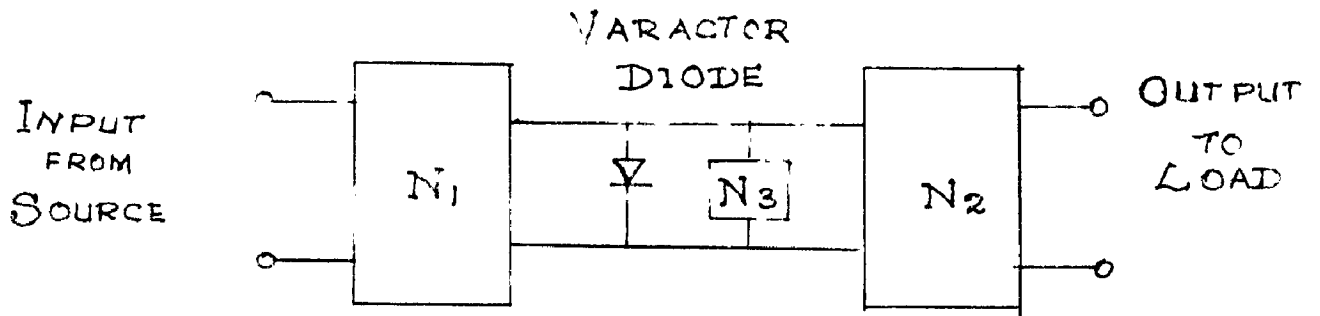


FIG. 2.4.

A BROAD BAND HARMONIC GENERATOR.

N_1 , N_2 and N_3 each consist of a capacitor and an inductor, which together with the diode are in series resonance at the input frequency, the third harmonic and the second harmonic respectively. To maximise the conversion efficiency, actual circuits tend to be more complex. Firstly there is an obvious necessity of resistively matching the circuit to both source and load. Secondly, the flow of input and idler frequency currents in the load and of the output and idler frequency currents in the source, must be prevented.

2.34 BANDWIDTH LIMITATIONS IN MULTIPLIERS

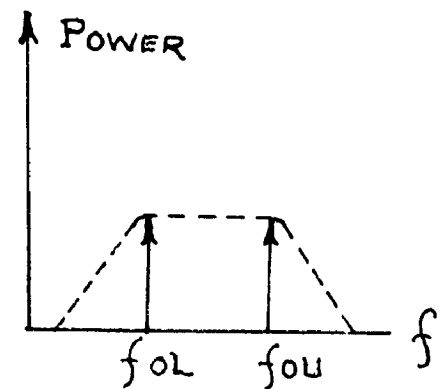
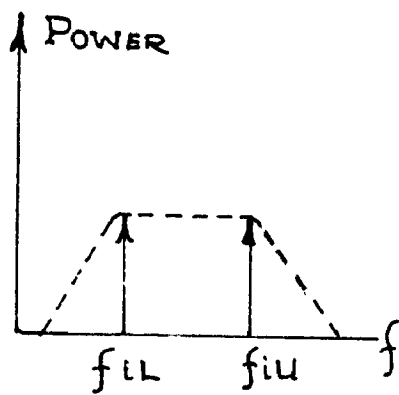
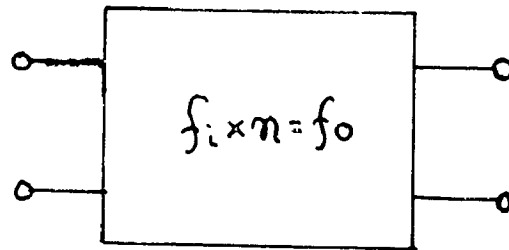
It is generally considered possible to construct chains of harmonic generators given flat output response ($\pm \frac{1}{2}$ db) over a 10% frequency range at S band and over 5% range at X-band by using relatively simple circuits for the networks N_1 , N_2 and N_3 of each harmonic generator. For achieving wider bandwidths, the proper synthesis techniques, based on the analysis of Bode⁽¹²⁾ and Fano⁽¹³⁾ are necessary. Such techniques have already been applied to the related matching problems encountered in parametric amplifiers⁽¹⁴⁾ and frequency converters⁽¹⁵⁾, for which fundamental bandwidth limitations have been determined. These limitations are determined in the same way for harmonic generators.

The bandwidth of a n -times multiplier is limited, fundamentally, by the requirement that no more than one harmonic should appear at the output simultaneously. Referring to fig. 2.5, the limiting bandwidth is

$$\Delta f \leq \frac{f_{oL}}{n} = f_{iL} \quad \dots \quad (2.36)$$

where, f_{oL} is the lower limit of output frequency.

f_{iL} is the lower limit of input frequency.



SINGLE FREQUENCY CONDITION

$$\underline{\text{BW OUTPUT} < \frac{f_{oL}}{n}}$$

FIG. 2.5

BAND WIDTH LIMITATIONS IN MULTIPLIERS

Equation (2.36) concludes that tripler or higher order multipliers would not be suitable for wider bandwidths. This arises because an increase in bandwidth results in networks N_1 , N_2 and N_3 , interfering with each other. The calculations show that, the doubler is limited to a maximum bandwidth of 40%, tripler to an approximately 29% and quadrupler to 22% and so on. These, however are the limitations imposed by the circuits used, whereas of more fundamental importance are those imposed by the diodes itself. These are associated with stray reactances of the diode encapsulation.

Considering the case of a doubler in which networks N_1 and N_2 need be considered. The optimum operating conditions are determined when the input and output reflections coefficients (and thus mismatch losses) take a constant minimum value over the desired band of frequencies, with complete rejection outside that band.

Bode⁽¹²⁾ has shown that in matching into an amplifier of input resistance R shunted by a capacitance C , for a constant reflection coefficient ρ over a bandwidth b Hz/Sec., the minimum value that ρ can take is given by

$$\rho = \exp(-\pi / bRC) \quad \dots \quad (2.37)$$

The input resistance R_1 for the diode in a harmonic generator circuit can be computed. R_1 is a function of both frequency and drive level, however, under conditions of constant ρ , the resultant variation is small, so that to a first approximation R_1 is constant. Using this value of R_1 , the diode capacitance at its optimum bias voltage and the midband input operating frequency of the harmonic generator, it is possible to calculate the quality factor Q_1 of the input circuit of harmonic generator. Thus equation (2.36)

becomes

$$\rho_{IN} = \exp(-\pi/BQ_1) \dots \quad (2.20)$$

where B is the fractional bandwidth of the system. The output reflection coefficient ρ_{OUT} can be calculated similarly, so that the variation with bandwidth of the total mismatch losses is known in fig. 2.6.

The total losses in a harmonic generator result from the series resistance of the varactor diode, the matching element, and the input and output mismatches. Since the former losses have little variation over the frequency band of interest, fig. 2.6 can be used to show the trade-off between conversion efficiency and bandwidth of a broadband harmonic generator.

The real problem in broad banding lies in the actual synthesis of suitable circuits and in particular of preventing or taking into account interaction between the input and output networks N_1 and N_2 . One method of avoiding this interaction is the separate odd and even harmonic components of the waveforms by means of a balanced circuit⁽¹⁶⁾. Although balanced doublers and triplers of this type have been used to obtain moderate bandwidths (10%), no attempts are known in which proper synthesis techniques have been applied in order to obtain wider bandwidths.

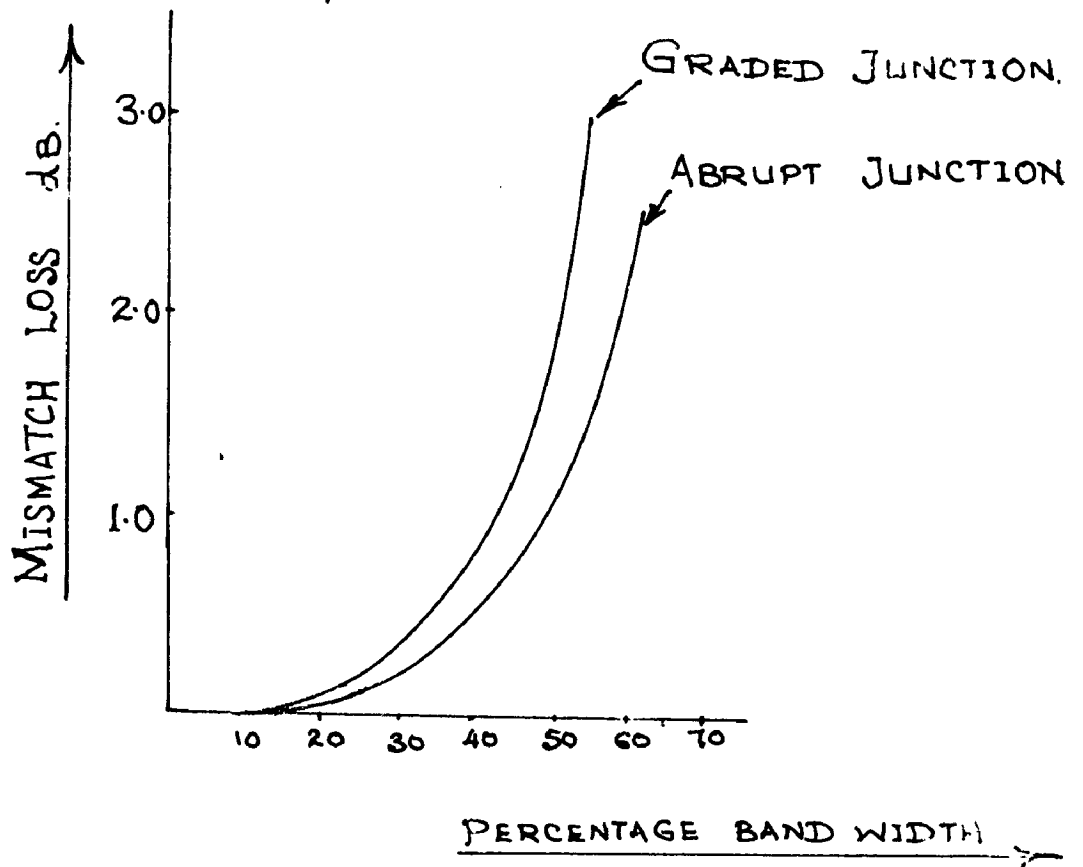


FIG. 2.6

MINIMUM MISMATCH LOSS FOR A.
BROAD BAND DOUBLER.

CHAPTER IIIDESIGN OF COMPONENTS FOR A BROAD BAND MULTIPLIER3.1 INTRODUCTION

This chapter describes the design of components for a broad band frequency quadrupler, the block diagram of which is given in fig. 3.1. The band pass filter used as an output frequency selecting circuit is of the interdigital type centred at about 1.84 GHz. The input low pass filter is designed for a cut off frequency of 600 MHz to allow only the fundamental frequency to pass through and to provide isolation between the source and the diode harmonic generator. Input matching to the step recovery diode is of lumped element Π -type (two-sections) network, whereas for output matching, a two-section quarter-wave transformer is used.

3.2 GENERAL PRINCIPLES OF MULTIPLIER CIRCUIT DESIGN

A satisfactory multiplier circuit should fulfill the following requirements.

1. It should reject unwanted frequencies and thus establish separate current paths for the desired frequencies.
2. It should match the source and the load impedance with the varactor input and output impedances, respectively.
3. It should provide a mechanical structure necessary to dissipate heat, which is internally generated under a specified environment.

Fig. 3.2 shows the schematic of a lumped circuit multiplier. Filters are resonant circuits adjacent to the varactor, separate different frequencies and permit impedance matching with little interaction. However, as the frequency increases both the electrical length of the interconnections and

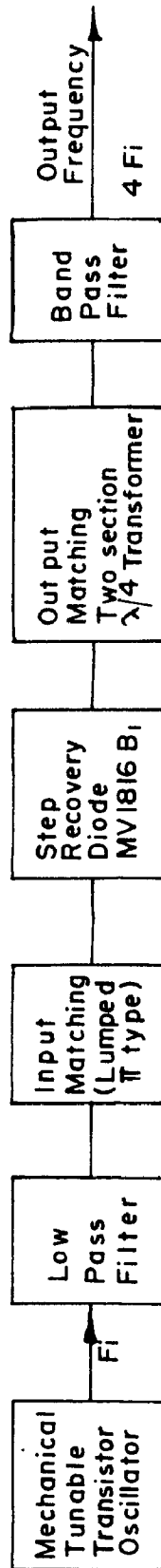


FIG.3-1 BLOCK DIAGRAM OF A BROADBAND FREQUENCY QUADRUPLER

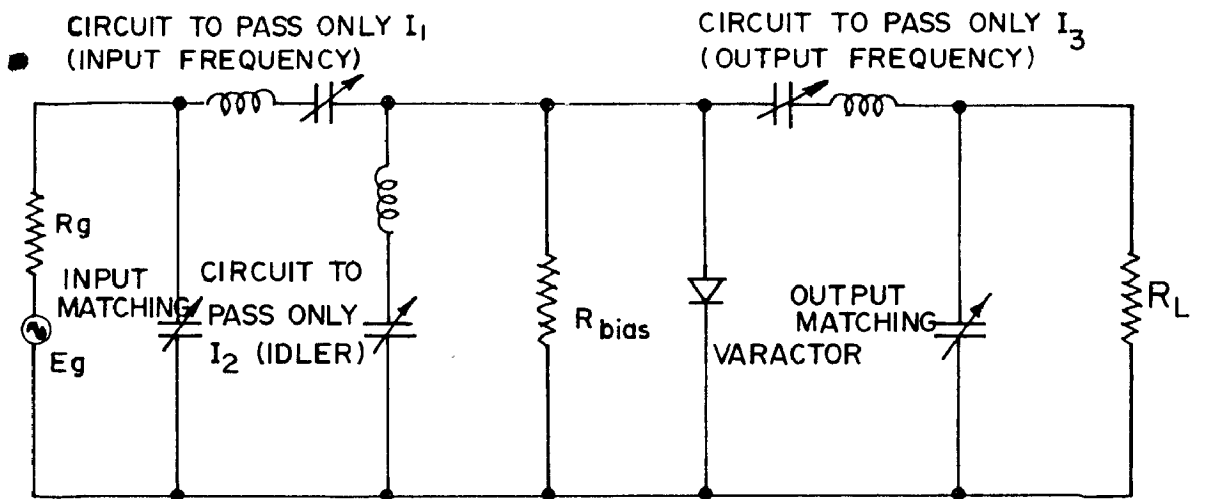


FIG.3-2 SCHEMATIC OF LUMPED CIRCUIT MULTIPLIER

the effects of the varactor parasitic reactances increases. These factors make the separation of frequencies without interaction difficult. Further, at high frequencies lumped element resonators no longer make adequate filters. Hence distributed circuits such as cavities, filters, etc., have to be used.

For a proper design, depending on the requirements of output frequency, output power, input frequency and bandwidth, the diode to be used should have a small lead inductance, a small series resistance and large degree of non-linearity.

Based on the above mentioned principles, a broad band quadrupler is designed and the design of the various components is given in the following sections.

3.3 THEORY OF LOW PASS FILTER DESIGN

At lower frequencies, a low pass filter is constructed from lumped circuit elements such as inductances and capacitances. The same prototype can be approximated at microwave frequencies using a cascade of alternating low and high impedance sections of transmission lines. It is often possible to represent a short length (less than quarter-wavelength) of line by a single reactive element. A short length of high characteristic impedance line terminated at both ends by a relatively low impedance has an effect equivalent to that of a series inductance given as

$$L = (Z_0 \ell / v) \text{ henries} \quad \dots \quad (3.1)$$

Similarly, a short length of low characteristic impedance line terminated at either end by a relatively high impedance has an effect equivalent to that of a shunt capacitance given as

$$C = \ell / Z_0 v \text{ farads} \quad \dots \quad (3.2)$$

In the above equations, l stands for the length of the line, V for the velocity of propagation along the transmission line and Z_0 for the characteristic impedance of the line. Such short sections of high Z_0 line and low - Z_0 line are the most common ways of realizing series inductance and shunt capacitance, respectively, in TEM- mode microwave filter structures.

An exact prototype low-pass distributed filter with sections of equal electrical length is shown in fig. 3.3(a). The characteristic impedances of different sections for a given VSWR pass-band ripple level and bandwidth are given in reference⁽¹⁷⁾. A typical insertion loss characteristic for a Chebyshev equiripple design is shown in fig.3.3(b). Its bandwidth (BW) is equal to the fractional bandwidth (W_q) of the quarter-wave transformer prototype defined by Young⁽¹⁸⁾, i.e.,

$$\text{Bandwidth (BW)} = W_q = \frac{4\theta_0'}{\pi} \dots (3.3)$$

where θ_0' is defined in fig. 3.3(b).

A is the maximum attenuation in decibels exhibited by the LPF in its stop band when all sections are multiples of one quarter-wavelength.

The only deviation from the exact design specification of an actual filter is due to the presence of capacitive discontinuities at the junctions. However, the method of compensation described by Levy and Rossi⁽¹⁹⁾ gives an exact realization of the cut off frequency. The magnitude of the fringing capacitances depends on the physical realization of the filter, e.g., for a given step between two impedances.

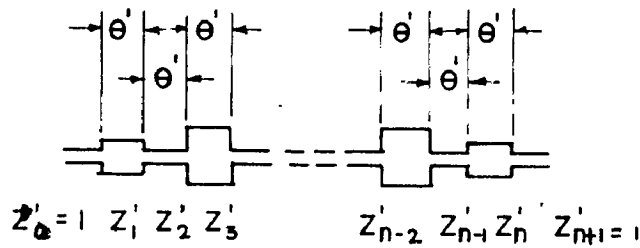


FIG.3.3(a) DISTRIBUTED LOW-PASS PROTOTYPE FILTER

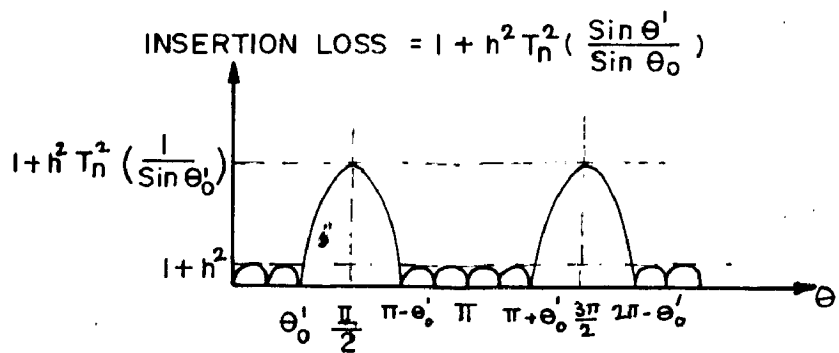


FIG.3.3(b) CHEBYSHEV EQUAL RIPPLE RESPONSE

$$\text{MAXIMUM ATTENUATION } A = 10 \log_{10} \left[1 + h^2 T_n^2 \left(\frac{1}{\sin \theta'_0} \right) \right]$$

$$\text{BANDWIDTH : } BW = \frac{4 \theta'_0}{\pi}$$

$$\text{RIPPLE VSWR : } S = 1 + 2h^2 + 2\sqrt{h^2 + h^4}$$

The low pass filter circuit is shown in fig.3.4(a). The terminating impedances are required to be equal so that an odd number of unit elements is used, i.e.; $Z'_{n+1} = 1$. Since the network is symmetrical

$$Z'_r = Z'_{n-r+1} \quad r = 1, 2 \dots n \dots \quad (3.4)$$

$$C_{r, r+1} = C_{n-r, n-r+1} \quad r = 0, 1, 2 \dots n \dots \quad (3.5)$$

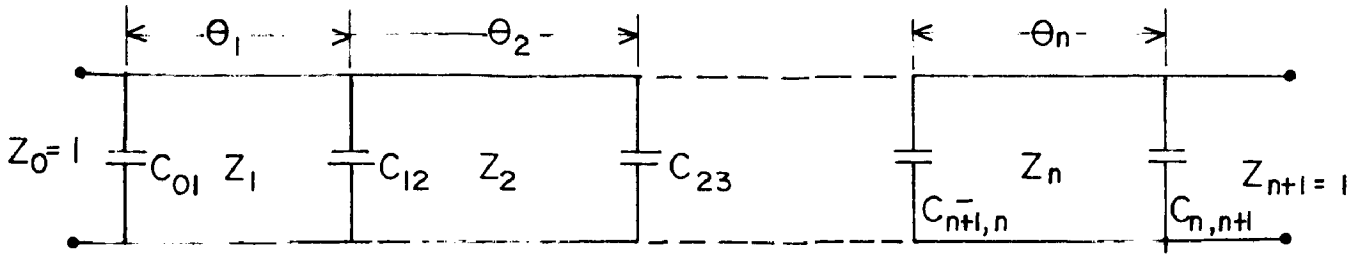
The symmetry means that the network may be split into a cascade of basic sections consisting of a unit element bounded by two equal shunt capacitors. The filter of fig. 3.4(a) is shown in fig. 3.4(b) in its basic sectional form. Now an exact equivalence between the filter and the prototype of fig.3.3(a) may be made at the cut off frequency by constraining the transfer matrices of corresponding sections to be equal at that frequency. This gives an exact realization of the cut off frequency of a practical low pass filter.

A typical basic section of fig. 3.4(b) is shown on the left-hand side of fig.3.4(c), and the corresponding prototype section on the right-hand side. Their equivalence at the cut off frequency results in the following two equations.

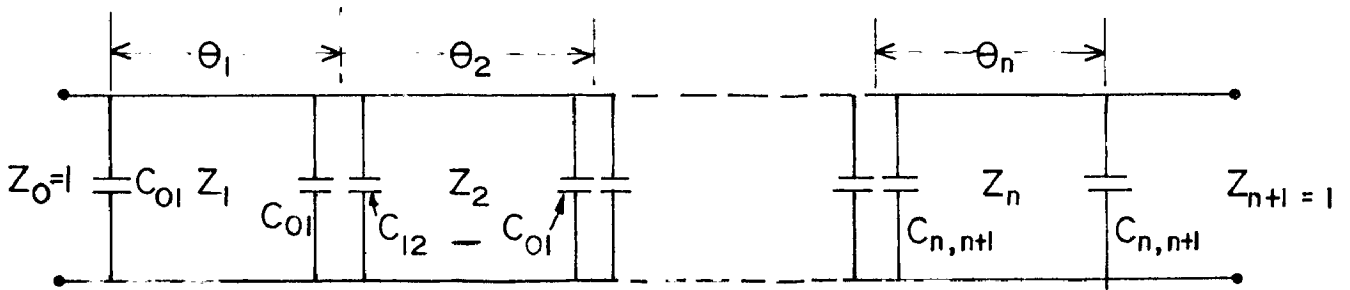
$$\cos \theta_o = \cos \theta'_o + \omega_o CZ' \sin \theta'_o \quad \dots \quad (3.6)$$

$$Z = \frac{Z' \sin \theta'_o}{\sin \theta_o} \quad \dots \quad (3.7)$$

The mathematical details of above equations are given in reference⁽¹⁹⁾.



(a)



(b)



(c)

FIG. 3-4 (a) CIRCUIT OF LOW PASS FILTER
 (b) SPLIT INTO BASIC SYMMETRIC SECTIONS
 (c) EQUIVALENCE TO BE ESTABLISHED

3.31 DESIGN OF A LOW PASS FILTER

This discusses the design procedure of a coaxial low pass filter having the following characteristics:

1. Pass band upto 485 MHz.
2. Greater than 20 dB attenuation in the frequency range of 1.74 GHz to 1.94 GHz (output frequency band)
3. No spurious responses below 2 GHz.

With the above specifications, a cut off frequency of 600 MHz will provide a sufficient design tolerance.

From the impedance tables given by Levy⁽¹⁷⁾, it is found that a five section filter with a bandwidth of 0.6 and ripple VSWR of 1.05 gives a maximum attenuation of 23 dB in the stop band.

From eqn. (3.3)

BW = 0.6 gives $\theta'_0 = 27^\circ$. Therefore the length of each section is 3.75 cms or 1.476". When $\theta'_0 = 27^\circ$, maximum attenuation occurs at a frequency, $f = \frac{90}{27} \times 600 = 2000 \text{ MHz}$ and second spurious pass band will be centred at frequency, $f' = \frac{180}{27} \times 600 = 4000 \text{ MHz}$. These fulfill the design requirements.

From Levy's tables, the value of the normalized impedances for different sections of the prototype filter are tabulated below.

TABLE 1

N = 5 , BW = 0.6 , VSWR = 1.05	
Section	Normalized impedance of prototype
1 & 5	1.536
2 & 4	0.4525
3	2.659

The whole centre conductor structure is held rigidly aligned by dielectric bushes ($\epsilon_r = 2.1$) surrounding low impedance sections.

Using the relation,

$$Z_0 = \frac{138}{\sqrt{\epsilon_r}} \log (b/a) \text{ ohms}$$

where, Z_0 is the characteristic impedance of the line.

ϵ_r is the relative dielectric constant.

b/a is the ratio of diameter of outer conductor to the inner conductor.

The ratio of diameters of each section can be calculated. The calculated diameter ratios for five sections and for the terminating sections (50Ω) are given in Table 2.

TABLE 3

Section	Impedance of prototype	Diameter ratio (b/a)
0 & 6	50	2.31
1 & 5	76.8	2.601
2 & 4 (in dielectric)	22.62	1.729
3	132.95	9.183

Selecting $b = 0.5625$ inches, we obtain

$$a_0 = a_6 = 0.244''$$

$$a_1 = a_5 = 0.1563''$$

$$a_2 = a_4 = 0.3260''$$

$$a_3 = 0.062''$$

For the exact realization of the cut off frequency, the length of each section is compensated by using eqn. (3.6). The values of fringing capacitances C_{01} , C_{12} and C_{23} obtained from Seale's graphical plots⁽²⁰⁾ are given in Table 3.

TABLE 3

Fringing capacitance	Value
C_{01}	0.02691 pF
C_{12}	0.08073 pF
C_{23}	0.11600 pF

So

$$C_{12} - C_{01} = 0.05382 \text{ pf}$$

$$C_{23} + C_{01} - C_{12} = 0.06218 \text{ pf.}$$

Now

$$\begin{aligned} \cos \theta_1 &= \cos \theta_1' + \omega_0 C Z_1' \sin \theta_1' \\ &= 0.8910 + 2\pi \times 0.6 \times 10^9 \times 26.91 \times 10^{-15} \times 76.80 \times 0.4540 \\ &= 0.8944 \end{aligned}$$

$$\text{So } \theta_1 = 26^\circ 34'$$

Similarly

$$\begin{aligned} \cos \theta_2 &= \cos \theta_2' + \omega_0 C Z_2' \sin \theta_2' \\ &= 0.8910 + 2\pi \times 0.6 \times 10^9 \times 53.82 \times 10^{-15} \times 32.8 \times 0.4540 \\ &= 0.8941 \end{aligned}$$

$$\text{So } \theta_2 = 26^\circ 35'$$

Again

$$\begin{aligned} \cos \theta_3 &= \cos \theta_3' + \omega_0 C Z_3' \sin \theta_3' \\ &= 0.8910 + 2\pi \times 0.6 \times 10^9 \times 62.18 \times 10^{-15} \times 132.95 \times 0.4540 \\ &= 0.90514 \end{aligned}$$

$$\text{so } \theta_3 = 25^\circ 10'$$

From the above calculations, it is found that the difference between θ_0 and θ'_0 is not much, so no attempt was taken to find the revised value of Z' .

Detailed calculations of the filter are given in Table 4.

TABLE 4

DETAILS OF CALCULATION OF 5-SECTION LOW-PASS FILTER

$N = 5$, $BW = 0.6$ ($\theta'_0 = 27$ degrees), ripple $VSWR = 1.05$
 Cut off = 600 MHz, Outer conductor diameter = 0.5625"

Section	Diameter of inner conductor (inches)	Final electrical length.	Final length (inches)
1 & 5	0.1563	25° 34'	1.453
2 & 4	0.326	26° 35'	1.454
3	0.062	25° 10'	1.376

Fig. 3.5 shows the complete drawing of the filter. The filter was tested for its cut-off and the measured response of the same is plotted in graph of fig.3.6. From this graph, it is obvious that a good agreement between the theory and practical design is achieved.

3-4 THEORY OF INTERDIGITAL BAND-PASS FILTER DESIGN

Interdigital line structures have in the past been regarded as of interest mainly for use as slow wave structures. However, a recent study has shown that interdigital line structures also have very interesting band-pass filter

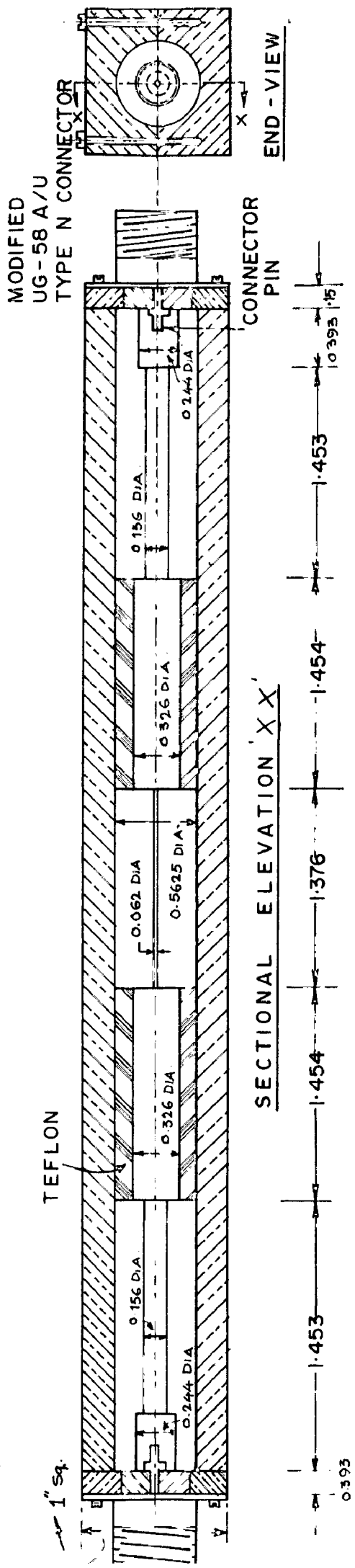




FIG. 3.5 DIAMENSIONS OF 5 SECTION LOW PASS FILTER

MATERIAL	BRASS	TEFLON
		

All dimensions are in inches

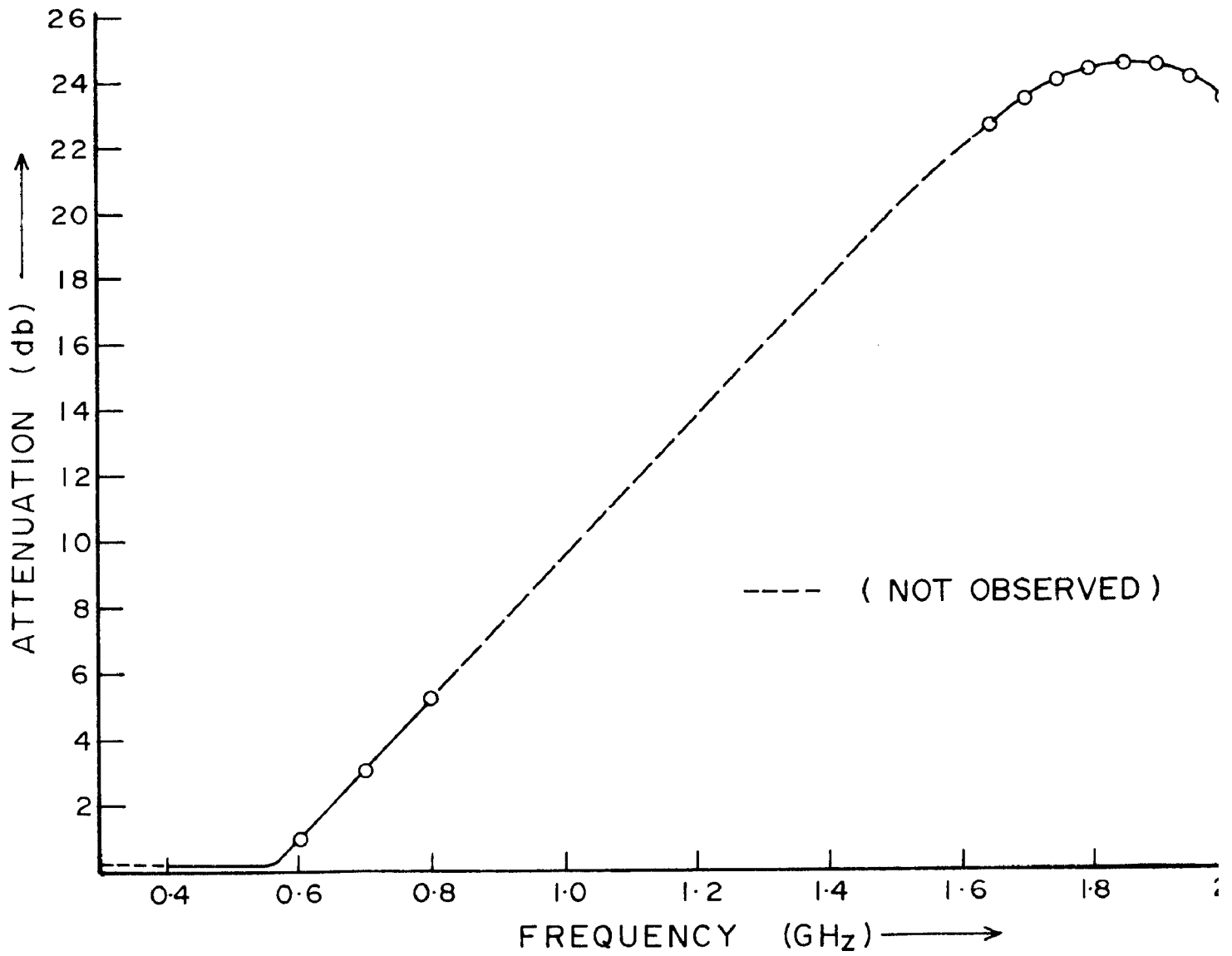


FIG3.6 LOW PASS FILTER CHARACTERISTICS

properties.

Fig. 3.7(a) shows one type of an interdigital filter. The structure, as shown, consists of a TEM-mode strip-line resonators between parallel ground planes. Each resonator element is a quarter-wavelength long at the mid frequency and is short circuited at one end and open circuited at the other end. Coupling is achieved by way of the fringing fields between adjacent resonator elements. In this structure, each line element serves as a resonator, except for the input and output line elements which have an impedance-matching function. Thus, an n -reactive element low-pass prototype will lead to an interdigital filter with $(n + 2)$ line elements. The design equations for this type yield the structural dimensions that will be most practical when the filter is of narrow or moderate bandwidth. The gaps between lines 0 and 1 and between lines n and $n + 1$ tend to become inconveniently small when the bandwidth is large, and the widths of bars 1 and n tend to become very small.

Fig. 3.7 (b) shows another type of interdigital filter with open circuited lines at the ends. The design equations for this type of interdigital filter give structural dimensions that are most practical when the filter is of wide bandwidth (say, around 30 percent bandwidth or greater). In this case, all of the line elements serve as resonators, including the open-circuited terminating line element at each end.

Interdigital band-pass filters have a number of attractive features.

1. They are very compact.
2. The tolerances required in their manufacture are relatively relaxed as a result of the relatively large spacing between resonator elements.

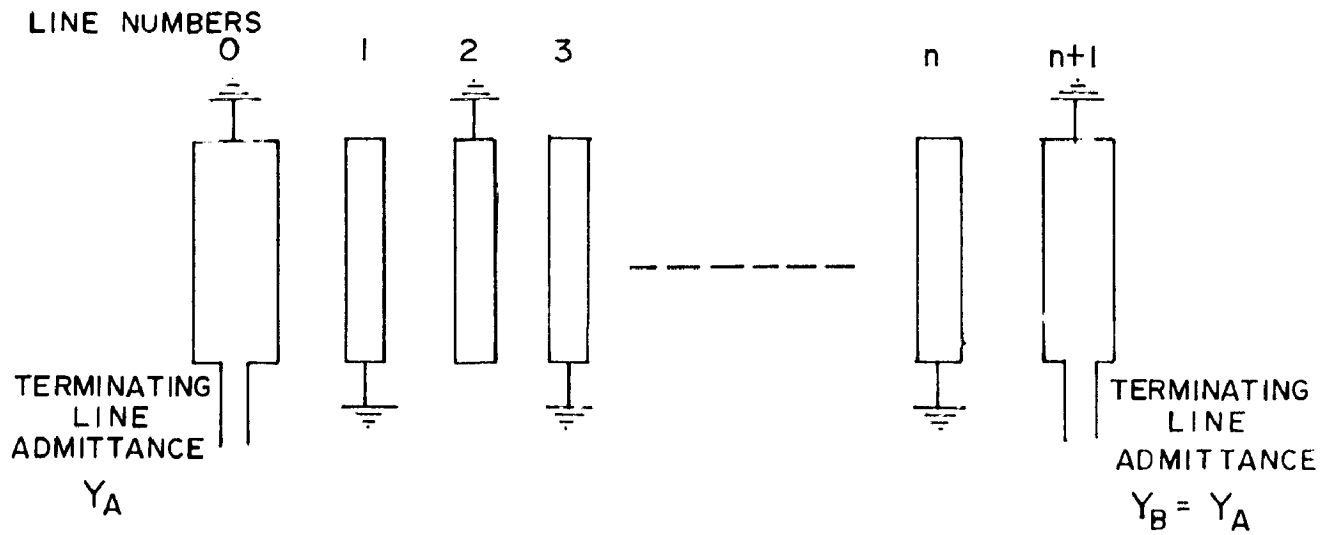


FIG. 3.7(a) INTER DIGITAL FILTER WITH SHORT-CIRCUITED LINES AT THE ENDS

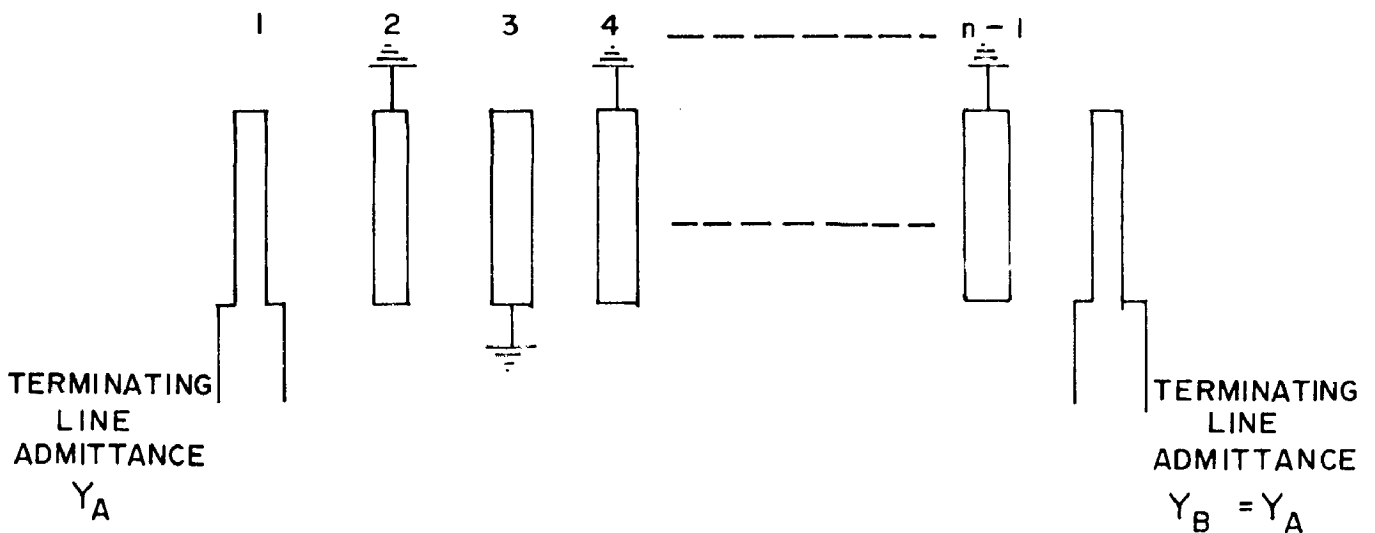


FIG. 3.7(b) INTER DIGITAL FILTER WITH OPEN-CIRCUITED LINES AT THE ENDS

3. The second pass band is centred at three times the centre frequency of the first pass-band, and there is no possibility of the spurious responses in between (while for the filters with half-wavelength, parallel coupled resonators, even the slightest mistuning will result in narrow spurious passbands at twice the frequency of the first pass-band centre).
4. The rates of cut-off and the attenuation in the stop bands are enhanced by multiple-order poles of attenuation at ω_c and at even multiples of the centre frequency of the first pass-band.
5. These filters can be fabricated in structural forms which are self-supporting so that dielectric material need not be used. Thus dielectric losses can be eliminated.

Since coupling between resonators is distributed in nature, it is convenient to work out the design of the resonator lines in terms of their capacitance to ground C_k per unit length, and the mutual capacitances $C_{k, k+1}$ per unit length between neighbouring lines k and $k+1$. These capacitances are illustrated in the cross sectional view of the line elements shown in fig. 3.6. This representation is not necessarily always highly accurate; it is conceivable that a significant amount of fringing capacitance could exist between a given line element and the line element beyond the nearest neighbour. However, at least for the geometries such as those shown in fig. 3.7(a) and (b), it was found that this representation gives a satisfactory degree of accuracy.

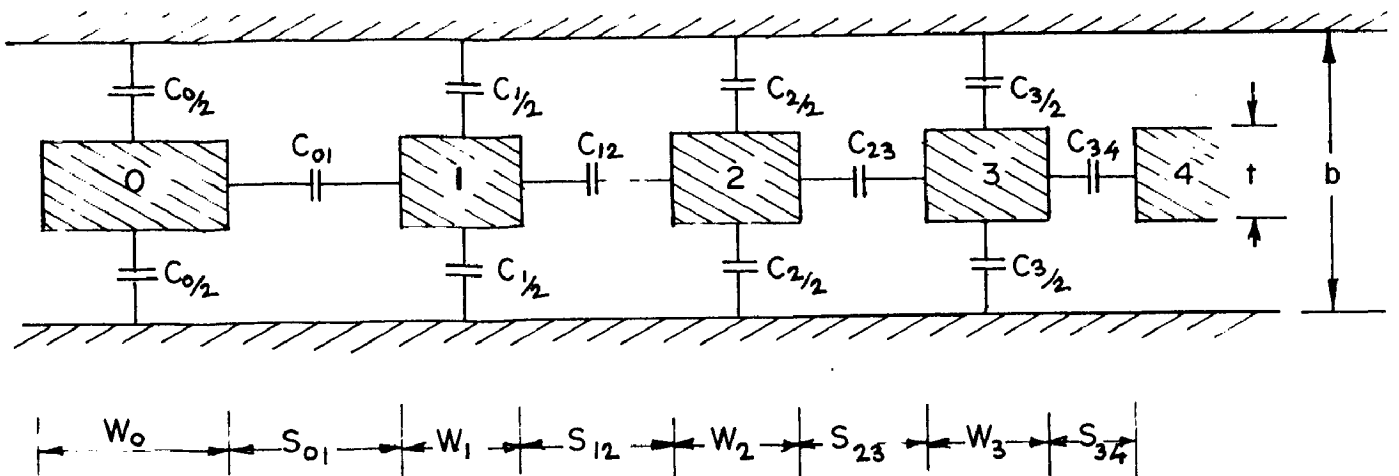


FIG. 3-8 CROSS SECTION OF AN ARRAY OF PARALLEL-COUPLED LINES BETWEEN GROUND PLANES.

3.41 LOW-PASS TO BAND-PASS TRANSFORMATION

The design equations to be described are based on the use of low-pass prototype filter structure, which is transferred to give the desired band-pass filter characteristics. Fig. 3.9 (a) shows a typical low-pass prototype specifying the elements g_k . The left side of fig. 3.9 (b) shows a typical Chebyshev low-pass response which can be achieved by using the prototype filters. Element values for this type of prototype filter networks, yielding different responses have been tabulated in reference (22).

The right side of fig. 3.9 (b) shows a band-pass filter response which is derived from the given low-pass prototype response, using the standard transformation technique. The band-pass filter response will have the same type of pass-band characteristics as the prototype, but the band-width of the band-pass filter can be specified arbitrarily. The attenuation is same for both low-pass and band-pass filters at frequencies ω' and ω , respectively and are related by the following mapping equation.

$$\omega' = \frac{2\omega_1}{\omega} \left| \frac{\omega - \omega_0}{\omega_0} \right| \quad \dots \quad (3.8)$$

where $\omega = \frac{\omega_2 - \omega_1}{\omega_0}$

The band-pass filter attenuation characteristics can be predicted by using the above equation. This transformation works well for filters of narrow or moderate band-width. The largest error is seen to occur on the high side of the pass-band where the narrowband mapping does not predict as large a rate of cut-off as actually occurs. The reason that the actual rate of cutoff tends to be unusually large on the high frequency side of the pass-band is

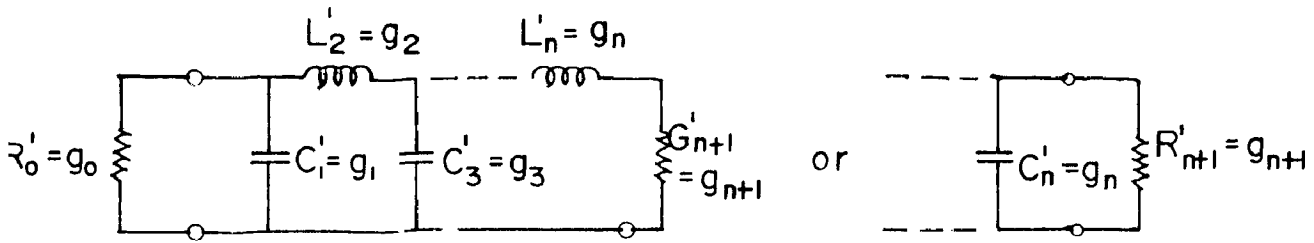
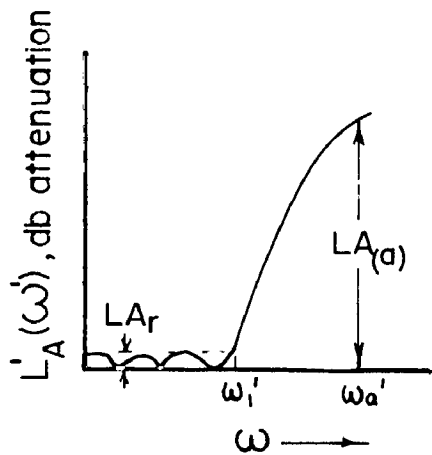
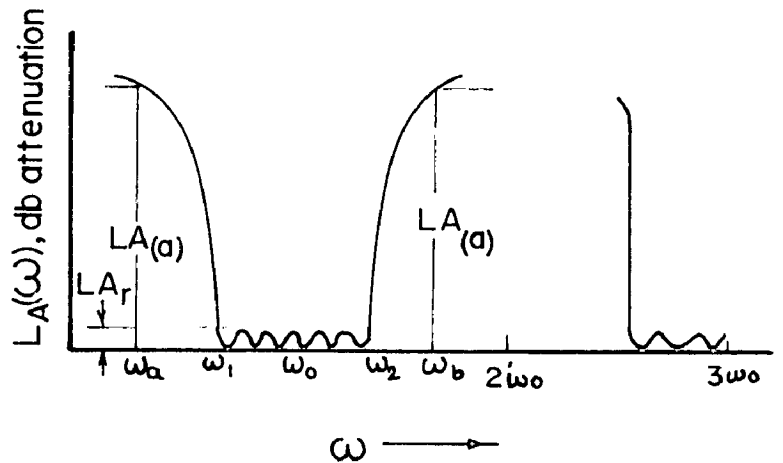


FIG.3-9(a) DEFINITION OF PROTOTYPE FILTER PARAMETERS

$g_0, g_1, g_2 \dots g_n, g_{n+1}$ AN ADDITIONAL PROTOTYPE PARAMETER ω'_1 IS DEFINED IN FIG.3-9 (b)



PROTOTYPE RESPONSE



BAND-PASS FILTER RESPONSE

$$L_A(\omega) = L'_A(\omega') \text{ db}$$

$$\omega_0 = \frac{\omega_2 + \omega_1}{2}$$

Where $\omega' = \frac{2\omega'_1}{W} \left| \frac{\omega - \omega_0}{\omega_0} \right|$ and W (fractional bandwidth) = $\frac{\omega_2 - \omega_1}{\omega_0}$

$$= \frac{\omega'_1}{W} \left(\frac{\omega}{\omega_0} - \frac{\omega_0}{\omega} \right)$$

FIG.3-9(b) RELATION BETWEEN THE LOW-PASS PROTOTYPE RESPONSE AND THE BAND-PASS FILTER RESPONSE

that the structure has infinite attenuation (theoretically) at the frequency for which the resonators lines are a quarter wavelength long.

3.42 BAND-PASS FILTERS AND THEIR RELATION TO LOW-PASS PROTOTYPES

In a microwave filter, it is much more practical to use a structure which approximates the circuit in fig. 3.10 (a), or its dual. In this structure all of the resonators are of the same type, and an effect like alternating series and shunt resonators is achieved by the introduction of "impedance inverters". The band-pass filter in fig. 3.10 (a) can be designed from a low-pass prototype as in fig. 3.9(a) by first converting the prototype to the equivalent low-pass prototype form as in fig. 3.10 (b) which uses only series inductances and impedance inverters in the filter structure. Then a low-pass to band-pass transformation can be applied to the circuit in fig. 3.10 (b) to yield the band-pass circuit in fig. 3.10(a). Same applies to the low-pass prototype using J' inverters (admittance inverters).

3.43 DESIGN PRINCIPLES

The requirements for a band-pass filter needed in the present application may be concisely stated as follows:

1. Pass-band in the range of 1.74 GHz to 1.94 GHz, i.e. the band-width is about 11% at a centre frequency of 1.84 GHz.
2. Very steep side-attenuation to the pass-band is required in order to obtain a better rejection of all unwanted harmonics.

According to the above mentioned requirements, a four resonator filter network should be sufficient to cover 11% band-width. A Tchebysheff filter with

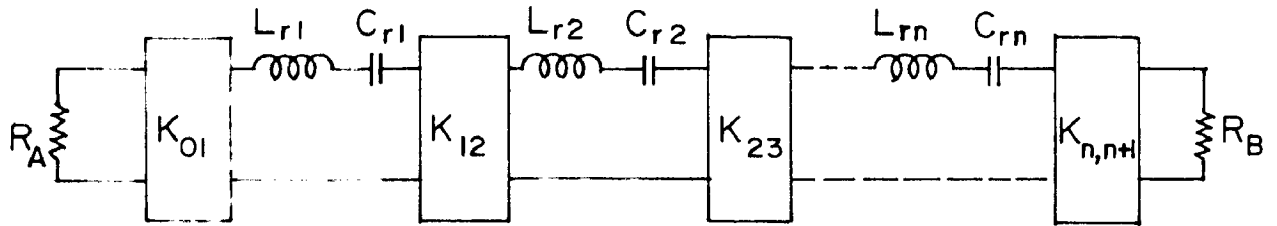


FIG.3-10(a) THE BAND-PASS FILTER CONVERTED TO USE ONLY SERIES RESONATORS AND IMPEDANCE INVERTERS

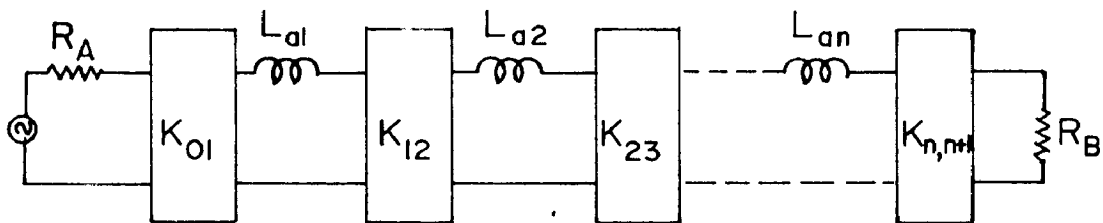


FIG.3-10(b) MODIFIED PROTOTYPE USING IMPEDANCE INVERTERS (K-INVERTERS)

a pass-band ripple of 0.5 db will be able to give a reasonably steep skirt attenuation characteristics. Suitable form of interdigital filter selected for this purpose is shown in fig. 3.7 (a). The approximate design equations for which, as given by Matthai⁽²²⁾, are tabulated below.

TABLE 5
DESIGN EQUATIONS FOR INTERDIGITAL FILTER

$$\theta_1 = \left(\pi / 2 \right) \frac{\omega_1}{\omega_0} = \frac{\pi}{2} \left(1 - \frac{\omega}{\omega_0} \right) \dots \quad (3.9)$$

$$\frac{J_{01}}{Y_A} = \frac{1}{\sqrt{\epsilon_0 \epsilon_1 \omega_1'}} \quad , \quad \left. \frac{J_{k,k+1}}{Y_A} \right|_{k=1 \text{ to } n-1} = \frac{1}{\omega_1' \sqrt{\epsilon_k \epsilon_{k+1}}} \dots \quad (3.10)$$

$$\frac{J_{n,n+1}}{Y_A} = \frac{1}{\sqrt{\epsilon_n \epsilon_{n+1} \omega_1'}} \quad \dots \quad (3.11)$$

$$\left. M_{k,k+1} \right|_{k=1 \text{ to } n-1} = \sqrt{\left(\frac{J_{k,k+1}}{Y_A} \right)^2 + \frac{\tan^2 \theta_1}{4}} \quad \dots \quad (3.12)$$

$$M_1 = Y_A \left(\frac{J_{01}}{Y_A} \sqrt{h+1} \right) \quad , \quad M_n = Y_A \left(\frac{J_{n,n+1}}{Y_A} \sqrt{h+1} \right) \quad \dots \quad (3.13)$$

where h is a dimensionless admittance scale factor to be specified arbitrarily so as to give a convenient admittance level in the filter.

The normalized self-capacitance C_k / ϵ per unit length for the line elements are:

$$\frac{C_0}{\epsilon} = \frac{376.7}{\sqrt{\epsilon_r}} \left(2 Y_A - M_1 \right) \dots\dots\dots (3.14)$$

$$\frac{C_1}{\epsilon} = \frac{376.7}{\sqrt{\epsilon_r}} \left[Y_A - M_1 + h Y_A \left\{ \frac{\tan \theta_1}{2} + \left(\frac{J_{01}}{Y_A} \right)^2 + N_{12} - \frac{J_{12}}{Y_A} \right\} \right] \dots (3.15)$$

$$\frac{C_k}{\epsilon} \Big|_{k=2 \text{ to } n-1} = \frac{376.7}{\sqrt{\epsilon_r}} h Y_A \left[N_{k-1,k} + N_{k,k+1} - \frac{J_{k-1,k}}{Y_A} - \frac{J_{k,k+1}}{Y_A} \right] \dots (3.16)$$

$$\frac{C_n}{\epsilon} = \frac{376.7}{\sqrt{\epsilon_r}} \left[Y_A - M_n + h Y_A \left\{ \frac{\tan \theta_1}{2} + \frac{J_{n,n+1}}{Y_A} + N_{n-1,n} - \frac{J_{n-1,n}}{Y_A} \right\} \right] \dots (3.17)$$

$$\frac{C_{n+1}}{\epsilon} = \frac{376.7}{\sqrt{\epsilon_r}} \left(2 Y_A - M_n \right) \dots\dots\dots (3.18)$$

where ϵ is the dielectric constant and ϵ_r is the relative dielectric constant in the medium of propagation.

The normalized mutual capacitances $C_{k,k+1}/\epsilon$ per unit length between adjacent line elements are

$$\frac{C_{01}}{\epsilon} = \frac{376.7}{\sqrt{\epsilon_r}} \left(M_1 - Y_A \right) \dots\dots\dots (3.19)$$

$$\frac{C_{k,k+1}}{\epsilon} \Big|_{k=1 \text{ to } n-1} = \frac{376.7}{\sqrt{\epsilon_r}} h Y_A \left(\frac{J_{k,k+1}}{Y_A} \right) \dots\dots\dots (3.20)$$

$$\frac{C_{n,n+1}}{\epsilon} = \frac{376.7}{\sqrt{\epsilon_r}} \left(M_n - Y_A \right) \dots\dots\dots (3.21)$$

CALCULATIONS

Required pass band = 1.74 GHz to 1.94 GHz

Hence centre frequency = 1.84 GHz

Fractional bandwidth (ω) = $\frac{200}{1840}$
 = 0.108

Quarter-wavelength at the centre frequency ($\frac{\lambda_0}{4}$) = 1.87"

Using equation (3.9)

$$\begin{aligned} \theta_1 &= \frac{\pi}{2} \left(1 - \frac{\omega}{2} \right) \\ &= \frac{\pi}{2} (1 - 0.054) \\ &= 1.482 \end{aligned}$$

The element values for Chebyshev filter having $\epsilon_0 = 1$, $\omega_1 = 1$ for $n = 4$ are given in Table 6.

TABLE 6

$\epsilon_1 = 1.6703$	$\epsilon_4 = 0.8419$
$\epsilon_2 = 1.1926$	$\epsilon_5 = 1.9841$
$\epsilon_3 = 2.3661$	

where ω_1 is equal ripple band edge for Chebyshev filter.

Computing J/Y_A and N parameters using equations (3.10), (3.11) and (3.13) and substituting the element values from Table 6.

$$\frac{J_{0,1}}{Y_A} = \frac{1}{\sqrt{1.6703}} = 0.7752$$

$$\frac{J_{1,2}}{Y_A} = \frac{1}{\sqrt{1.6703 \times 1.1926}} = 0.7092$$

$$\frac{J_{2,3}}{Y_A} = \frac{1}{\sqrt{1.1926 \times 2.3661}} = 0.5957$$

Since $\epsilon_3 \epsilon_4 = \epsilon_1 \epsilon_2$

$$\text{So } \frac{J_{3,4}}{Y_A} = \frac{J_{1,2}}{Y_A} = 0.7092$$

Again $\epsilon_4 \epsilon_5 = \epsilon_0 \epsilon_1$

$$\text{So } \frac{J_{4,5}}{Y_A} = \frac{J_{0,1}}{Y_A} = 0.7752$$

$$N_{1,2} = \sqrt{\left(\frac{J_{1,2}}{Y_A}\right)^2 + \frac{1}{3} \cdot \tan^2 \theta_1}$$

$$= \sqrt{(0.7092)^2 + 31.36}$$

$$= 5.646$$

$$N_{2,3} = \sqrt{(0.5957)^2 + 31.36}$$

$$= 5.632$$

$$N_{3,4} = N_{1,2} \quad \text{since} \quad \frac{J_{3,4}}{Y_A} = \frac{J_{1,2}}{Y_A}$$

One of the prime considerations in the choice of admittance scale factor, h is that the line dimensions must be such that the resonators should have a high unloaded Q . The dimensions that give optimum resonator Q 's in structures such as interdigital filters are not known. However, it is known that for air-filled, coaxial-line resonators the optimum Q will result when the line impedance is about 76 ohms, and various approximate studies suggest that the optimum impedance for strip-line resonators is not greatly different. It was therefore concluded that for optimum h , the following condition should be satisfied.

$$\frac{2 C_{k-1,k}}{\epsilon} + \frac{C_k}{\epsilon} + \frac{2 C_{k,k+1}}{\epsilon} \left| \begin{array}{l} k = \frac{n}{2} \text{ for } n \text{ even} \\ = (n+1)/2 \text{ for } n \text{ odd} \end{array} \right. = (\text{around } 5.4)$$

putting $k = 2$

$$\frac{2 C_{1,2}}{\epsilon} + \frac{C_2}{\epsilon} + \frac{2 C_{2,3}}{\epsilon} = 5.4 \quad \dots \quad (3.22)$$

Using equations (3.16), $\frac{C_2}{\epsilon}$ is obtained in terms of h as given below:

$$\begin{aligned} \frac{C_2}{\epsilon} &= \frac{376.7 h Y_A}{\sqrt{\epsilon_r}} \left[N_{1,2} + N_{2,3} - \frac{J_{1,2}}{Y_A} - \frac{J_{2,3}}{Y_A} \right] \\ &= (376.7 \times 0.02) \left[5.646 + 5.632 - 0.7092 - 0.5957 \right] h \\ &= 75.13 h \end{aligned}$$

Now

$$\begin{aligned} \frac{C_{1,2}}{\epsilon} &= \frac{376.7 h Y_A}{\sqrt{\epsilon_F}} \left[\frac{J_{1,2}}{Y_A} \right] \\ &= (376.7 \times 0.02) (0.7092) h \\ &= 5.342 h \end{aligned}$$

Similarly

$$\frac{C_{2,2}}{\epsilon} = 4.487 h$$

Substituting the values of $\frac{C_{1,2}}{\epsilon}$, $\frac{C_{2,2}}{\epsilon}$ and $\frac{C_2}{\epsilon}$ in equation (3.22), the required value of h is obtained.

$$2(5.342) h + 75.13 h + 2(4.487)h = 5.4$$

$$\begin{aligned} h &= \frac{5.4}{94.768} \\ &= 0.05698 \end{aligned}$$

Now

$$\begin{aligned} M_1 &= Y_A \left[\frac{J_{0,1}}{Y_A} \sqrt{h} + 1 \right] \\ &= 0.02 \left[0.7752 \sqrt{0.05698} + 1 \right] \\ &= 0.0237 \end{aligned}$$

Since

$$\frac{J_{4,5}}{Y_A} = \frac{J_{0,1}}{Y_A}, \text{ so } M_4 = M_1$$

The normalized self-capacitances are calculated by using equations (3.14), (3.15), (3.16), (3.17) and (3.18).

$$\begin{aligned} \frac{C_0}{\epsilon} &= \frac{376.7}{\sqrt{\epsilon_r}} (2 Y_A - M_1) \\ &= 376.7 (2 \times 0.02 - 0.0237) \\ &= 6.141 \end{aligned}$$

$$\begin{aligned} \frac{C_1}{\epsilon} &= \frac{376.7}{\sqrt{\epsilon_r}} \left[Y_A - M_1 + h Y_A \left\{ \frac{\tan \theta_1}{2} + \left(\frac{J_{0,1,2}}{Y_A} \right)^2 + M_{1,2} - \frac{J_{1,2}}{Y_A} \right\} \right] \\ &\approx 3.39 \end{aligned}$$

$$\begin{aligned} \frac{C_2}{\epsilon} &= 75.13 \times h \\ &= 75.13 \times 0.057 \\ &= 4.283 \end{aligned}$$

$$\frac{C_{2,3}}{\epsilon} = \frac{C_2}{\epsilon} \quad \text{since } M_{3,4} = M_{1,2} \quad \text{and} \quad \frac{J_{3,4}}{Y_A} = \frac{J_{1,2}}{Y_A}$$

$$\frac{C_4}{\epsilon} = \frac{C_1}{\epsilon} \quad \text{since } M_1 = M_4, \quad \frac{J_{4,5}}{Y_A} = \frac{J_{0,1}}{Y_A}$$

$$M_{3,4} = M_{1,2}, \quad \frac{J_{3,4}}{Y_A} = \frac{J_{1,2}}{Y_A}$$

$$\frac{C_{n+1}}{\epsilon} = \frac{376.7}{\sqrt{\epsilon_r}} (2 Y_A - M_n)$$

$$\frac{C_5}{\epsilon} = 6.141$$

Normalized mutual capacitances per unit length between adjacent lines are calculated by using equations (3.19), (3.20) and (3.21).

$$\frac{G_{0,1}}{\epsilon} = \frac{376.7}{\sqrt{\epsilon_r}} (N_1 - I_A)$$

$$= 1.394$$

$$\frac{G_{1,2}}{\epsilon} = 5.342 h$$

$$= 0.3045$$

$$\frac{G_{2,3}}{\epsilon} = 4.487 \times 0.057$$

$$= 0.2558$$

$$\frac{G_{3,4}}{\epsilon} = \frac{G_{1,2}}{\epsilon} \quad \text{since} \quad \frac{J_{3,4}}{I_A} = \frac{J_{1,2}}{I_A}$$

$$\frac{G_{4,5}}{\epsilon} = \frac{G_{0,1}}{\epsilon} \quad \text{since} \quad N_1 = N_4$$

The computed parameters are tabulated below.

TABLE 7

k	$\frac{J_{k,k+1}}{I_A}$	$N_{k,k+1}$	$\frac{G_{k,k+1}}{\epsilon}$	k	$\frac{G_k}{\epsilon}$
0 and 4	0.7752		1.394	0 and 5	6.141
1 and 3	0.7090	5.846	0.3045	1 and 4	3.39
2	0.5957	5.632	0.2558	2 and 3	4.283

$$\omega = 0.109$$

$$I_A = 0.02 \text{ ambs}$$

$$\theta_1 = 1.482$$

$$N_1 = N_4 = 0.0237$$

$$h = 0.05698$$

Calculation of cross sectional dimensions of bar and spacing between them.

The circular cylindrical rods as resonators were used because of several fabrication advantages over rectangular bars. The design data of coupled circular cylindrical rods between parallel ground planes, and a design method for using the data to synthesize filters are given in reference (23). The geometry of the periodic, circular cylindrical rods between parallel ground planes and the dimensional notations are shown in fig. 3.11.

The first step in obtaining the dimensions of the structure from specified normalized capacitances is to draw horizontal lines in the graph of fig. 3.12 corresponding to the values of $\frac{C_m}{\epsilon}$ (normalized mutual capacitance) for $k = 0, 1, 2$. Next the coordinates of the intersections of constant $\frac{C_m}{\epsilon}$ with the family of constant d/b curves are noted and plotted as shown on the graph of fig. 3.13. Smooth curves are then drawn on the graph of fig. 3.13 through points of constant C_m/ϵ , thus obtaining curves of constant C_m/ϵ .

Next it is useful to partition the filter configuration of fig. 3.11 into smaller subsections as shown in fig. 3.14. Each subsection consists of a normalized capacitance to ground and the normalized coupling capacitances to the right and to the left. For determining the normalized rod diameters and normalized spacings, each sub-section is considered separately.

Let block III be chosen as an example. On the graph of fig. 3.13 several auxiliary curves of constant d/b are drawn in the vicinity of one half value of the required normalized capacitance to ground ($\frac{1}{2} \frac{C_m}{\epsilon} = 2.143$). The objective of drawing auxiliary curves is to find unique intersections with the constant curves of $\frac{C_m}{\epsilon} = 0.2358$ and 0.3045 in such a way that

the sum of the ordinates of the intersections totals $\frac{C_1}{\epsilon} = \frac{C_2}{\epsilon} = 4.253$. This gives $\frac{d_2}{b} = 0.345$. The same procedure is repeated for other two blocks. It was found that $d_1/b = 0.325$ and $\frac{d_0}{b} = 0.516$.

The respective normalized spacings, $(s_{k,k+1}/b)$ are obtained by summing the abscissa values which correspond to the same mutual capacitance.

Abscissa values corresponding to their mutual capacitances are tabulated below:

TABLE 2

$C_{k,k+1}$	Abscissa value $(\frac{1}{2}) \frac{s}{b}$
C_{01}	0.140
C_{01})	0.110
C_{12})	0.322
C_{12})	0.325
C_{23})	0.350

Therefore,

$$\frac{s_{01}}{b} = 0.140 + 0.110 = \frac{s_{45}}{b}$$

$$\frac{s_{12}}{b} = 0.322 + 0.325 = 0.647 = \frac{s_{34}}{b}$$

$$\frac{s_{23}}{b} = 0.350 + 0.350 = 0.70$$

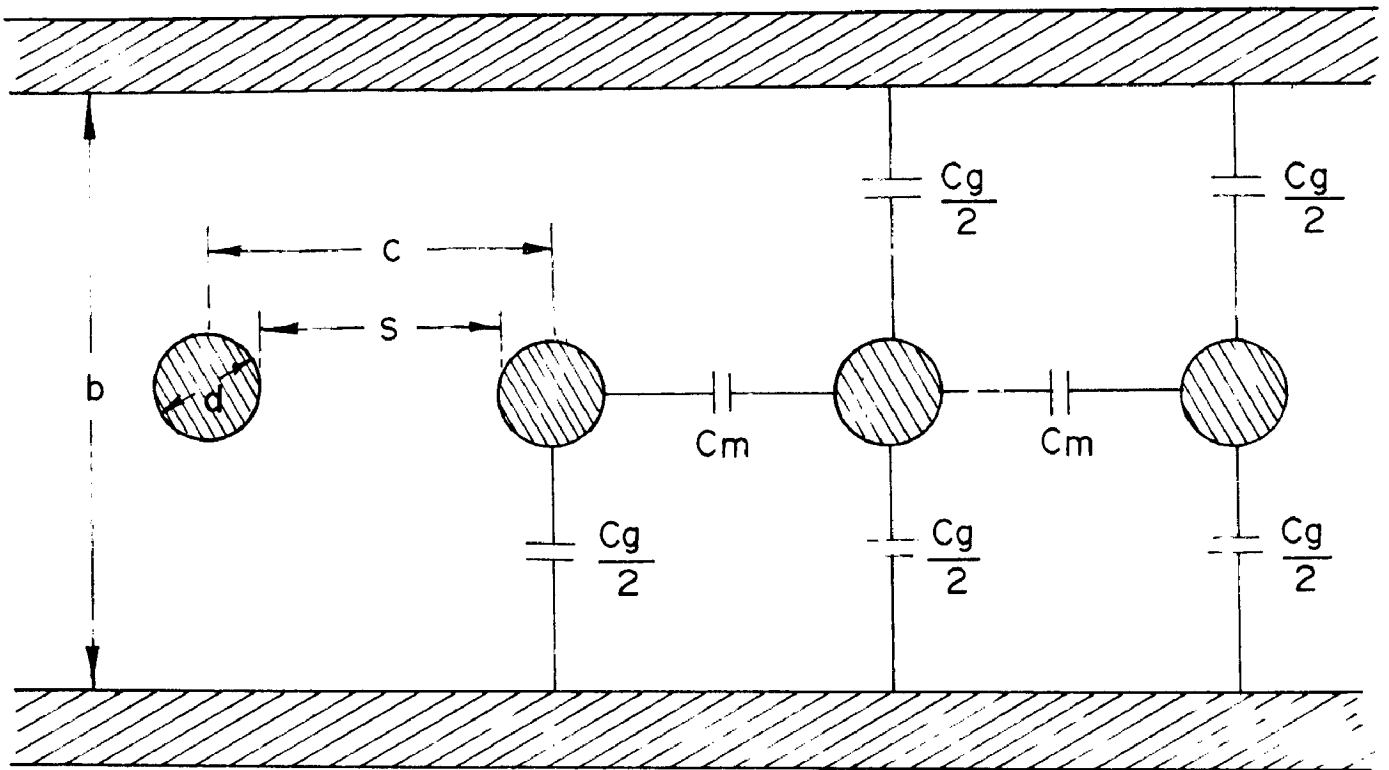


FIG. 3-11 COUPLED CIRCULAR CYLINDRICAL RODS
BETWEEN PARALLEL GROUND PLANES

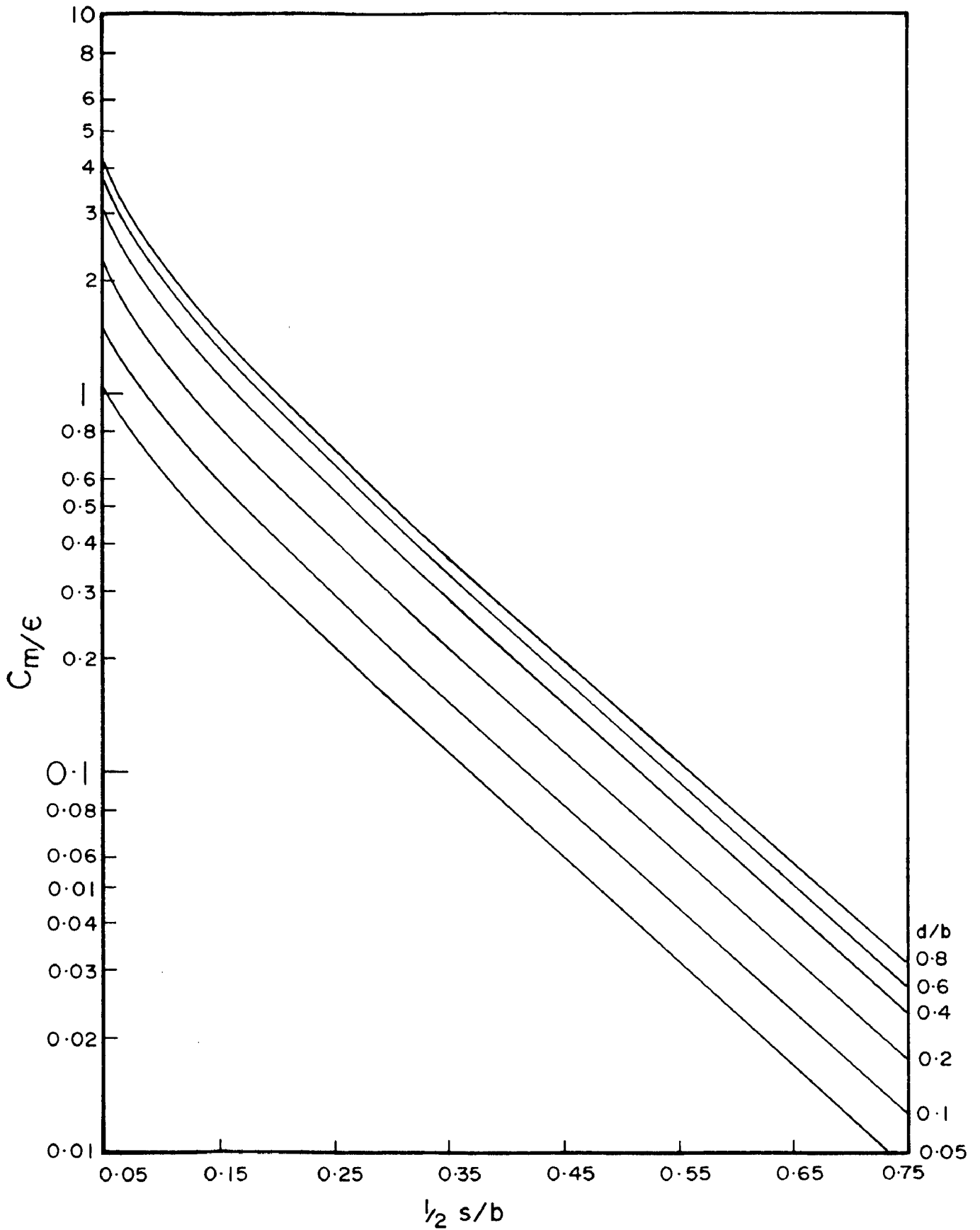


FIG. 3-12 GRAPH OF C_m/ϵ (NORMALIZED MUTUAL CAPACITANCE) Vs. $(\frac{1}{2})^{s/b}$ (NORMALIZED HALF SPACING)

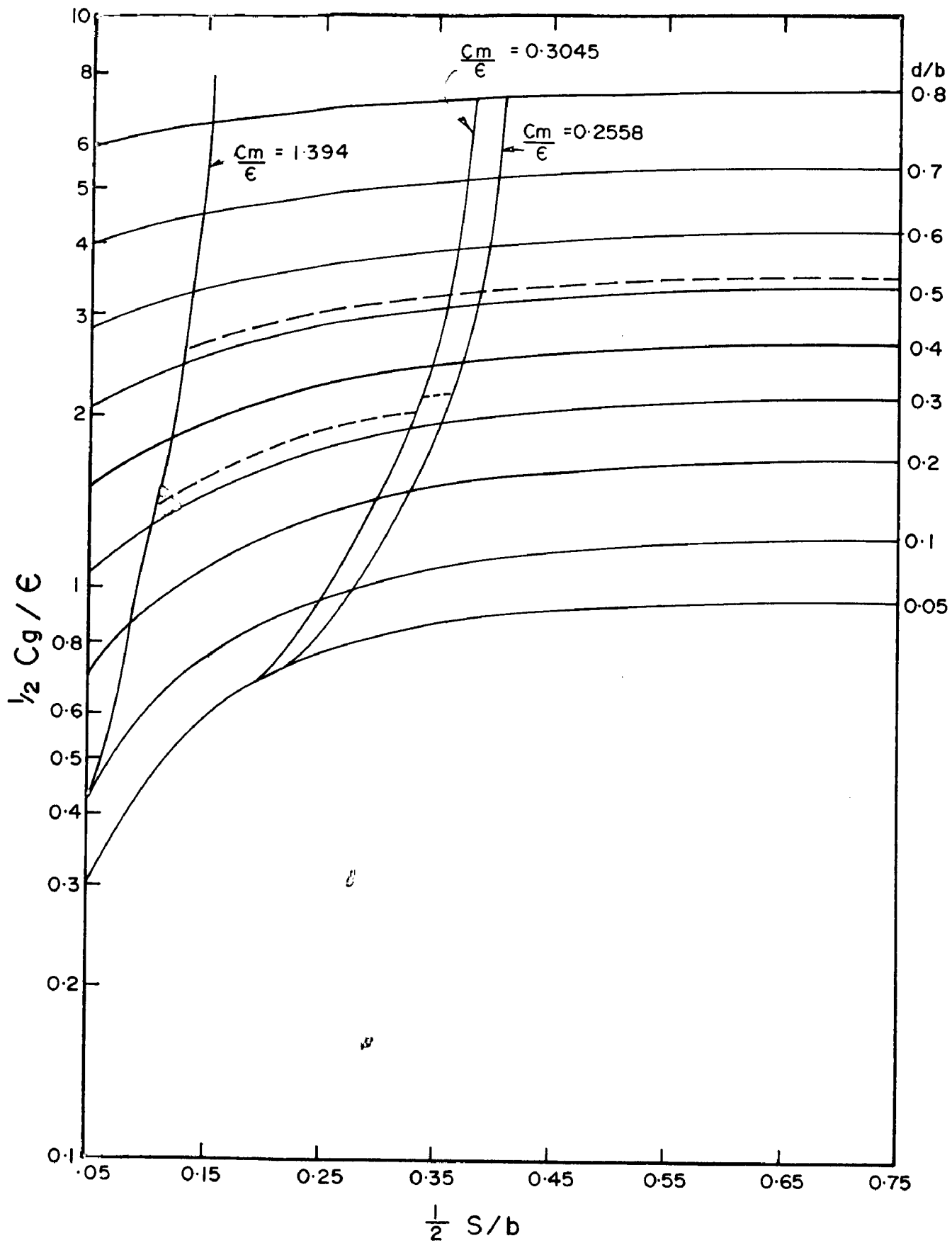


FIG. 3-13 DETERMINATION OF THE NORMALIZED DIAMETERS AND THE ADJACENT SPACINGS

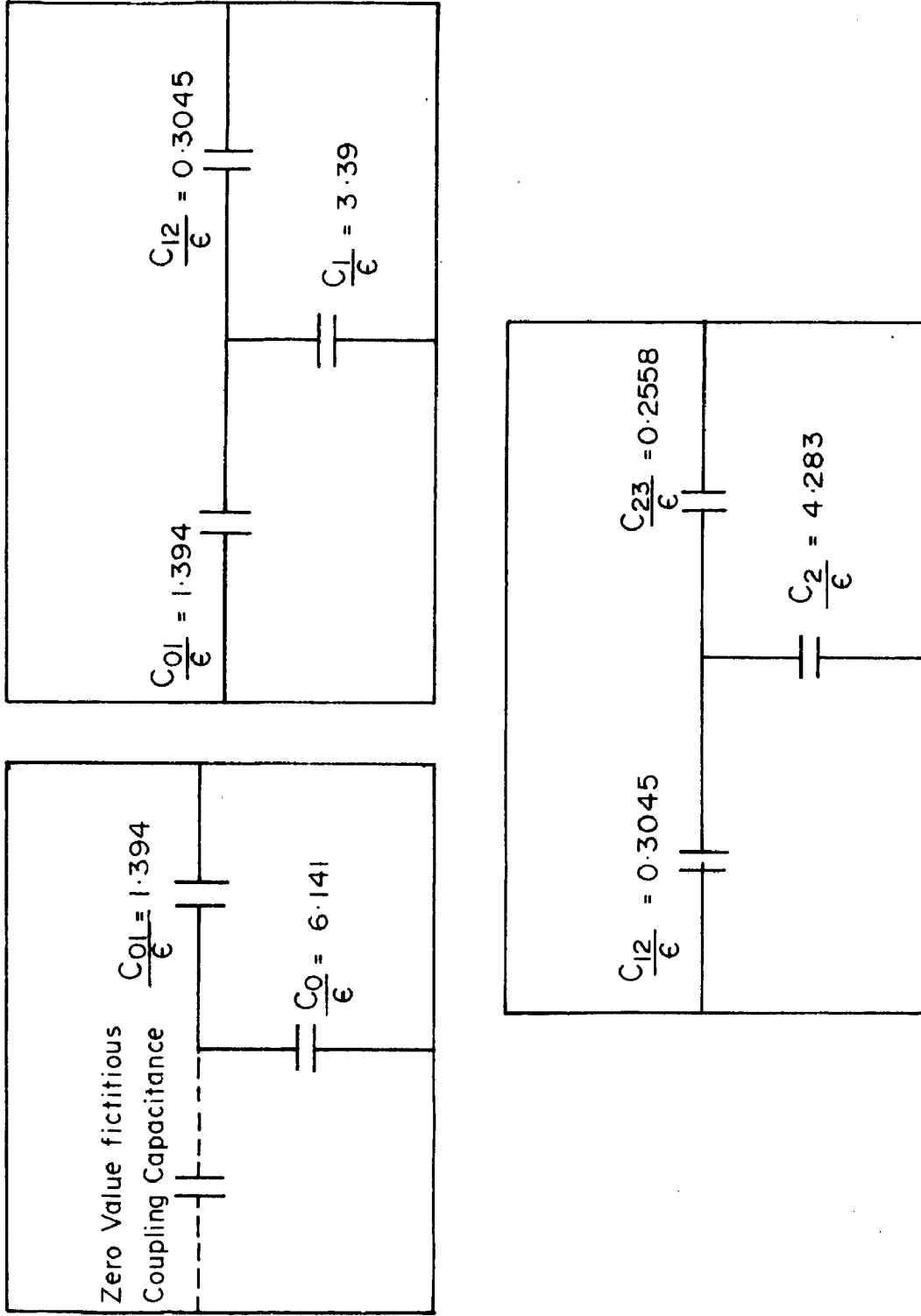


FIG. 3.14 GROUPINGS OF SELF AND MUTUAL CAPACITANCES USED IN THE DESIGN

Taking $b = 0.625''$ (ground plane spacing) we obtain

$$d_0 = d_5 = 0.3225''$$

$$d_1 = d_4 = 0.2032''$$

$$d_2 = d_3 = 0.2156''$$

$$S_{01} = S_{45} = 0.1563''$$

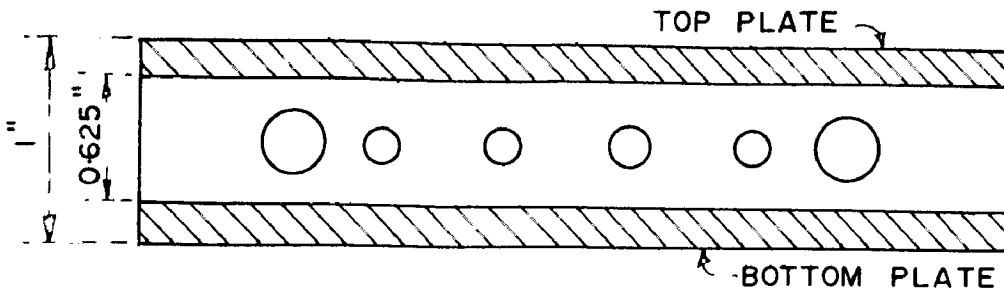
$$S_{12} = S_{34} = 0.4043''$$

$$S_{23} = 0.4375''$$

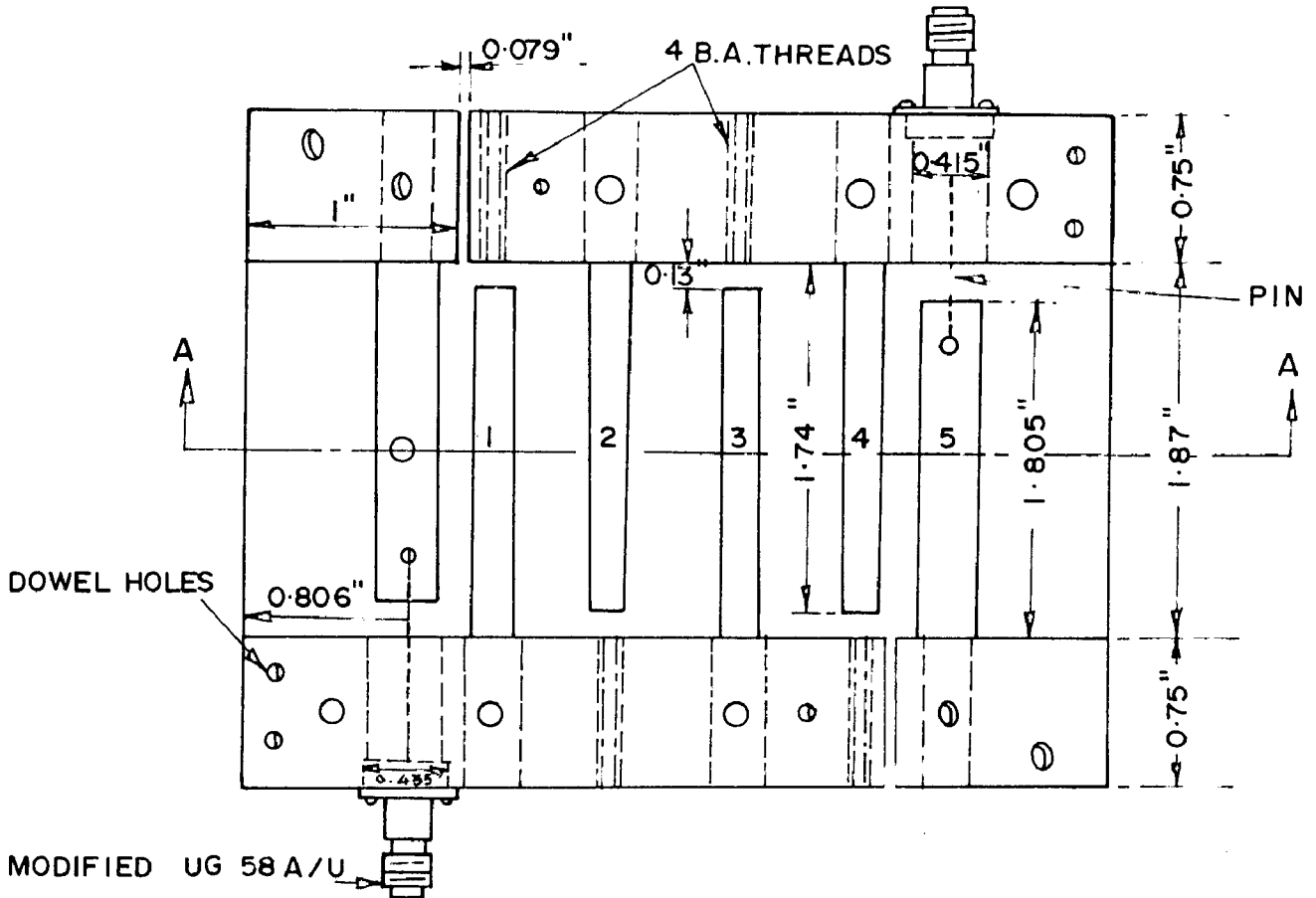
Fig. 3.15 shows a complete drawing of the filter with the cover plate removed. The short-circuiting side walls of the structure are spaced exactly a quarter-wavelength apart at the midband frequency of $f_0 = 1.84$ GHz ($\frac{\lambda_0}{4} = 1.87''$). Because of the capacitance between the open-circuited ends of the resonator elements and the sidewalls, it was necessary to foreshorten them slightly so as to maintain their resonant frequency at 1.84 GHz. For the pass-band VSWR to be closely controlled, it is desirable to have the spacing between the end resonators and the adjacent impedance transforming section adjustable for small changes in spacing.

3.41 BAND-PASS FILTER CHARACTERISTICS

When the filter was first tested, the insertion loss and VSWR were too high. This situation was improved by adjusting properly the spacings between the terminating resonators and the resonators adjacent to them. The spacing S_{01} and S_{45} were decreased for better performance of the filter. The adjustments of these spacings were very critical, even a change of few mils could degrade the overall filter response.



SECTION AA



TOP VIEW , TOP PLATE REMOVED

ROD DIAMETERS AND SPACING BETWEEN ADJACENT RODS

K	DIAMETER OF ROD K	K	SPACING BETWEEN ADJACENT RODS
0 and 5	0.322"	0 and 1 } 4 " 5 }	0.157"
1 and 4	0.203"	1 and 2 } 3 " 4 }	0.4043"
2 and 3	0.216"	2 and 3	0.4375"

FIG. 3.15

The experimental set-ups for the measurement of insertion loss and VSWR are given in fig. 3.16 and 3.17, respectively.

For the measurement of insertion loss, a 30 dB directional coupler was introduced between the signal generator and the filter. The input power to the filter is calculated by measuring power at the coupled port of the directional coupler, for different generator frequencies. The corresponding output power is measured at the filter output. The input voltage standing wave ratio of the band-pass filter was measured at different frequencies using the standard VSWR measurement techniques. Fig. 3.18 is a plot of frequency versus attenuation and fig. 3.19 is a plot of frequency versus VSWR.

3.4.5 COMPARISON BETWEEN THEORETICAL DESIGN AND EXPERIMENTAL PERFORMANCE

Fig. 3.18 shows the measured as well as the theoretical attenuation characteristics of the filter. The measured fractional band-width is found to be less than the designed value. This shrinkage in band-width is likely to be there due to the approximate nature of the design equations. Thus to compensate for the shrinkage in band-width, it is always necessary to design the filter for the fractional band-width which is about 5 to 6 percent higher than the actual desired band-width.

The shift of the centre-frequency of the filter towards the low frequency side results from the resonators being slightly loaded by the "end-capacitances". The centre frequency could be raised by reducing the length of the resonator; however this was not tried since the final aim was to study the behaviour of a broad-band microwave source using varactors. Because of the shift in the

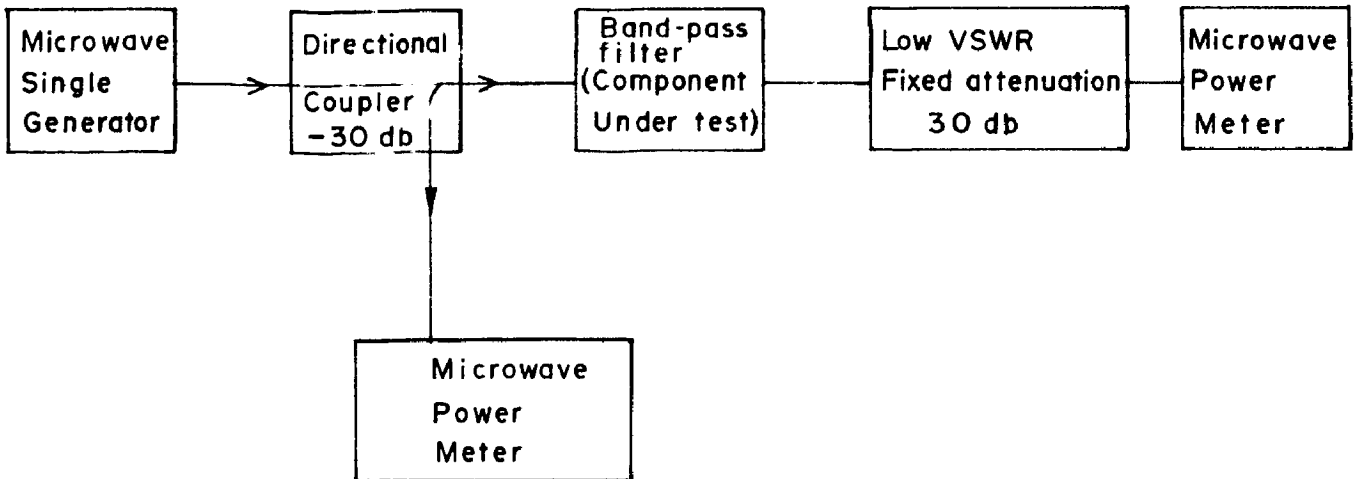


FIG.3.16 INSERTION LOSS MEASURING SET-UP

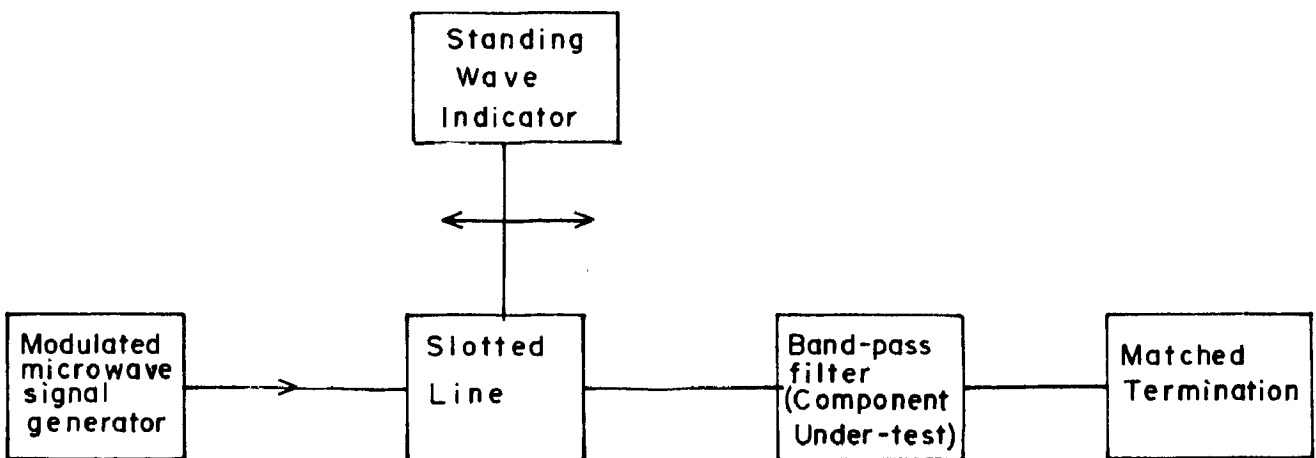


FIG.3.17 VSWR MEASURING SET-UP

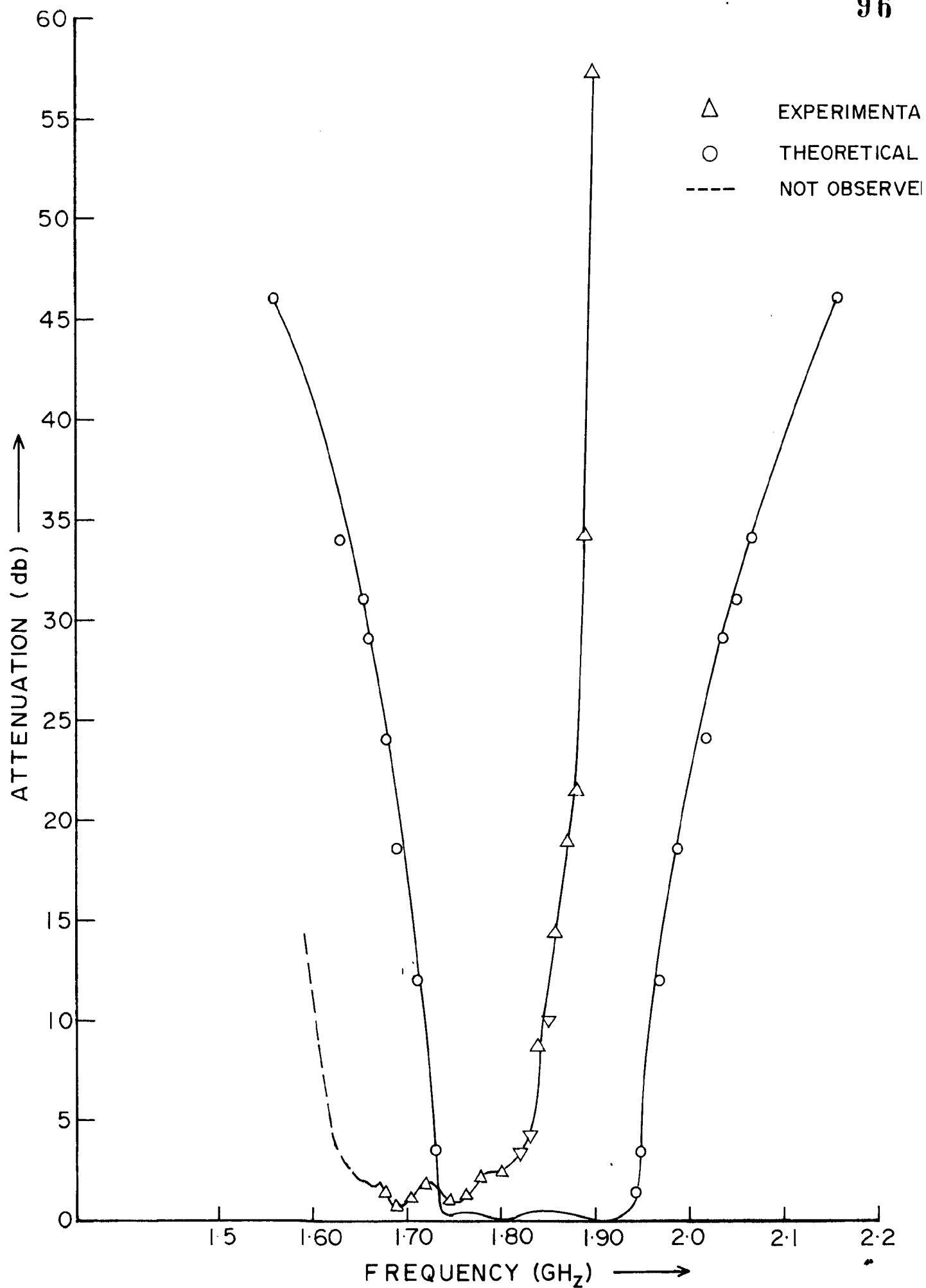


FIG. 3.18 BAND-PASS FILTER CHARACTERISTICS

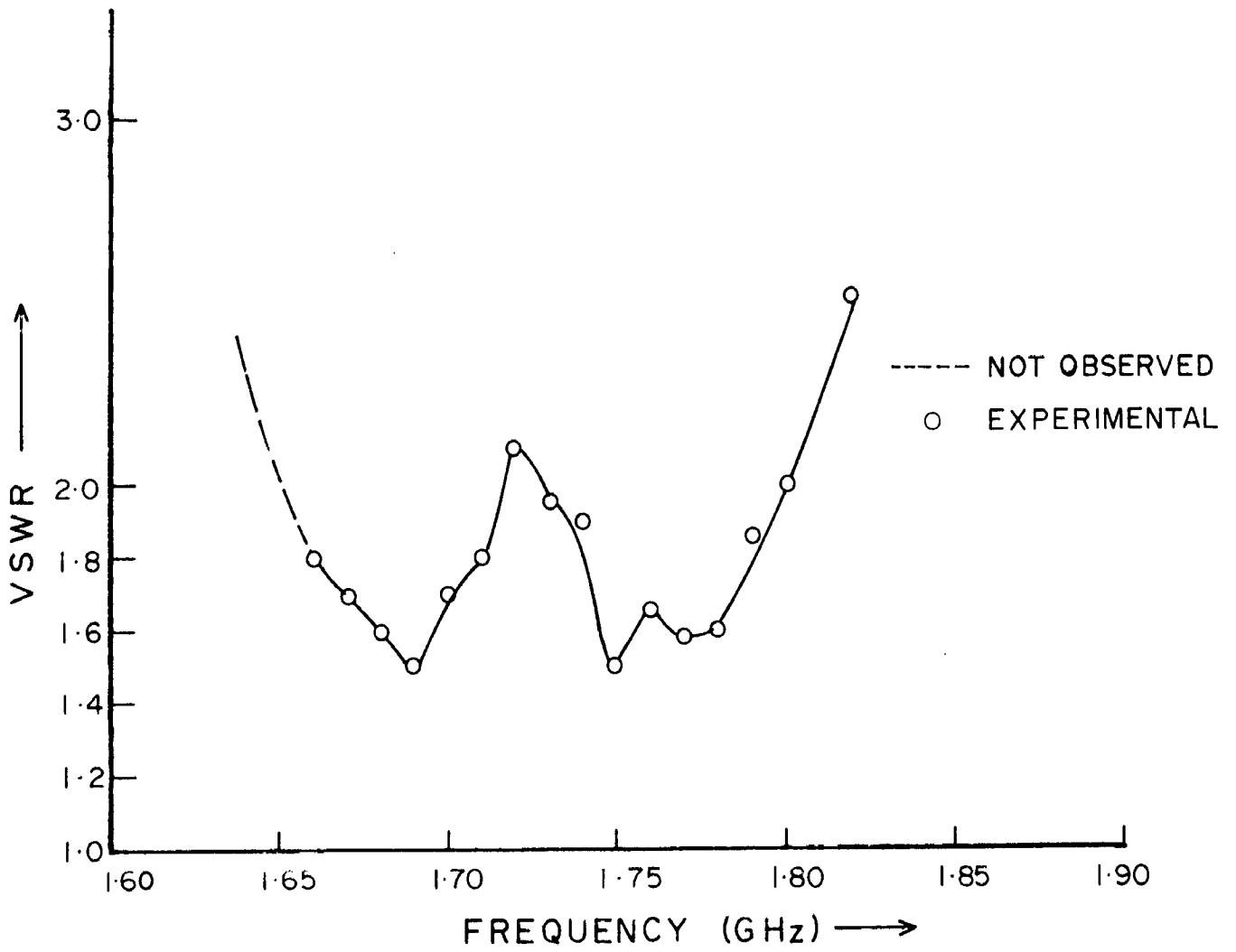


FIG. 3.19 FREQUENCY VERSUS VSWR

centre frequency of the filter towards the low frequency side, the overall frequency range of the multiplier is accordingly changed.

The measured pass-band insertion loss for the filter was found to be quite high as compared to the designed value. One of the possible reasons for this is that the practically achieved unloaded Q 's of the resonators is low compared to the designed value. The practical value is always less than the calculated value owing to mechanical surface finish, lossy electrical contacts.

3.5 DESIGN OF TRANSISTOR POWER OSCILLATOR, MECHANICALLY TUNABLE FROM 410 TO 450 MHz

For the testing purpose of the broadband frequency quadrupler, a primary source (mechanically tunable UHF transistor oscillator) was built. When operating in UHF range, the important characteristics of the power transistors are:

1. Maximum collector dissipation.
2. Maximum peak collector current.
3. Maximum collector voltage.
4. High-frequency current-gain figure of merit f_T .

The most important consideration for the r.f. power transistor is the power-dissipation capability. The maximum power that can be dissipated before thermal runaway occurs depends to a great extent on how well the heat generated within the transistor is removed. When heat is removed by conduction the amount removed is an inverse function of thermal resistance. A good r.f.

power transistor, therefore is characterized by a low value of thermal resistance. An rf transistor must be capable of handling high peak collector currents to provide substantial power output. The maximum peak-collector-current rating is usually limited by the practical consideration that the current amplification factor varies approximately inversely with emitter current at high values of emitter-current density. The maximum peak collector-current rating, therefore, may be established by considering the amount of reduction in the current gain which can be tolerated at high frequencies.

The maximum collector-voltage rating of an rf power transistor must be sufficiently high to avoid breakdown under conditions of a strong reactive loading. The rf transistor must be capable of withstanding high VSWR without collector-junction breakdown.

The high-frequency current-gain figure of merit (f_T) is essential in determination of the power-gain capability of a particular rf power transistor. The f_T of an rf transistor varies with dc emitter current and usually decreases at very high levels of current. A good rf power transistor should be characterized by a high value of f_T at high levels of dc emitter current or collector current.

3.5.1 OSCILLATOR DESIGN

Requirements for the high-power oscillator are as follows:

1. Tunable from 410 to 450 MHz.
2. Minimum power output should not be less than 1.5 watts.
3. All other harmonics and spurious frequencies should be down by a minimum of 20 db.

The clapp type (modified colpitts)⁽²⁴⁾ configuration is selected for this purpose because it is highly insensitive to changes in transistor parameters. Fig. 3.20 shows the Clapp oscillator circuit using 2N3375 which is capable of providing the desired power output in the required frequency range of 400- 450 MHz. In this circuit, the collector is grounded for maximum heat dissipation. Therefore, the power output is taken from the base circuit. Frequency of oscillations is determined by L and C₃ in the tank circuit and the capacitances C₁ and C₂ serve only to realize a certain feedback ratio. The ratio and the absolute values of the capacitances C₁ and C₂ can be adjusted in such a manner that the frequency of oscillation becomes practically independent of fluctuations in the collector capacitance due to supply voltage variations. The tuning is provided largely by capacitor C₃. Capacitance C₄ is adjusted for optimum match to the load of 50 ohms.

The dc parameters for the network are calculated as follows:

The maximum continuous collector current rating for 2N3375 is 500 mA. So keeping,

$$I_c = 250 \text{ mA} \quad \dots\dots\dots (3.23)$$

$$\text{Let } V_{cc} = 28 \text{ volts} \quad \dots\dots\dots (3.24)$$

Assuming a 25% efficiency for class A operation, for a power output of 2.0 watts, there should be a power dissipation of 8.0 watts in the transistor.

$$\text{Therefore, } I_c \times V_{CE} = 8.0 \text{ watts} \quad \dots\dots (3.25)$$

Substituting I_c from equation (3.23) in the above expression, gives

$$V_{CE} = 32 \text{ volts}$$

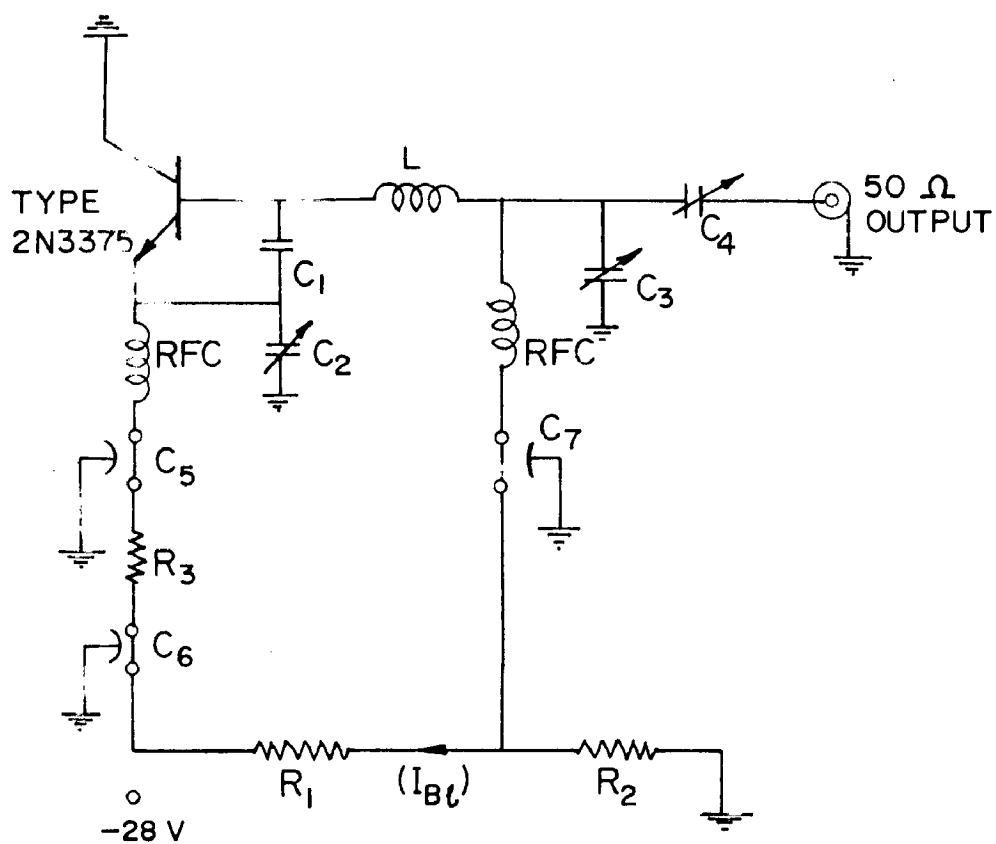


FIG. 3-20 A CLAPP OSCILLATOR CIRCUIT

$$\omega^2 \approx \frac{1}{LC_3} \quad \text{if} \quad \frac{C_1 C_2}{C_1 + C_2} > C_3$$

So the voltage drop across $R_3 = 4$ volts.

$$R_3 = \frac{4}{0.250} = 16 \text{ ohms} \quad \dots \quad (3.26)$$

The maximum rating of V_{BE} for 2N375 is 4 volts. So a value of $V_{BE} = 0.6$ volts can be easily selected. Therefore,

$$\text{Voltage drop across } R_1 = 4.6 \text{ volts}$$

$$\text{Voltage drop across } R_2 = 23.4 \text{ volts.}$$

Keeping the bleeder current (I_{B1}) = 30 mA

$$\text{base current} \approx \frac{I_C}{h_{fe}} \approx 16 \text{ mA}$$

hence

$$R_1 = \frac{4.6}{0.03} \approx 153 \text{ ohms}$$

$$R_2 = \frac{23.4}{0.046} \approx 510 \text{ ohms}$$

While adjusting for maximum power output and optimum biasing, the experimental values of R_1 , R_2 and R_3 differed slightly from the calculated values. The experimental values for all the components are listed below.

C_1	-	1.0 μ f, bead ceramic.
C_5, C_6, C_7	-	1000 pf, feed through.
C_2, C_3, C_4	-	0.8 - 10 pf, Johanson.
R_1	-	100 ohms, 0.5 W.
R_2	-	480 ohms, 3.0 W.
R_3	-	10 ohms, 2.0 W.

Experimentally it was found that the oscillator was highly stable and no undesired harmonics lie within the output frequency band. The final output response of the oscillator is shown in Graph of fig. 3.21.

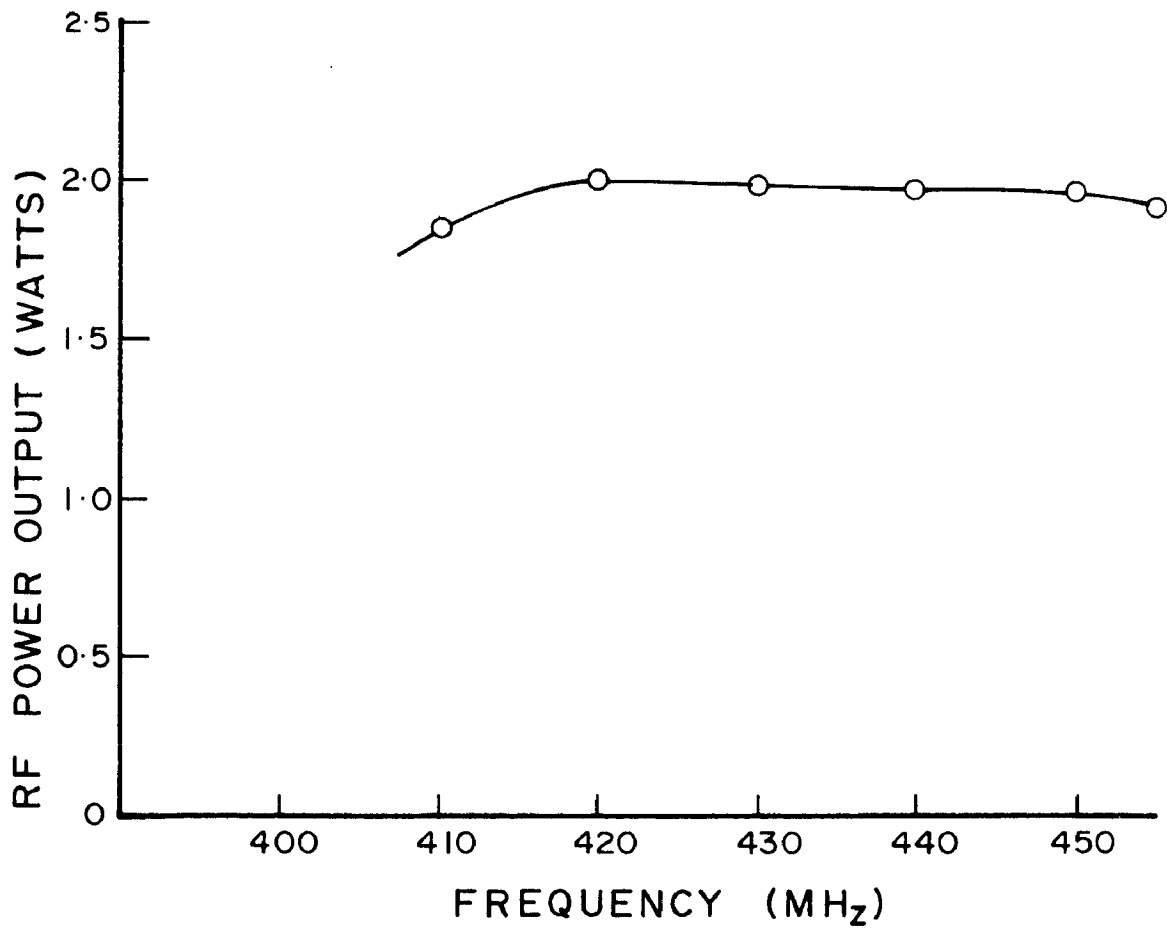


FIG.3-21 FREQUENCY VERSUS OUT PUT POWER

CHAPTER IV

MEASUREMENTS ON THE BROADBAND HARMONIC GENERATOR

4.1 INTRODUCTION

The broadband frequency quadrupler was assembled and tested. Design procedures for various components, needed for the same have already been described in chapter III. This chapter deals with the integration aspect of the broadband multiplier, describes the experimental set-up used for measuring it's performance and presents a discussion on the results obtained.

4.2 EXPERIMENTAL SET-UP

The block schematic of the frequency multiplier was given in fig. 3.1. According to the schematic, various components were assembled and the quadrupler was tested for its bandwidth and conversion efficiency. A block schematic of the measurement set-up is shown in fig. 4.1. The output of the broadband multiplier was fed to a 30 db strip line directional coupler, the direct output of which goes to the power meter through an attenuator and a frequency meter. The power output from the coupled port is fed to Tektronix 1120 spectrum analyser for studying the spectral response of the output wave. A 50-ohm, 20 db attenuator inserted in the direct arm brings down the power within the measuring range of the power meter besides eliminating a frequency pulling of the multiplier when the frequency meter is tuned for its resonance dip.

4.2.1 MULTIPLIER TESTING

Fig. 4.2 shows the arrangement of a shunt mounted step recovery diode with the input and output matching networks. Shunt mode was preferred for maximum

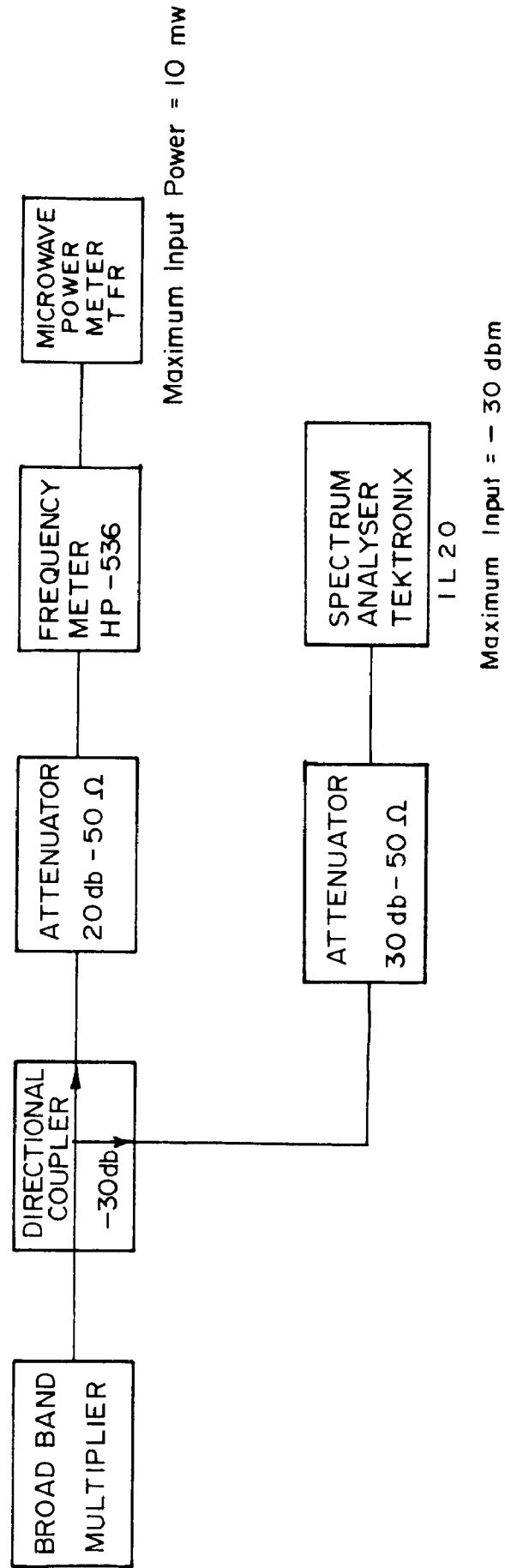
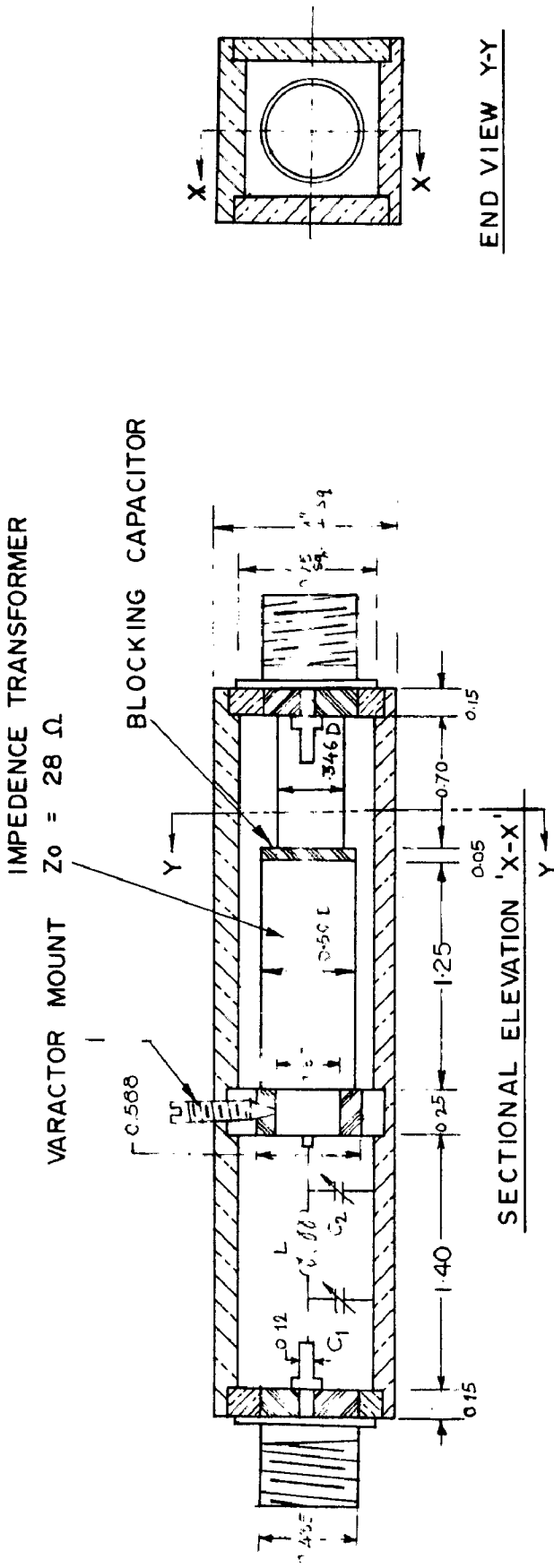
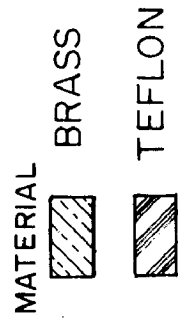


FIG. 4.1 EXPERIMENTAL SET-UP



C₁ and C₂ 1-20 pf JHONSON CAPACITORS



All dimensions are in inches

FIG. 4.2 SECTIONAL VIEW OF THE DIODE MOUNT WITH NARROW BAND INPUT AND OUTPUT MATCHING SECTIONS

heat dissipation, since a grounding of the varactor provides a direct heat sink. In order to avoid dc short circuiting of the step recovery diode, a blocking capacitor was used as shown in fig. 4.2. A pencil line resistance across the varactor as a bias resistance was preferred in order to eliminate parasitic resonances. Matching of the diode to the source and load was accomplished by using an ordinary lumped element single Π -section network and single section quarter-wave transformer, respectively.

The output response of the multiplier is given in fig. 4.3. It may be seen that the multiplier gives a maximum output of 400 mw at a frequency of 1.693 GHz. The response of this multiplier is such that it gives a 2 db bandwidth of 46 MHz and a 3 db bandwidth of 51 MHz. It is apparent from these measurements that the bandwidth obtained is very small. The multiplier behaves more or less like a narrowband multiplier.

Since the bandwidth obtained in the above case is very small, it was considered necessary to ^{use} multi-section broadband matching networks instead of single networks. The matching sections were broadbanded by using a two stage Π -section network for input matching and a two-section quarter-wave transformer for output matching. This schematic is illustrated in fig. 4.4. A brief design of this broadband output matching network is given in the following section.

4.3 DESIGN OF OUTPUT MATCHING NETWORK

The output resistance (R_{out}) of the diode for frequency quadrupling is given by⁽²⁵⁾

$$R_{out} = \frac{20}{C_{eff}^2}$$

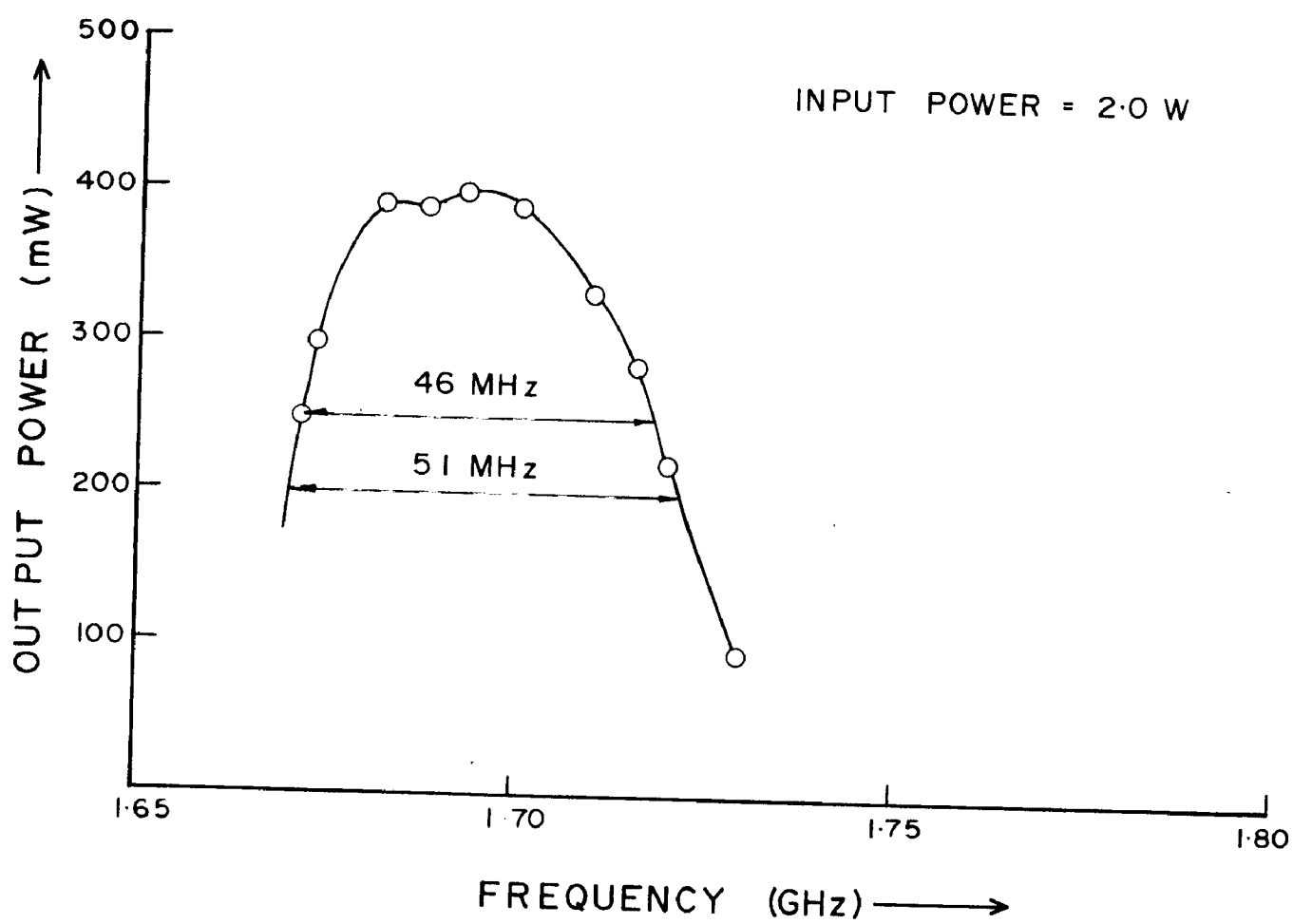


FIG. 4.3

where:

C_0 is the diode capacitance in pf at -6 volts

f_{in} is the input frequency in GHz.

Substituting for C_0 and f_{in} , it is found that

$$R_{out} \approx 17 \Omega$$

This is now to be matched to the line characteristic impedance of 50 .
Hence the impedance ratio (r) = $\frac{50}{17} \approx 3$. The desired bandwidth of the transformer is $\approx \frac{1.8 - 1.6}{1.7} \times 100 \approx 12\%$. It will therefore be sufficient if a matching transformer is designed for a 20% bandwidth and an impedance ratio of 3.

From Young's tables^(26,27), it is found that a two-section transformer provides the desired impedance matching over a 20% bandwidth with pass-band VSWR of 1.01. Since this pass-band VSWR is not very high, it was considered adequate if a two-section transformer is used. Referring to Young's tables⁽²⁷⁾ the impedances for a two-section Tchebysheff quarter-wave transformer (for an impedance ratio of 3 and fractional bandwidth of 0.2) are found to be

$$Z_1 = 1.3207 \quad (4.1)$$

and

$$Z_2 = 2.27 \quad (4.2)$$

where Z_1 and Z_2 are the normalized impedances of the two quarter-wave sections.

So that

$$Z_0 = 1, \text{ and } Z_{N+1} = r \quad (4.3)$$

for the terminating line impedances on the left and right, respectively.

For actual fabrication of the transformer, a cylindrical centre conductor was located in an enclosure having a square cross section (see fig. 4.4). For such a structure, the characteristic impedance is given by the equation

$$Z_0 = \frac{138}{\sqrt{\epsilon_r}} \log_{10} \frac{b}{a} + 3.54 \quad (4.4)$$

where a is the diameter of inner conductor and b is the length of one side of the square outer conductor.

The ratios $\frac{b}{a}$ for the two sections can be now calculated from the above equation. The calculated $\frac{b}{a}$ ratios for these sections are given in Table 9.

TABLE 9

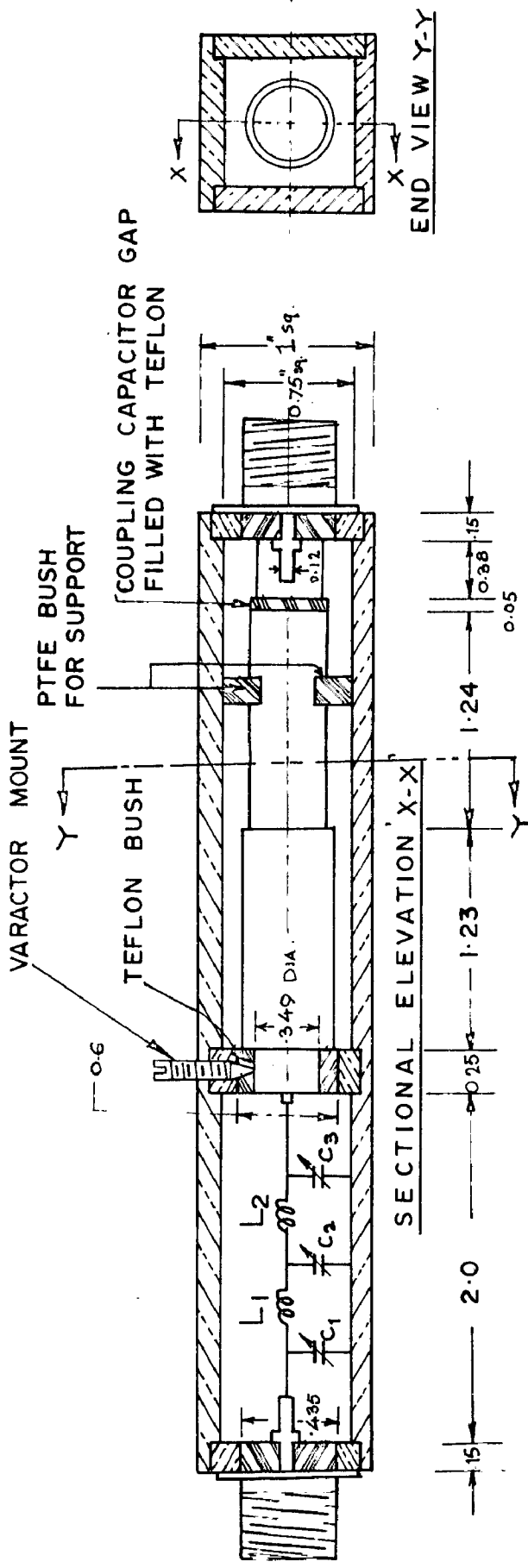
Section	Impedance	Ratio b/a
1	22.44	1.37
2	38.6	1.80

Selecting $b = 0.75''$, we obtain



$$a_1 = 0.547''$$

$$a_2 = 0.416''$$

In order to take into account the reactive loading of the line, the length



C₁, C₂ and C₃ 1 - 20pt. JHONSON CAPACITORS

MATERIAL	BRASS	TEFLON
		

All dimensions are in inches

FIG.4-4 SECTIONAL VIEW OF THE DIODE MOUNT WITH BROAD BAND INPUT AND OUTPUT MATCHING SECTIONS.

of each section was kept slightly less than quarter-wave length at the centre frequency of 1.7 MHz . A detailed drawing of the diode mount with the broadband input and output matching sections is given in fig. 4.4.

4.4 RESULTS

Finally the multiplier was tested with broadband input and output matching networks. While optimising the multiplier for power output, bandwidth and spectral purity, it is expected that the power output and bandwidth of the multiplier depend to a great deal on the matching conditions of the diode and the source. The fact that is so was also experimentally observed. Different sets of readings were taken for different matching conditions between the diode and the source. These are plotted in figs. 4.5(a), 4.5(b), 4.5(c) and 4.5(d). From these plots, it can be seen that for a broadband operation, the efficiency obtainable is relatively small. The measurements on the frequency multiplier indicate a maximum 2 db bandwidth of 135 MHz with all other harmonic and spurious frequencies down to a minimum of 40 db. The power output over the entire 135 MHz bandwidth was at least 155 mW. This corresponds to an efficiency of ^{approx.} eight percent. From other sets of measurements, shown in figs. 4.5(a) to 4.5(e), it might be observed that it is possible to obtain a larger power output i.e. efficiency by varying the matching conditions. The resulting bandwidth in that case is however smaller than 135 MHz . These graphs illustrate that the efficiency and bandwidth are inter-dependent. Larger efficiency can be obtained if the bandwidth is reduced. Alternately, a large bandwidth operation, necessarily results in a reduction in the overall conversion efficiency of the multiplier.

INPUT POWER = 2.0 W

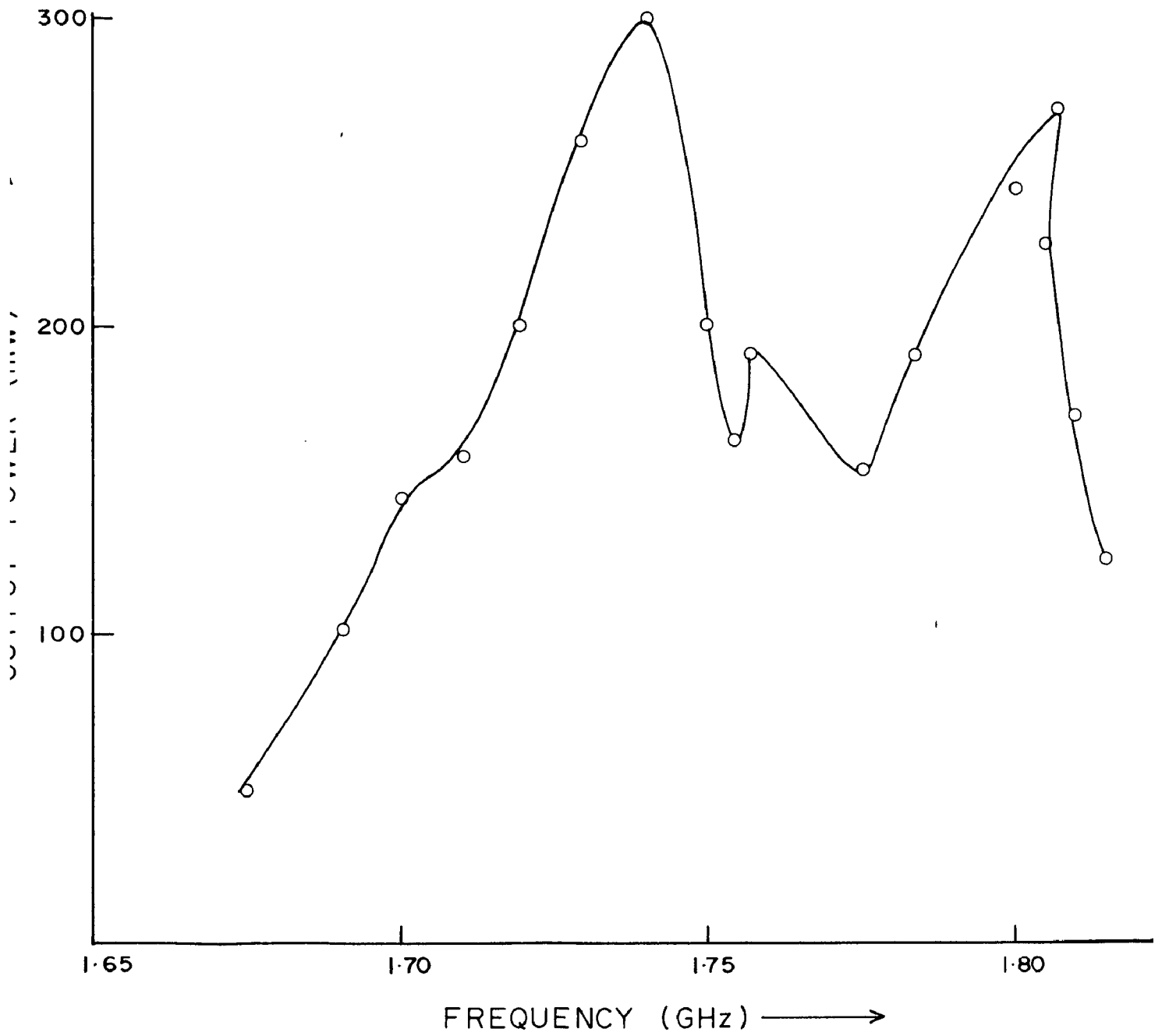


FIG. 4.5 (a)

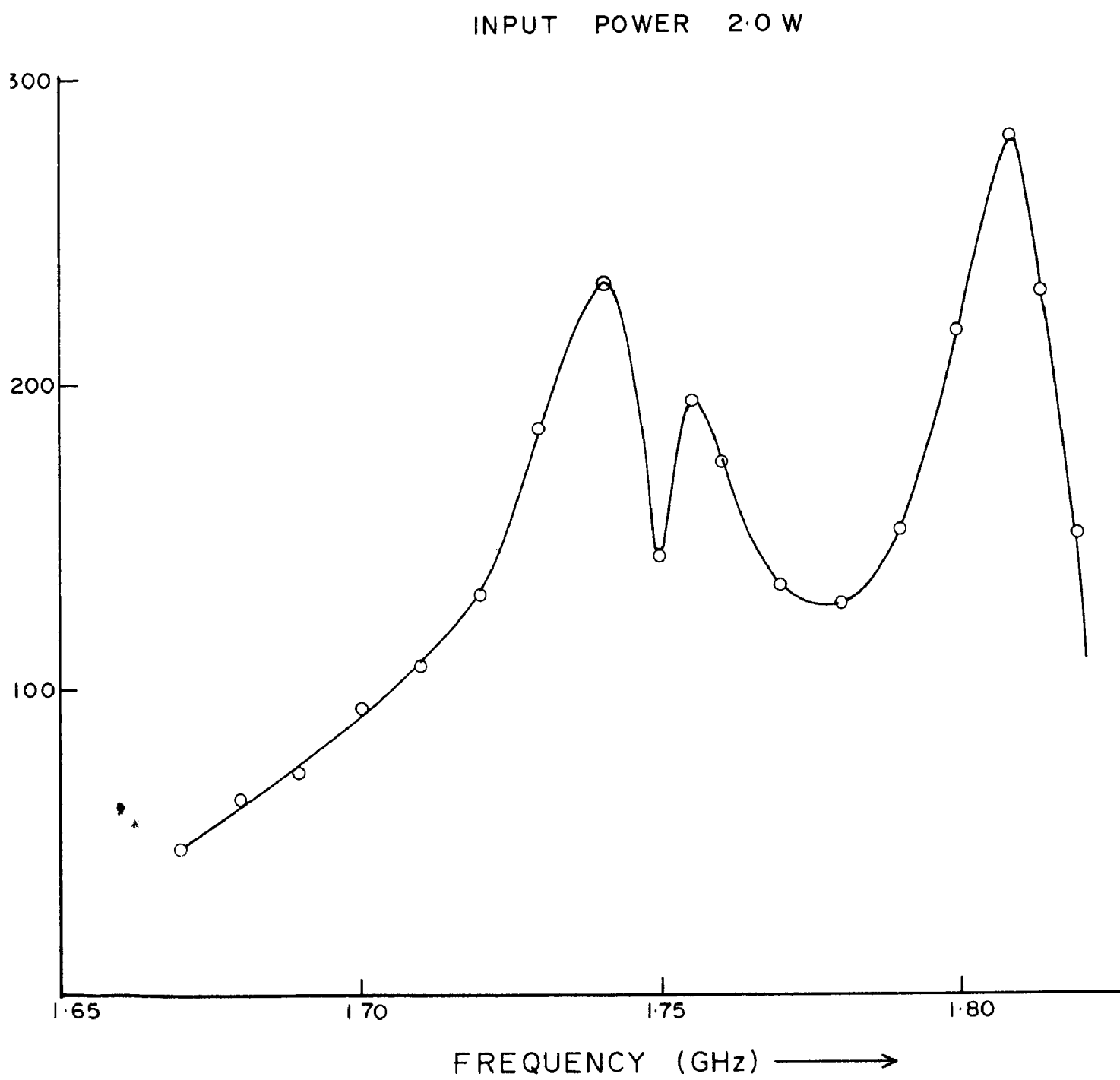


FIG. 4.5 (b)

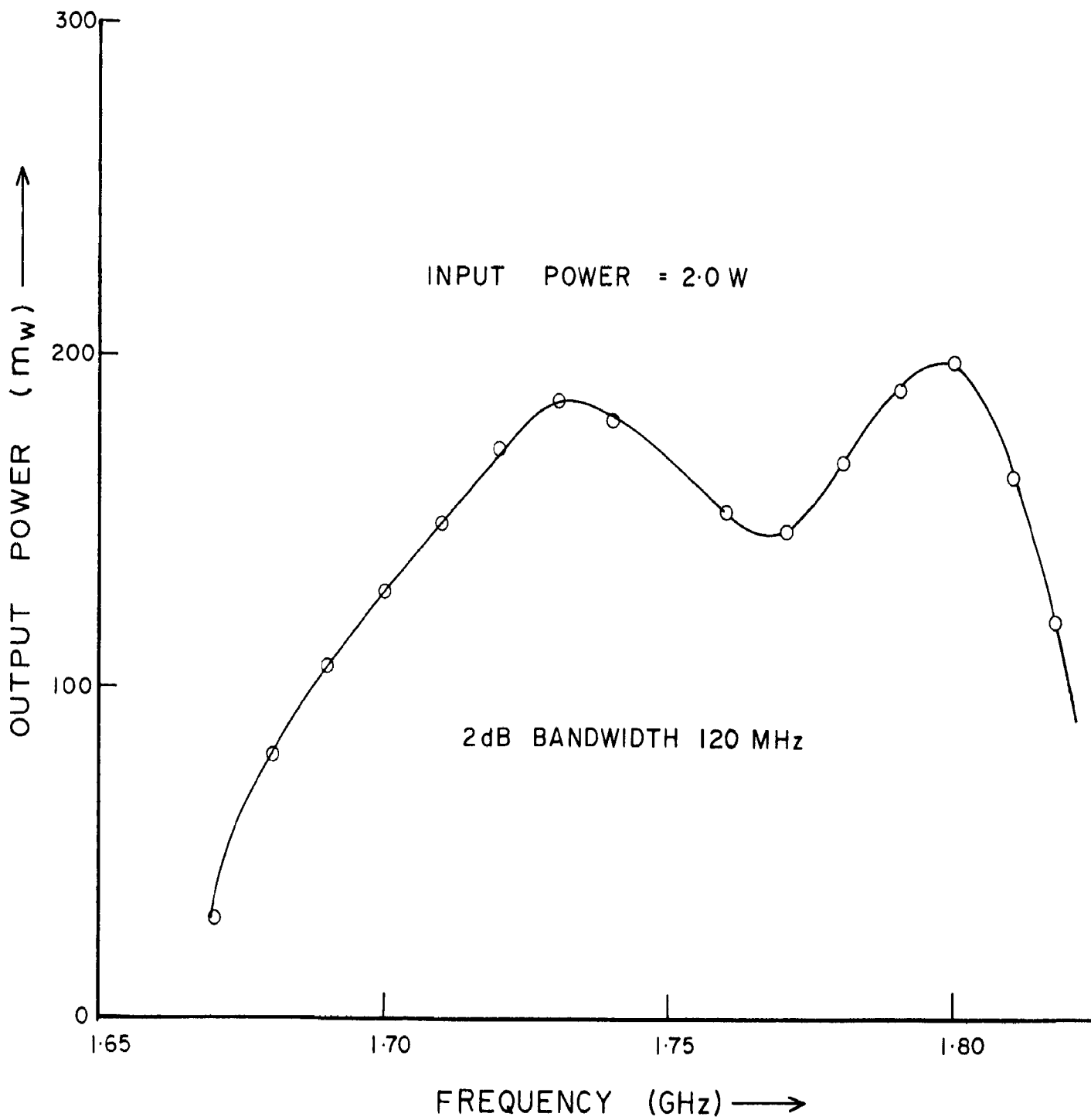


FIG. 4.5 (c)

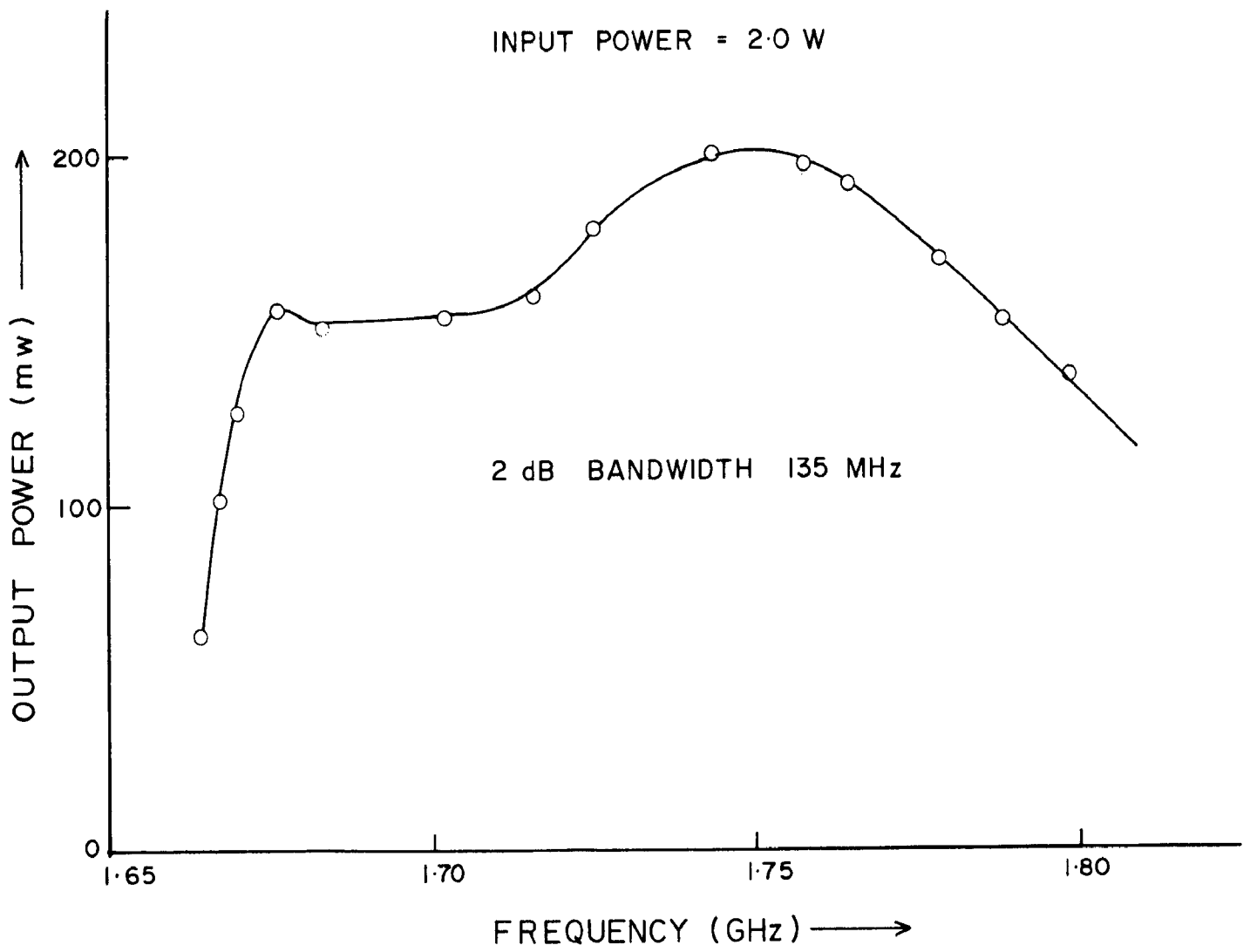


FIG. 4.5 (d)

The photographs of the broadband frequency quadrupler and the diode mount with its input and output matching networks are given in figs. 4.6 and 4.7, respectively.

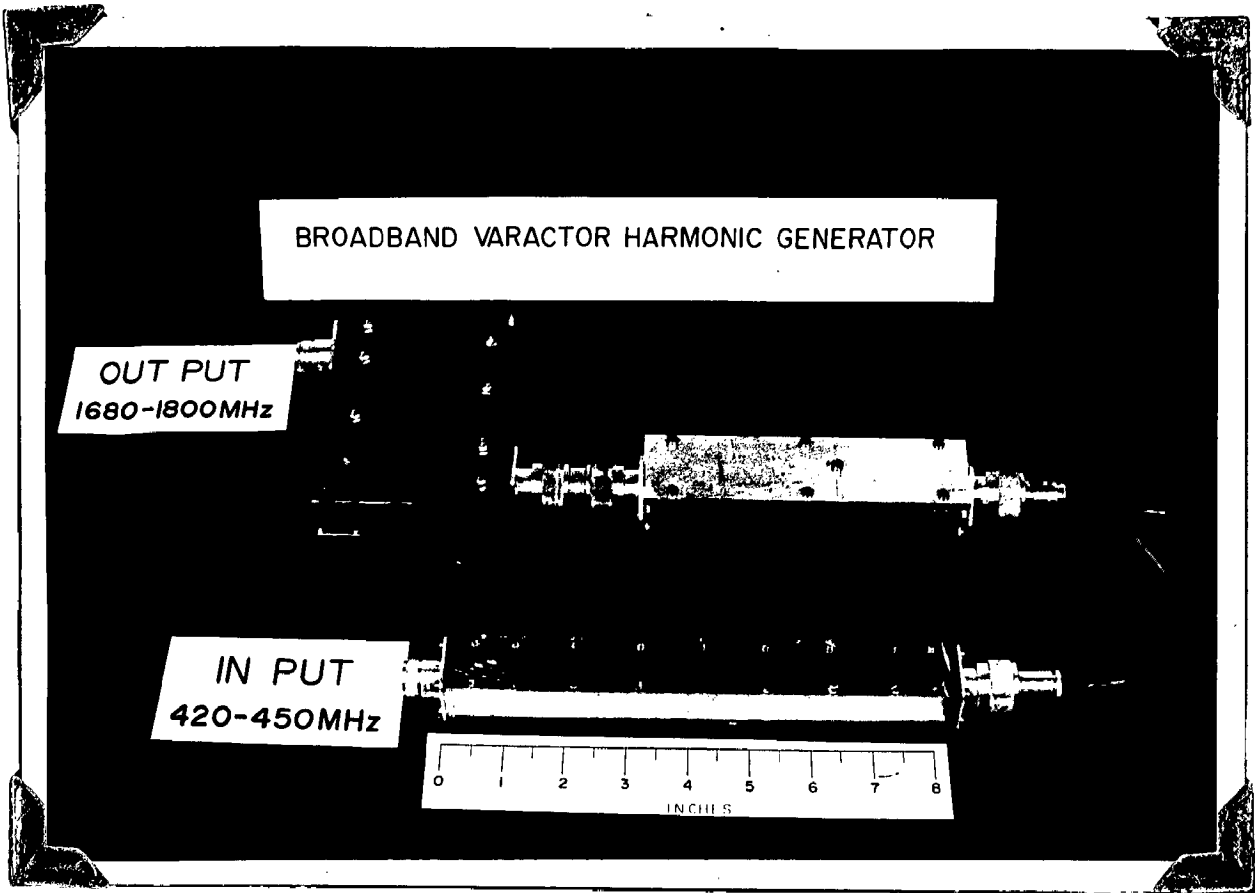


FIG. 4.6

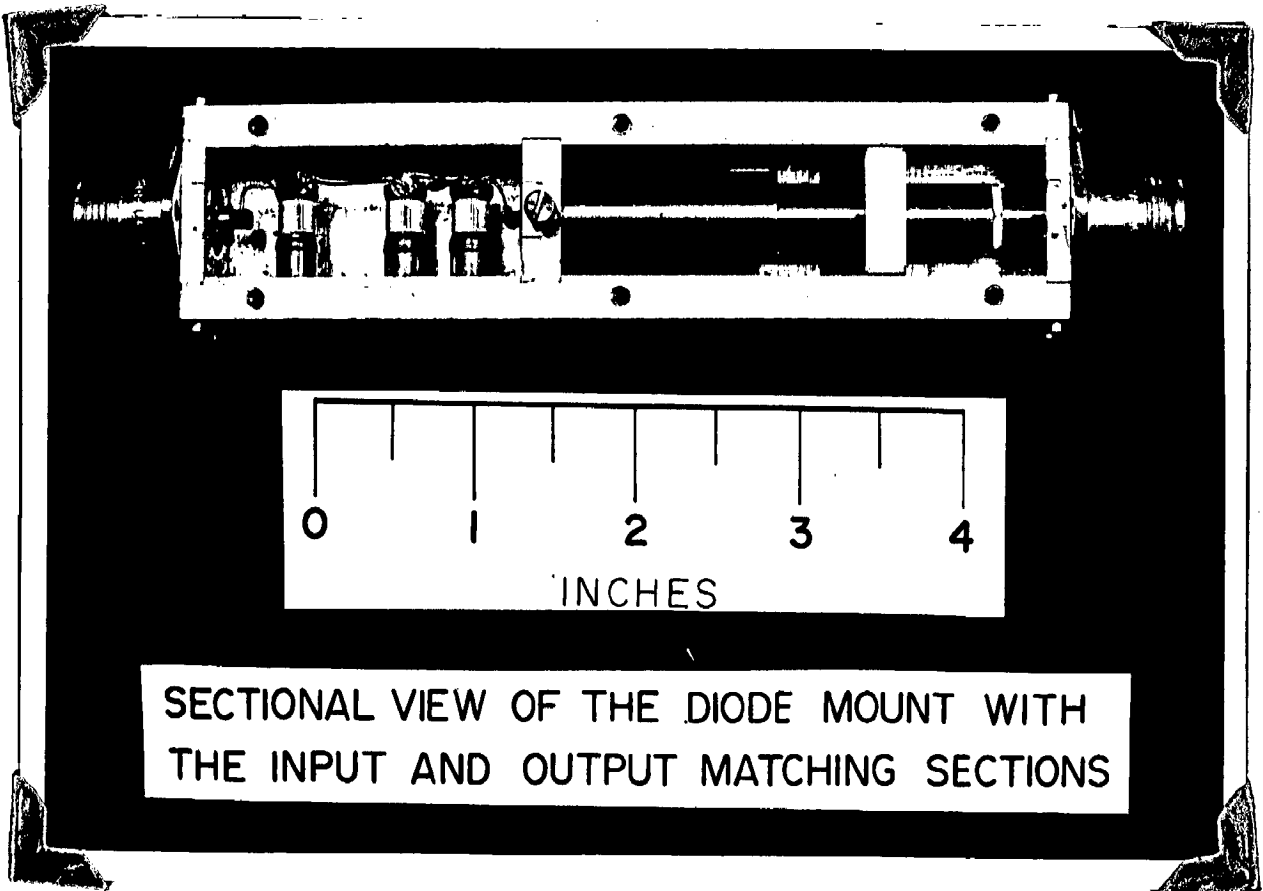


FIG. 4.7

CHAPTER V

SUMMARY, CONCLUSION AND SCOPE FOR FURTHER STUDY

5.1 SUMMARY AND CONCLUSION

In this thesis, a study of the broadband varactor harmonic generator was presented. The primary object was to obtain a broadband frequency multiplication consistent with a good overall performance. A frequency quadrupler using a step recovery diode was actually designed, fabricated and tested.

The first two chapters of this thesis deal with the physics of varactor diodes, principles of frequency multiplication using conventional (depletion layer) varactors and step recovery diodes and other circuit considerations in designing varactor multipliers. Varactor frequency multipliers can be categorised as spot frequency (i.e. narrowband) multipliers and broadband frequency multipliers. Large signal analysis of spot frequency varactor (conventional) multipliers with and without idlers was described in detail and the advantages of using idlers have been clearly explained.

A description of a broadband frequency multiplier with its basic block schematic explaining the function of each part was given and the bandwidth limitations arising from a requirement of having only one harmonic appear at the output have been explained.

The later part of the thesis dealt with the design of UHF oscillator, input and output filters, needed in the assembly of a broadband multiplier and the testing of the integrated unit. The input lowpass filter was designed for a cut-off frequency of 600 MHz. Function of this filter was to allow only the fundamental frequency to pass through and to provide isolation between the

source and the diode harmonic generator for the output frequency range of 1.74 GHz to 1.94 GHz. The bandpass filter used as an output frequency selecting circuit was of interdigital type. This filter was designed for a bandwidth of 10.8% centred at 1.84 GHz. However, a shift in centre frequency towards the low frequency side was observed when the filter was actually fabricated and tested. A UHF mechanically tunable oscillator was built to serve as a primary source for the frequency multiplier and was tested for its power output and spectral purity. After testing and adjusting these components individually, the frequency multiplier was assembled and tested.

Different sets of readings were taken for different matching conditions between the diode and the source. These have been plotted in figs. 4.5 (a), 4.5 (b), 4.5 (c) and 4.5 (d). From these plots, it is seen that for broadband operation, the conversion efficiency obtainable is relatively small. This was in any case expected to be so. In one typical case the efficiency of the frequency quadrupler was measured to be atleast eight percent over a bandwidth of 125 MHz.

5.3 SCOPE FOR FURTHER STUDY

The bandwidth of an n -times multiplier is limited, fundamentally, by the requirement that no more than one harmonic should appear at the output simultaneously. For example, a simple frequency tripler if designed to have more than 29% bandwidth, the output circuit passes fourth and second harmonics when the harmonic generator is operated at the lower and higher edges of its frequency band, respectively. In the same way a frequency doubler is limited to have a maximum bandwidth of 40%. In practice, however, the stray reactances

associated with the diode and the physical realization of the required circuit will tend to further reduce the useful bandwidth.

Varactor harmonic generators for broader bandwidth operation (than is possible with a single diode) can be designed by using balanced circuits.⁽¹⁶⁾ These balanced circuits avoid the possibility of interaction of different harmonics at the output by separating even and odd harmonic components of the waveform. A simple balanced circuit is shown in fig. 5.1. In order to separate the even and odd harmonic components, it is necessary that the drive currents to the two diodes be in antiphase. This is achieved by means of a transformer as shown. The vector sum of the resultant voltage waveforms contains only the even harmonics and the vector difference only odd harmonics. Thus since the output circuit of fig. 5.1 forms the vector sum, it suppresses odd harmonics. Doublers using such balanced circuits can have bandwidths of the order of an octave.

The output filters for such balanced multipliers can be of interdigital or digital elliptic type. These elliptic function filters⁽²⁶⁾ have very sharp cut-off response whereas the sharp cut-off response in the case of an interdigital filter can only be achieved by having larger number of resonators and high value of passband ripple. Because of the increase in number of resonators, the alignment and tuning of the resonators is rendered more difficult while adjusting the filter for optimum response. Furthermore, the fabrication becomes costly and tedious. Elliptic function filters, because of their steep skirt characteristics, when used in balanced multipliers will provide better rejection for all unwanted harmonic frequencies. Since these elliptic filters are suited to wideband (greater than 30 percent) designs, they can not be used for unbalanced frequency multipliers excepting for the unbalanced doubler. No work

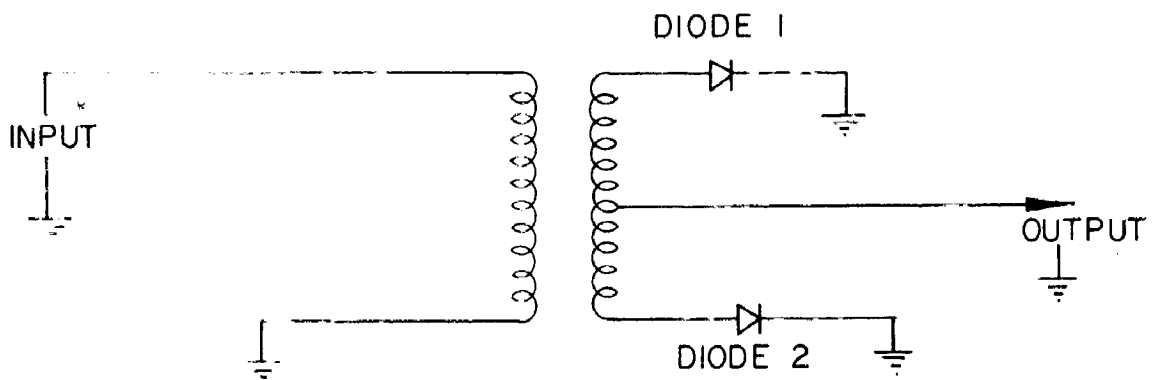


FIG. 5-1 BALANCED CIRCUIT

has so far been reported in the literature, where the above mentioned concepts have been utilised to evolve optimal designs. This is consequently an area that is open for further investigation.

On the theoretical side also this field is wide open for further work. The dependence of conversion efficiency on the bandwidth is still unknown. Also the analysis of broadband varactor multipliers with and without idlers is still incomplete. This thesis work can be extended over any of the lines suggested above.

REFERENCES

1. H.A. Moten, "Microwave semiconductor devices and their circuit applications", McGraw-Hill, Chapter 7.
2. G. Staffner, "High-power varactor diodes: theory and application", Motorola Semiconductor Products Inc. Application note AM-107.
3. P. Ponzio and A.P. Refuso, "Varactor applications", N.I.E. Press, 1962, Chapter 6.
4. H.D. Hall, "Step-recovery diodes and their use in frequency multiplication", Microwave, pp.70-76, September 1965.
5. S.L. Kramer, "Harmonic generation, rectification and lifetime evaluation the step recovery diode", Proc. IRE, Vol.50, pp.1050-1070, July 1962.
6. G. Schaffner, "Charge storage varactors boost harmonic power", Electronics, Vol.57, pp.62-67, July 1964.
7. G.H. Pogo, "Frequency conversion with nonlinear reactance", J. Res. NBS, Vol.60, pp.227-229, May 1957.
8. J.H. Manley and H.H. Hepp, "Some general properties of nonlinear elements; part-1, general energy relations", Proc. IRE, Vol.60, pp.006-013, July 1960.
9. H. Hall, and S. Hamilton, "Sharp radio harmonic generation with step recovery diodes", The Microwave Journal, Vol.10, pp.60-70, April 1967.

10. J.O. Scanlan and P.J.R. Laybourn, "Analysis of varactor multipliers with idlers", *The Radio and Electronic Engineer*, Vol.31, pp.359-367, June 1966.
11. J. O. Scanlan and P.J.R. Laybourn, "Large-signal analysis of varactor harmonic generators without idlers", *The Radio and Electronic Engineer*, Vol.112, pp.1515-1522, August 1965.
12. H.W. Bode, "Network analysis and feedback amplifier design", Van Nostrand, New York, 1945, pp.360-368.
13. R.M. Fano, "Theoretical limitations on the broadband matching of arbitrary impedances", *J. Franklin Inst.* Vol.249, pp.87-93, 139-154, January and February, 1950.
14. G.L. Matthaei, "A study of the optimum design of wideband parametric amplifiers and up converters", *Trans IRE on Microwave Theory and Techniques*, MTT-9, pp.23-26, Jan. 1961.
15. E.S. Kuh, "Theory and design of wideband parametric converters", *Proc. IRE*, Vol.50, pp.31-36, Jan. 1962.
16. D.J. Wright, "Wide tuning range solid-state sources" *Proc. of the Joint symposium on Microwave applications of semiconductors*, Vol.5, pp.36/1 - 36/5, June-July, 1965.
17. H. Levy, "Tables of element values for the distributed low-pass prototype filter", *IEEE Trans. on Microwave, Theory and Techniques*, Vol. MTT-13, pp.514-536, September 1965.

18. L. Young, "Stepped-impedance transformer and filter prototypes",
IRE Trans. on Microwave Theory and Techniques, Vol. MTT-10,
pp. 339-359, September 1962.
19. R. Levy and T.E. Rossi, "Precise design of coaxial low-pass filters",
IEEE Trans. on Microwave Theory and Techniques, Vol. MTT-16,
pp. 142-146, March 1968.
20. P. I. Soale, "The computation of coaxial line step capacitances",
IEEE Trans. on Microwave Theory and Technique, Vol. MTT-15,
pp. 48-53, January 1967.
21. J.T. Bolljahn and G.L. Matthaei, "A study of the phase and filter
properties of arrays of parallel conductors between ground planes",
Proc. IRE, Vol. 50, pp. 299-311, March 1962.
22. Matthaei, Young and Jones, "Microwave filters impedance-matching
networks and coupling structures", McGraw-Hill, Chapter 10.
23. E. G. Cristal, "Coupled circular cylindrical rods between parallel
ground planes", IEEE Trans. on Microwave Theory and Techniques,
Vol. MTT-12, pp. 429-440, July 1964.
24. Gartner, "Transistor principles, design and application", Van Nostrand,
New York, Chapter 17.
25. J. Cochran, "24 watts at 1 GHz, with step recovery varactors", Motorola
Semiconductor Products Inc. Application note AN-228.

26. Leo Young, "Tables for cascaded homogeneous quarter-wave impedance transformers", IRE Trans. PG MTT-7, pp.233-237, April 1959.
27. Leo Young, "Tables for cascaded homogeneous quarter-wave impedance transformers", IRE Trans. PG MTT-8, pp.243-244, March 1960.
28. M.G. Horton and H.J. Wessel, "The digital elliptic filter - A compact sharp cut off design for wide band stop or band-pass requirements", IEEE Trans. on Microwave Theory and Techniques, Vol. MTT-15, pp.307-314, May 1967.

UNIVERSITY OF ROORKEE
ROORKEE

REPORT OF THE EXAMINERS FOR AWARD OF M.E. DEGREE.

- | | |
|---|--|
| 1. Name of the candidate | Miss Neelam Rani Gupta |
| 2. Department | E & C.E. Deptt. |
| 3. Specialised subject | M.E. Microwaves |
| 4. Title of dissertation | A Study of Broadband Varactor Harmonic Generators. |
| 5. The Viva-Voce Examination was held on January, 1971, at Roorkee. | |

(Note: The examiner is requested to give here a ~~short~~ concise report not exceeding 100 words).

The presentation of Miss Neelam Rani Gupta was very good and the work explained in the Thesis is of a standard that I would consider equivalent to any Master's Degree in U.S.A. I recommend that here thesis may be accepted for the award of M.E. Degree.

The dissertation is approved.

Sd. (A.K.Kamal)

Signature of Internal Examiner

Signature of External Examiner.

~~XXXXXXXXXX~~

UNIVERSITY OF ROORKEE
ROORKEE

No. Ex/1318 /PF/NRG

Dated May 26, 1971.

Copy forwarded for information to:-